Charles University

Faculty of Science

Department of physical and macromolecular chemistry

Mgr. Nadiia Velychkivska

Investigation of external stimuli-influenced temperature-sensitive polymers behavior studied by spectroscopic methods

Doctoral thesis

Supervisor: Mgr. Larisa Starovoytova, PhD

Consultant: RNDr. Jan Labuta, PhD

Institute of Macromolecular Chemistry CAS

Prague 2020

Univerzita Karlova

Přírodovědecká fakulta

Katedra fyzikální a makromolekulární chemie

Mgr. Nadiia Velychkivska

Výzkum vlivu vnějších podnětů na chování teplotně-citlivých polymerů pomocí spektroskopických metod

Dizertační práce

Školitel: Mgr. Larisa Starovoytova, PhD

Konzultant: RNDr. Jan Labuta, PhD

Ústav makromolekulární chemie AV ČR, v. v. i.

Praha 2020

Declaration:

I declare that I have written this thesis independently under the supervision of Mgr. Larisa Starovoytova, PhD. and RNDr. Jan Labuta, PhD. I did not submit this work, or a part of it, to obtain another university degree. To the best of my knowledge, I have cited all the sources I have used.

Prague, 24.06.2020 Nadiia Velychkivska

Acknowledgments

I would like to acknowledge my supervisor Mgr. Larisa Starovoytova, PhD., for her support and guidance during my PhD studies. She has been an essential source of advice on the experimental tools and required knowledge in the field of polymer science. I would like also to express special gratitude to my advisor RNDr. Jan Labuta, PhD., for his motivation, willingness to assist, and technical knowledge. I appreciate highly his guidance given during the experimental work, data processing and physico-chemical analyses as well as the friendly working environment he provided during my fellowships in Japan.

I would also like to thank to my colleagues in the NMR spectroscopy department for their kind help and support. Additionally, I am very grateful to Nikolay Kotov, PhD., Uliana Kostiv, PhD., Anna Golunova, PhD., for their support, help and good times throughout my PhD. I appreciate highly the valuable advice given by Sergey Filippov, PhD., (SAXS and DLS) doc. RNDr. Lenka Hanyková, Dr., (on DSC and OM), and Jonathan P. Hill, PhD., (on macromolecular and supramolecular systems). I am also very thankful to RNDr. Ondřej Sedláček, PhD., for synthesizing the porphyrin-PNIPAM conjugates used in this work.

I am very grateful to the Institute of Macromolecular Chemistry, the Charles University, the Visegrad Scholarship (№ 51910789) for providing financial support of my PhD studies in Prague, and to the National Institute for Materials Science for supporting my research stays in Japan.

Last but not least, I would like to express my gratitude to my family members and friends all over the world. A special thanks to my mom Hanna for her unconditional love, faith, and encouragement that gave me the strength to follow my dreams.

Table of Contents

Abstract

Temperature-sensitive polymers or “smart” polymers are materials that undergo phase separation initiated by temperature change. Some of these polymers possess phase separation temperatures close to human body temperature (37 °C), thus offering a wide range of potential applications in controlled drug release or gene delivery systems, bioseparations, tissue engineering, etc. Of the polymers with a phase separation temperature close to 37 °C, poly(*N*-isopropylacrylamide) (PNIPAM) and poly(vinyl methyl ether) (PVME) are perhaps the most important and were selected as the subjects of this study. In this work, these two polymers have been examined in the presence of low molecular weight additives, and their colloidal stability evaluated using ^{1}H NMR (nuclear magnetic resonance) and time-resolved ^{1}H NMR spin-spin relaxation time T_2 experiments. An improved model of the two exchangeable states was applied for a more detailed characterization of the phase separation process. The main focus of this study was to determine the influence of additives on the phase separation behavior of the polymers (phase separation temperature, width of transition, maximum number of polymer chains participating in phase separation), reversibility of the phase separation, dynamics of solvent molecules (water and additive), interactions between solvent molecules, additives and polymer chains. Another objective of this thesis was to perform a thorough characterisation of temperature-sensitive porphyrin-PNIPAM conjugates by a variety of physico-chemical methods. Thermodynamic parameters associated with the phase separation phenomenon were obtained by NMR spectroscopy and compared with data obtained by differential scanning calorimetry. Phase diagrams based on Flory-Huggins theory were constructed and the influence of the concentration and length of the polymer chain on phase separation was evaluated. Small angle X-ray scattering (SAXS) provided information about the internal structure of aggregated, phase-separated, and protonated structures of the conjugates. Protonation occurring in the porphyrin-PNIPAM conjugates was studied by UV-Vis spectrophotometry, SAXS, NMR, and dynamic light scattering (DLS). During the protonation process, the colour of the conjugate solutions changes from red to green, accompanied by a change in geometry of the porphyrin core. The colour change is fully reversible and can be used as a visual indicator for sensing applications. Additionally, a co-nonsolvency effect was observed for the conjugates and was studied by NMR, DLS and optical microscope.

Keywords: PVME, PNIPAM, porphyrin−PNIPAM, phase separation, co-nonsolvency, pH responsiveness, ^{1}H NMR, T_2 spin−spin relaxation time.

Abstrakt

Teplotně-citlivé neboli “chytré” polymery jsou materiály, které procházejí fázovou separací při aplikaci vnějších podnětů, zde teploty Některé z těchto polymerů mají kritickou teplotu fázové separace blízkou fyziologické teplotě lidského těla (37 °C), což nabízí širokou škálu potenciálních aplikací v systémech řízeného uvolňování léčiv nebo systémech pro přenos genů, bioseparace, tkáňového inženýrství atd. Mezi polymery s teplotou fázové separace blízkou 37 °C byly pro bližší studium vybrány poly (*N*-isopropylakrylamid) (PNIPAM) a poly (vinylmethylether) (PVME). Tyto dva polymery byly zkoumány v přítomnosti nízkomolekulárních přiměsí a jejich koloidní stabilita byla hodnocena hlavně pomocí ^{1}H NMR spektroskopie vysokého rozlišení a časově rozlišených ^{1}H NMR spin-spinových relaxačních experimentů. Pro podrobnější charakterizaci fázové separace byl použit vylepšený dvoustavový model. Hlavní důraz byl kladen na vliv příměsí na chování polymerů během fázové separace (teplota fázového přechodu, šířka přechodu, maximální počet polymerních řetězců, které se účastní fázové separace), reverzibilita fázové separace, a dále byla sledována dynamika molekul rozpouštědla (vody) a příměsi, interakce mezi molekulami rozpouštědla, příměsi a polymerních řetězců. Dalším cílem této práce byla důkladná charakterizace teplotně-citlivých konjugátů PNIPAMu a porfyrinem různými fyzikálně-chemickými metodami. Termodynamické parametry spojené s jevem fázové separace byly získány NMR spektroskopií a porovnány s daty z diferenciální skenovací kalorimetrie. Byly zkonstruovány fázové diagramy odvozené z Flory-Hugginsovi teorie. Byl charakterizován vliv koncentrace a délky polymerního řetězce na fázovou separaci. Maloúhlový rozptyl rentgenového záření (SAXS) poskytl informace o vnitřní struktuře agregátů, fázově separovaných a protonovaných struktur konjugátu porfyrin-PNIPAM. Jev protonace, který se vyskytuje u konjugátů porfyrin-PNIPAM byl studován pomocí UV-Vis spektrofotometrie, SAXS, NMR a dynamického rozptylu světla (DLS). Během procesu protonace se barva roztoku konjugátu změnila z červené na zelenou, což je doprovázeno i změnou geometrie porfyrinového jádra. Změna barvy související s procesem protonace je plně reverzibilní a tento konjugát může být použit jako kolorimetrický senzor. Rovněž byl u konjugátů pozorován co-nonsolvency efekt který byl studován pomocí NMR, DLS a optického mikroskopu.

Klíčová slova: PVME, PNIPAM, porfyrin−PNIPAM, fázová separace, co-nonsolvency efekt, pH citlivost, ^{1}H NMR, T_2 spin-spinový relaxační čas.

List of abbreviations

DLS – dynamic light scattering

DMSO – dimethyl sulfoxide

D_2O – deuterated water

DSC – differential scanning calorimetry

EtOH – ethanol

H_2O – water

LCST – lower critical solution temperature

MeOD – methanol-d_4 (CD_3OD)

MeOH – methanol

NaCl – sodium chloride

NMR – nuclear magnetic resonance

PNIPAM – poly(*N*-isopropylacrylamide)

PVME – poly(vinyl methyl ether)

SAXS – small angle X-ray scattering

(*S*)-CSA – (*S*)-camphor sulfonic acid

T_2 – spin-spin relaxation time

t-BuAM – *tert*-butyl amine

t-BuOH – *tert*-butyl alcohol

t-BuME – *tert*-butyl methyl ether,

t-BuMK – *tert*-butyl methyl ketone

UCST – upper critical solution temperature

Introduction

1.1 Temperature-sensitive polymers and the phase separation phenomenon

Stimuli-responsive, so-called "smart" or "intelligent" polymers are materials that change their behavior according to an external stimuli.[1] These stimuli can be categorized as physical, chemical, or biochemical. Physical stimuli include variation in solution temperature, application of electric or magnetic field, mechanical forces, ultrasound or light irradiation.[2,3] Chemical stimuli include variation in pH or ionic strength or addition of chemical agents such as salts and metals.[3,4] Biochemical stimuli are associated with the addition of bioactive compounds, like enzymes, proteins, amino acids, antigen/antibodies, polysaccharides.[5]

Temperature-sensitive polymers are environmentally-responsive materials which compose a class of "smart" polymers, as they undergo a solubility transition under the influence of an external stimulus, herein temperature.[2] In aqueous solutions, the solubility variation in temperature-sensitive polymers is also known as a phase separation phenomenon. The molecular mechanism behind reversible phase separation corresponds to a coil–globule transition[2,6] during which hydrated polymer chains with expanded coil conformations collapse to fairly compact globular-like structures.[7,8] In other words, a binary polymer-solvent mixture undergoes a temperature-induced phase separation from a one-phase system (i.e. fully mixed) to a two-phase system (i.e. aggregated and separated).[9,10] When phase separation of a polymer solution occurs with increasing temperature, the polymer solution exhibits so-called lower critical solution temperature (LCST) behaviour. LCST is the minimum temperature below which a polymer-solvent mixture is miscible at all concentrations (Figure 1.1). On the other hand, a phase separation occurring with decreasing temperature is called upper critical solution temperature (UCST) behaviour.[12] UCST is the maximum temperature above which a polymer solution forms a single phase stable state. LCST and UCST are critical points lying at the intersections of binodal and spinodal curves (Figure 1.1). UCST and LCST temperatures for certain polymers in aqueous media are basic parameters important for the design and development of polymeric systems with practical applications.[9,11,12]

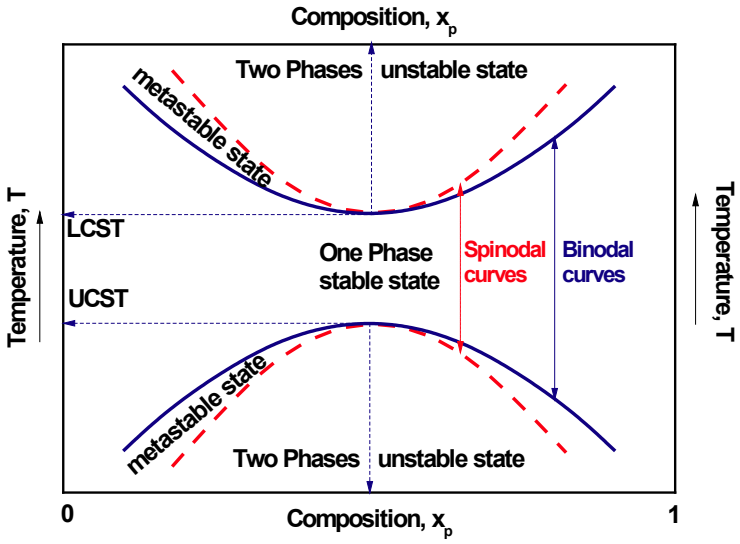

Figure 1.1. Schematic phase diagram of temperature vs. composition including both LCST and UCST behaviour for polymer binary solution.

Numerous non-ionic water-soluble temperature-sensitive polymers (e.g. families of N-substituted poly[(meth)acrylamide]s, poly(ether)s, poly(oxazoline)s) show an LCST type phase separation.[10,12-14] These polymers typically contain both hydrophobic (e.g. vinyl backbone, methyl groups) and hydrophilic groups (e.g. ether, carbonyl, or amide groups) and thus are amphiphilic in nature.[12] The dissolution of non-ionic polymer in water leads to the formation of hydrogen bonds between water molecules and hydrophilic polymer groups. At the same time, a water cage is formed around the respective hydrophobic groups being supported by the formation of new hydrogen bonds between water-water molecules surrounding the polymer chains.[15] UCST or LCST is a temperature when balance is shifted towards polymer-polymer hydrophobic groups interactions which leads to phase separation of the polymer from the medium. The balance of these interactions then could be described using thermodynamic approach.

From a thermodynamic point of view the free energy change of a system can be represented by the Gibbs equation[15]:

$$\Delta G = \Delta H - T\Delta S, \quad (1)$$

where ΔG is the Gibbs free energy change, ΔH is enthalpy change and ΔS is entropy change connected with the phase separation process.

The process of phase separation becomes energetically favourable when the entropic term predominates over the enthalpic term.[16] Temperature elevation causes an increase in entropy of water molecules, which becomes large enough to provoke spontaneous association of hydrophobic polymer groups present on polymer chains. The collapse of the individual polymer chains is called a microphase separation, while visible aggregation of the polymer in solution is called a macrophase separation.[9] Also, it is worth mentioning that while LCST behaviour of a temperature-sensitive polymer is a process driven by entropy, UCST behaviour is a process driven by enthalpy.[11,16] For example a schematic depiction of the coil–globule transition and the macroscopic phase separation in a real sample are displayed in Figure 1.2. Reaching LCST or UCST a phase-separated system turns opaque with aggregated particle sizes (>20 nm) comparable with visible light wavelength and, hence, scatters light.

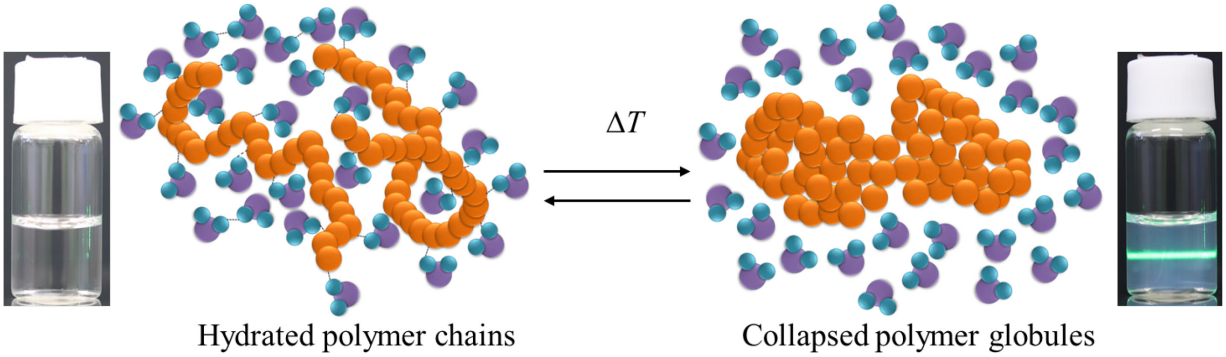

Figure 1.2. A schematic representation of a coil–globule transition in a polymer solution and its macroscopic detection by a green light laser pointer (532 nm). Key: orange circles = polymer chains, blue circles = H atoms, violet circles = O atoms. Vials show photographs of aqueous poly(*N*-isopropyl acrylamide) solution below (left) and above the phase separation temperature (right).

In some aqueous solutions of temperature-sensitive polymers, a hysteresis phenomenon is observed. This phenomenon is represented by a difference in the phase separation (demixing) temperature during heating and mixing temperature during cooling cycles. This hysteresis behaviour is attributed to limited diffusion of water molecules into dense globular structures (above LCST), which delay the polymer transition back to coil state

(below LCST).[10] Presence or absence of hysteresis allows evaluating the rigidness or looseness, respectively, of polymer globules upon their return to coil state.

As a result of phase separation, temperature-sensitive polymer systems can form well-defined self-assembled nano-organized structures, which morphologies and physico-chemical properties can be designed as desired. Nowadays, there is a huge variety of polymeric structures starting from polymer nanoparticles, micelles, physically and covalently crosslinked hydrogels, interpenetrating networks, etc., which are used as effective carriers to deliver therapeutic molecules in a range of biomedical applications spanning from bioseparation, through tissue engineering, up to drugs and genes delivery.[11,17-19] In this research, the formation of polymer globules and tuning of phase separation temperature for two homopolymers were studied for the potential biomedical purposes.

1.1.1 Poly(vinyl methyl ether)

The first system presented in this work is a temperature-sensitive poly(vinyl methyl ether) (PVME) (Figure 1.3). Depending on PVME concentration and molecular weight its aqueous solutions undergo the LCST-type phase separation in the temperature range 32–40 °C.[12,20] The phase separation is caused by a change of polymer-water interactions, namely by competition between hydrophobic and hydrogen bonding interactions.[21] Thermoresponsiveness of PVME makes it a suitable candidate for miscellaneous industrial and medical applications.[22]

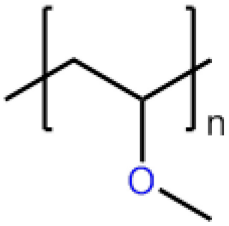

Figure 1.3. A chemical structure of a temperature-sensitive poly(vinyl methyl ether) (PVME).

Y. Maeda and co-authors studied phase separation of PVME aqueous solution in both H_2O and D_2O using infrared spectroscopy.[23] The authors indicated that hydrophobic and

hydrophilic parts of PVME behave differently during phase separation. Above the LCST most of hydrophobic methyl groups are found in a dehydrated state, whereas the ether oxygen groups remain only partially dehydrated. Phase separation temperature of PVME in D_2O solution was observed higher than that in H_2O solution for about 1 °C, which was attributed to stronger hydrogen bonding between D_2O molecules and PVME than in the case of H_2O.

Maeda *et al.* also studied the temperature-driven phase separation of PVME in binary alcohol/water mixtures by micro-Raman spectroscopy.[22] They found that solvation/dehydration of the alkyl group of PVME is governed by the hydrophobicity of the added alcohols in the order of methanol (MeOH) < ethanol (EtOH) < 2-propanol (2-PrOH) < *tert*-butanol (*t*-BuOH). Interestingly, the co-nonsolvency effect was observed in the case of 2-PrOH and *t*-BuOH in the range ca. 0.10-0.30 weight fraction of the alcohol in the ternary mixtures. The co-nonsolvency effect is discussed in detail in the part 1.1.2. Furthermore, the co-nonsolvency effect was also observed for PVME in water/1-propanol (PrOH) mixtures.[24] An addition of PrOH to PVME aqueous solutions promotes a rapid decrease in the difference between the surface tension of PVME and PrOH aqueous solution. This effect is well pronounced when the PrOH weight fraction exceeds 0.1 and surface behaviour changes from adsorption to depletion. It follows that with an increase of additive hydrophobicity the phase separation temperature of PVME decreases (considering the same concentration of additive) in the following order MeOH < EtOH < 2-PrOH < *t*-BuOH.

Additionally, Maeda *et al.* explored the influence of tetraalkylammonium ions on phase separation of PVME.[25] They observed an increase of a phase separation temperature in the order of methyl < ethyl < *n*-propyl < *n*-butyl ions addition, which is opposite to the effect observed by the addition of alcohol solvents. The authors suggested that it is because a positive charge of tetraalkylammonium ions is located at the surface of the complex, which increases the hydrophilicity of PVME and as a result, increases phase separation temperature.

K. Van Durme and co-workers investigated the influence of sodium chloride (NaCl) on the phase separation of an aqueous solution of PVME.[26] The NaCl addition decreases phase separation temperature as well as extends phase separation interval, by partial disruption of polymer-water interactions.

Spěváček and Hanyková showed that ^{1}H nuclear magnetic resonance (^{1}H NMR) spectroscopy can be effectively used for investigation of PVME phase separation.[27] Spin-spin and spin-lattice relaxation measurements revealed that in dilute PVME/D_2O solutions

polymer globules have compact structure, compared to semi-dilute and concentrated solutions, in which a certain amount of D_2O molecules is bound to the polymer globules. In addition, the authors detected fast and slow chemical exchange between free and bound water states for semi-dilute (2-10 wt.%) and concentrated (20-60 wt.%) polymer solutions, respectively.[28] The work presented in this thesis is in many ways a continuation of deeper understanding of PVME phase separation behaviour and its tuning by other than temperature stimuli.

1.1.2 Poly(*N*-isopropyl acrylamide)

Another system of interest in this study is poly(*N*-isopropyl acrylamide) (PNIPAM), a well-known temperature-sensitive water-soluble polymer with a sharp phase separation around 32 °C (chemical structure in Figure 1.4).[2,29] This separation process is reversible, as PNIPAM dissolves easily in aqueous media when the temperature drops below its phase separation temperature. Heskins and Guillet[30] were the first who reported the LCST-type behaviour for an aqueous solution of PNIPAM, and since then, around 9000 manuscripts were published on this topic.[31] Because LCST of PNIPAM is close to human body temperature (37 °C), PNIPAM is a prominent candidate for various biomedical applications, e.g. in drug and gene delivery.[32]

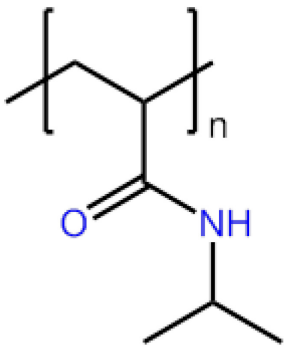

Figure 1.4. A chemical structure of a temperature-sensitive poly(N-isopropylacrylamide) (PNIPAM).

One of the ways to influence PNIPAM phase separation temperature is to add another solvent. Interestingly, an addition of a certain amount of good solvent to an aqueous solution of PNIPAM leads to a co-nonsolvency phenomenon.[33] A good solvent is a solvent in which polymer chains exist in expanded coil conformation ($A_2>0$, where A_2 is a second osmotic virial coefficient), while in poor solvent polymer coil tends to tighten and minimize polymer-solvent interactions ($A_2<0$).[34] The co-nonsolvency phenomenon is visually detected when at constant temperature and pressure a transparent aqueous PNIPAM solution becomes turbid upon the addition of a specific amount of a co-solvent (in which the PNIPAM itself is fully soluble), for example MeOH, EtOH, tetrahydrofuran or 1,4-dioxane.[35] One of the most thoroughly studied examples of co-nonsolvency is the phase separation of PNIPAM in water upon addition of MeOH.[36] In recent work, Xue *et al.* concluded that the phase separation in PNIPAM/water/MeOH mixtures depends on the solvent composition and temperature, as well as on the polymer molar mass, concentration, and end-group structure.[37] However, the molecular origin of the co-nonsolvency phenomenon still remains unclear. Tanaka *et al.* suggest that co-nonsolvency in PNIPAM/water/MeOH mixtures has a competitive character of hydrogen bonds established between PNIPAM-water and PNIPAM-MeOH.[38] Pica and Graziano supported this suggestion and proposed that MeOH interacts preferentially with isopropyl groups for basic geometric reasons, while H_2O interacts preferentially with amide groups.[36] However, Zhang and Wu note that the conformational transition is driven rather by solvent quality changes (MeOH and water form complexes in which PNIPAM is insoluble) than by local polymer-solvent interactions.[37,39]

Another way to modulate the phase separation temperature of PNIPAM is salt addition. The Hofmeister series classify salts by the ability to promote solubilisation or precipitation of macromolecules in aqueous solution.[40] Kosmotropes (e.g. CO_3^{2-}, SO_4^{2-}, Cl^-, HPO_4^{2-}) are strongly hydrated anions and therefore, reduce the solubility of proteins and macromolecules dissolved in water and show a so-called salting-out effect, while chaotropes (e.g. SCN^-, ClO_4^-, I^-) destabilize folded macromolecules (in other words solubilize macromolecules), resulting in a so-called salting-in behaviour. These effects were experimentally demonstrated for PNIPAM via rheological studies.[41] Interestingly, in the latter cited work a two-step phase separation for PNIPAM was observed: when KCl (kosmotrope) promotes a decrease in LCST, KBr has no influence on LCST, while KSCN (chaotrope) shifts PNIPAM LCST to higher temperatures. Kosmotrope anions such as Cl^- are more hydrophilic compared to SCN^-, and prefer interaction with water molecules than with polymer chains,

causing polymer dehydration and consequently lead to a decrease of a polymer LCST. The opposite effect occurs when chaotrope anions SCN^- because of their pronounced hydrophobicity. These anions form charged complexes with PNIPAM causing an increase in the polymer LCST.[40-44] In general, the presence of salts in polymer solution changes the hydrogen bonding network established by water molecules, and this phenomenon is typically more pronounced for anions than for cations.

Despite the plethora of LCST tuning possibilities of PNIPAM for various biomedical applications, the effects of small non-ionic (and into some degree functional) molecules on PNIPAM phase behaviour are not particularly well documented. Therefore, we have decided to study the influence of additives with different functional groups (amine, alcohol, ether and ketone) onto the LCST as well as other aspects of PNIPAM phase separation process.

1.1.3 Porphyrin derivatives

Porphine is the simplest macrocyclic tetrapyrrole and consists of four pyrrole units joined by four methine bridges (Figure 1.5). Porphyrins are substituted derivatives of porphine which are ubiquitous in nature. Haem is one of the best-known porphyrins being a cofactor of the protein haemoglobin, the pigment in red blood cells. Haem is an iron coordinated porphyrin complex that plays an essential role in vascular oxygen transport. Another well-known member of the porphyrin family is chlorophyll, which is a magnesium coordinated porphyrin. It is a green pigment in plants that plays a critical role in photosynthesis by absorbing sunlight energy and producing oxygen. Haem and chlorophyll are often called "The colours of life" due to the respective red colour of blood and green colour of leaves. Porphyrin and its derivatives are deeply coloured compounds due to a delocalized aromatic system consisting of 26π electrons (e.g. supporting aromaticity Hückel's rule). The π electronic system of porphyrins is responsible for their unique electronic, optical, redox, catalytic, self-assembly, magnetic, and other properties.[45]

Porphyrins can coordinate cationic species, especially transition metal cations, and these complexes exhibit unique functions depending on the metalating species. Porphyrins can coordinate most of the transition metals (Fe, Co, Cu, Zn, Hg, Pd, Pt, etc) in a square-planar configuration, forming metalloporphyrin complexes. Porphyrins without a metal cation

in their structure are called free-base porphyrins.[46] Stone and Fleischer reported that metal cations incorporated into the porphyrin structure can further coordinate electron-donating ligands in the axial positions above and below the plane of the porphyrin macrocycle. Besides metals coordination, these systems are used for sensing analytes such as alcohols, carbon monoxide, pyridine, etc.

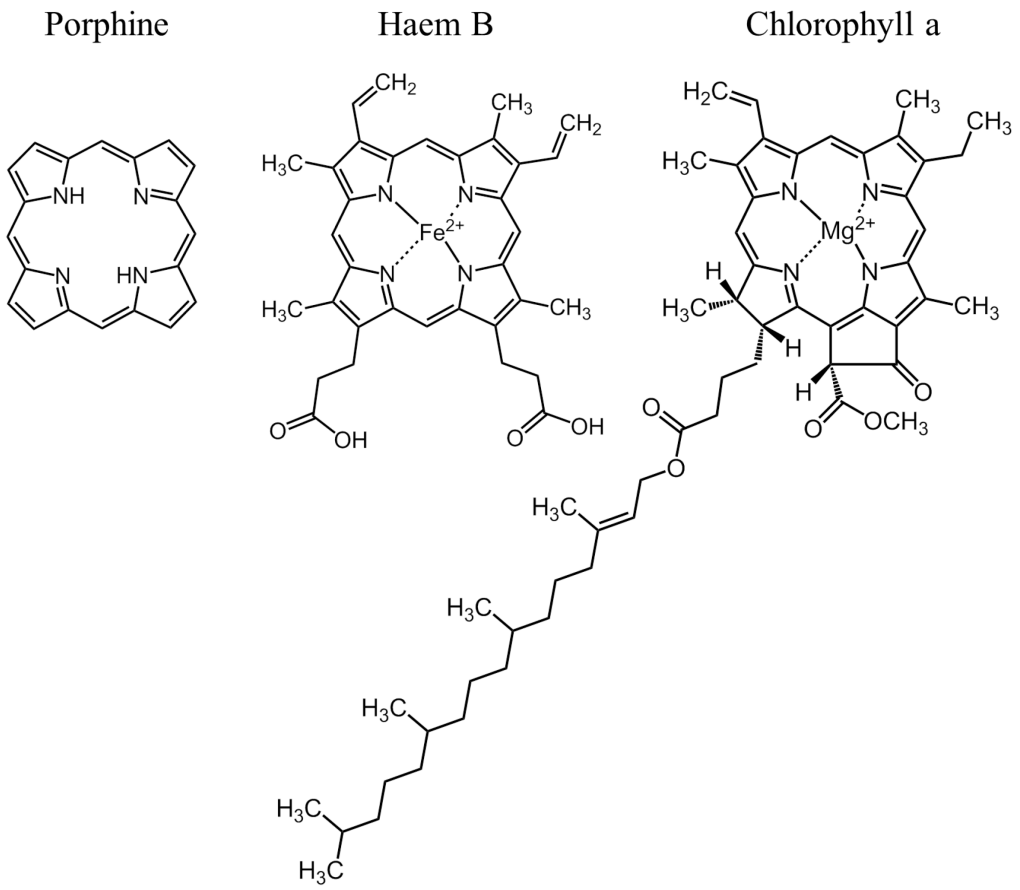

Figure 1.5. Chemical formulae of porphine and some well-known porphyrins: haem and chlorophyll a.

Porphyrin derivatives show sensing properties towards various anions. For instance, antioxidant-substituted tetrapyrazinoporphyrazine has been used as a fluorescent sensor for fluoride anions (F^-).[47] Upon addition of F^- the colour of solutions in organic solvent changed from gray-blue to green.[47] Ishihara et al. reported on reversible photo-redox switches based on 5,15-bis(3,5-di-tert-butyl-4-hydroxyphenyl)-substituted porphyrins which can be repeatedly used both as an F^- anion sensor and a photo-memory sensor.[48] Another example, β,β′-

disulfonamidequinoxaline-appended porphyrin derivatives were used as anion sensors for F^-, $H_2PO_4^-$, $CH_3CO_2^-$, Cl^-, HSO_4^-, Br^-, I^- anions.[49]

Decades ago, Dolphin reported on the ability of natural and synthetic porphyrins to form aggregates.[50] These, similar to other highly conjugated systems, self-associate in the solution due to strong intermolecular van der Waals forces between its porphyrin units.[51,52] Porphyrin molecules form a so-called J-aggregates and H-aggregates. J-aggregates are structures that exhibit the bathrochromically shifted J-bands (or red shift), whereas H-aggregates exhibit hypsochromically shifted H-bands bands (or blue shift) and these effects are explained in terms of molecular exciton theory.[53] J-aggregated structures exhibit the characteristic formation of a side-by-side or end-to-end molecules arrangement, whereas H-aggregates form face-to-face assemblies.[54] These structures show photocatalytic properties, widely exploited in molecular devices as optical switchers. The large extinction coefficients of porphyrin chromophores have great promise in use as photo-electronic components while their well-defined redox potentials suggest many electrochemical applications based on this feature.

The porphyrins are capable of adopting various tautomeric structures. They are usually planar in form, however, they can be distorted into saddle-like non-planar structures by various mechanisms including protonation (Figure 1.6).[46] Double protonation of porphyrin core is a highly cooperative two-step process with the core geometry change confirmed by X-ray crystal structure[48] as well as *ab initio* calculations.[55] The interaction with one proton forms a monocation and thus makes one inner nitrogen protonated. This process is more energy demanding because the energy barrier for the addition of the first proton is greater than that for the addition of the second proton. Free-base porphyrin is a planar molecule with lone-pairs of electrons on unprotonated nitrogen atoms directed towards the centre of the ring. This sterically unfavourable position of nonbonding electron pair demands more energy for the tilt of the first pyrrole ring up or down upon binding the first proton. The addition of the second proton to the opposite inner nitrogen promotes formation of dication. This process is less energy demanding as compared to the monoprotonation, partially due to better accessibility of nitrogen lone-pair electrons. The second protonation is high positively cooperative process. This well corresponds with the situation that porphyrins are usually found in either free-base or dication form and the monocation form is undetectable due to low abundance. Upon diprotonation, the solution colour changes from red to green due to the geometry change allowing straightforwardly following the process by the naked eye. Note, the protonation

process is a reversible process and can be turned back by addition of a base. Tautomerism and switching between planar- and saddle-like shapes[56] of porphyrins makes them applicable for enantiomeric purity detection[57], selective anions detection[58] or for determination of trace water impurities in organic solvents.[59]

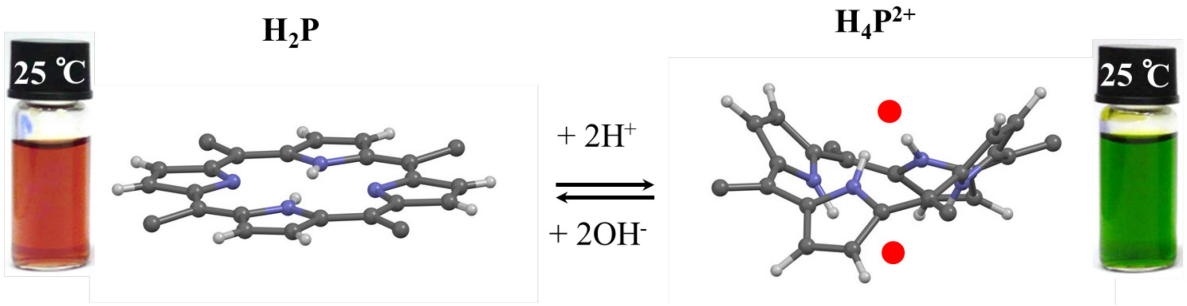

Figure 1.6. Scheme of protonation of porphyrin core. Free-base form and dication form of porphyrin is denoted as H_2P and H_4P^{2+}, respectively. Colour coding: white = H atoms, grey = C atoms, blue = N atoms, red circles denote acid anions. Vials show photographs of aqueous porphyrin-PNIPAM solution at neutral pH (red colour; left) and acidic pH (green colour; right).

In aqueous media porphyrin molecules self-aggregate due to non-covalent interactions, such as hydrophobic interactions and π-stacking. Hydrophobic interactions exert themselves as a tendency of nonpolar macrocyclic cores of porphyrins to form associates in aqueous solutions. Some π-stacked porphyrin derivatives (derivatized with suitable polar groups in *meso* positions) have a parallel orientation of two or more planar π-conjugated structures with an interplanar separation of 3.4-3.6 Å between the macrocycles.[60] Nevertheless, Hunter and Sanders noted that face-to-face stacking is not commonly observed due to strong electrostatic repulsion between the π-electrons. As a result, an attractive offset stacking or T-shape geometry is detected.

Conjugation of porphyrin with polymers introduces promising novel multi-responsive materials. These materials show properties applicable in the field of material science[61] and for biomedical purposes (e.g. photodynamic therapy).[62-64] They are ideal for these purposes since they are available in high yield from relatively well-established synthetic routes. A huge variety of methods are used for studying porphyrin derivatives. For example, NMR (as well as UV-Vis and fluorescence spectroscopy) for construction of stoichiometric binding model[65], UV-Vis spectrophotometry and fluorescence spectroscopy for observing a photoredox switching between hydroquinone and quinonoid states[48], protonation/guest

binding[66], circular dichroism spectroscopy for molecular recognition of chiral molecules, J-aggregates formation or porphyrin-surfactant complexes, etc.[54] Conjugates of porphyrin with PNIPAM were studied and used as a highly sensitive polymeric sensor for uranyl ion (UO_2^{2+})[67], or porphyrin conjugates with PNIPAM, poly(methacrylic acid) (PMAA) and poly(2-hydroxylethyl methacrylate) (PHEMA) were used as a metal sensing systems.[68] However, further scrutiny of physico-chemical properties of this system should bring valuable insight into the properties of the systems and the ability to tune these properties for desired applications. To fill this missing knowledge, the phase behaviour of porphyrin-PNIPAM conjugates was studied by our group using a set of advanced experimental techniques and obtained results are presented in this thesis.

1.2 Experimental methods

1.2.1 The basics of NMR spectroscopy

Nuclear magnetic resonance (NMR) spectroscopy is a well-established technique for examination of structure, dynamics and chemical environment of molecules. NMR was initially developed in the late 1940s and later, in 1952, Felix Bloch and Edward Purcell were jointly awarded the Nobel Prize in Physics 'for their development of new methods for nuclear magnetic precession measurements and discoveries in connection therewith.[69] The next breakthrough in the field of NMR Spectroscopy was made by Richard R. Ernst, who was awarded the Nobel Prize in Chemistry in 1991, for the development of Fourier Transform (FT) and 2-dimensional NMR Spectroscopy. Nowadays, these techniques applied to proton (^{1}H) NMR, carbon (^{13}C) NMR and many other NMR active nuclei are basic and indispensable tools in chemistry, biology and medicine.

NMR Spectroscopy is based on the magnetic properties of the atomic nucleus and particularly favourable nuclei for NMR are ^{1}H, ^{13}C, ^{19}F, ^{31}P. Nuclei with a spin quantum number (m_s) of ½ possess a nuclear magnetic moment, and when it is placed in an external magnetic field occupy two possible quantum states. In the lower energy state, magnetic moments of the nuclear spin are aligned with the external magnetic field, whereas in the higher energy state, magnetic moments of the nuclear spin have the opposite direction to the external magnetic field. In a large population of nuclei at the condition of thermal equilibrium, slightly more than half exists in the lower energy state and slightly less than half exists in the higher energy state.[70-72] The energy gap (ΔE) between these two states can be represented using the following equation:

$$\Delta E = \gamma h B_0 / 2\pi, \tag{2}$$

where h is the Planck's constant, γ is the gyromagnetic ratio (a characteristic constant of a nucleus) and B_o is the strength of the external magnetic field.

The sum of individual magnetic moment vectors is called the net magnetization vector **M**. The net magnetization is aligned in the direction of the lower energy state or here in the positive z-direction (Figure 1.7). Application of a radio frequency pulse tilts the net magnetization away from z-axis which causes the net magnetization to precess around z-axis

with the Larmor frequency (ω_0). In order to tilt the magnetization radio-frequency pulse perpendicular to z-axis has to be applied at the resonance condition close to Larmor frequency (ω_0):

$$\omega_0 = \gamma B_0, \tag{3}$$

where ω_0 is the nuclei's intrinsic Larmor frequency.

After the exposure of the radio frequency pulse, the sample's net magnetization returns to its equilibrium position in the positive z-direction. The precession motion of the net magnetization induces an oscillating current in the probe head receiver coil of the NMR spectrometer. This oscillating current is called free induction decay (FID). The FID is a representation of NMR spectrum in the time domain that is converted to the frequency domain via Fourier transformation.

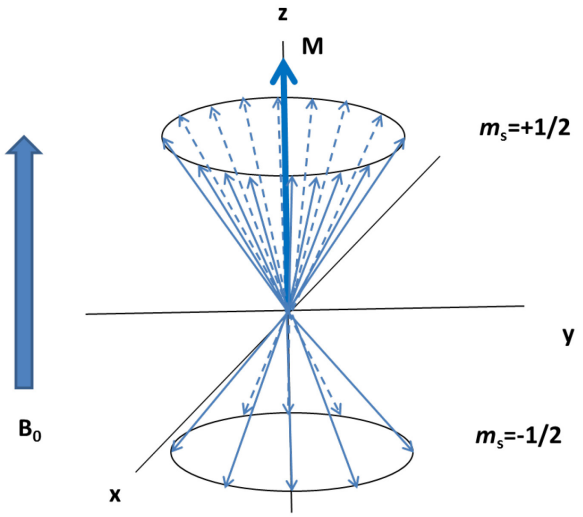

Figure 1.7. The net macroscopic magnetization of a sample in an external magnetic field B_0.

A particularly important feature of NMR spectroscopy is its high sensitivity to even slight variations of the local chemical environment, which provide changes in Larmor frequency of examined nucleus. An external magnetic field B_o applied on a sample induces electron circulation around nuclei, which produce a small magnetic field in the opposite direction to the applied external field. This effect is called magnetic shielding and Larmor frequency for nuclei under the influence of the local magnetic field is given by:

$$\omega_0 = \gamma B_0(1 - \sigma), \tag{4}$$

where σ is a shielding constant of the particular nucleus.

From equation (4), one can see that Larmor frequency is dependent on the strength of the applied magnetic field, which is the reason why chemical shift δ was introduced and is represented in ppm (part per million) units:

$$\delta = \frac{\nu_{sample} - \nu_{standard}}{\nu_{spectrometer}} \times 10^6, \quad (5)$$

where ν_{sample} is the resonance frequency of the sample (in Hz), $\nu_{standard}$ is the frequency of a standard reference compound (in Hz), typically used compound is tetramethylsilane (TMS), and $\nu_{spectrometer}$ is the operating frequency of the spectrometer (in Hz).

Another characteristic parameter of the NMR signal (besides the chemical shift) is the signal intensity. The integrated intensity of the NMR resonance is an area under the resonance curve, and it is proportional to the number of nuclei (e.g. protons) to which the peak corresponds. The integrated resonance intensities are widely used in quantitative analysis of macromolecular and supramolecular systems, for instance, to confirm chemical structure or copolymer composition, etc.[73]

1.2.2 Characterization of phase separation by NMR

Phase separation behaviour in polymer systems can be effectively studied using high resolution NMR spectroscopy. Both qualitative (signal shape and intensity) and quantitative (signal integrated intensity) information on phase separation can be obtained using ^{1}H NMR spectra. A typical approach we utilize in this work is described below. PNIPAM in D_2O has been used as an exemplary system (Figure 1.8).

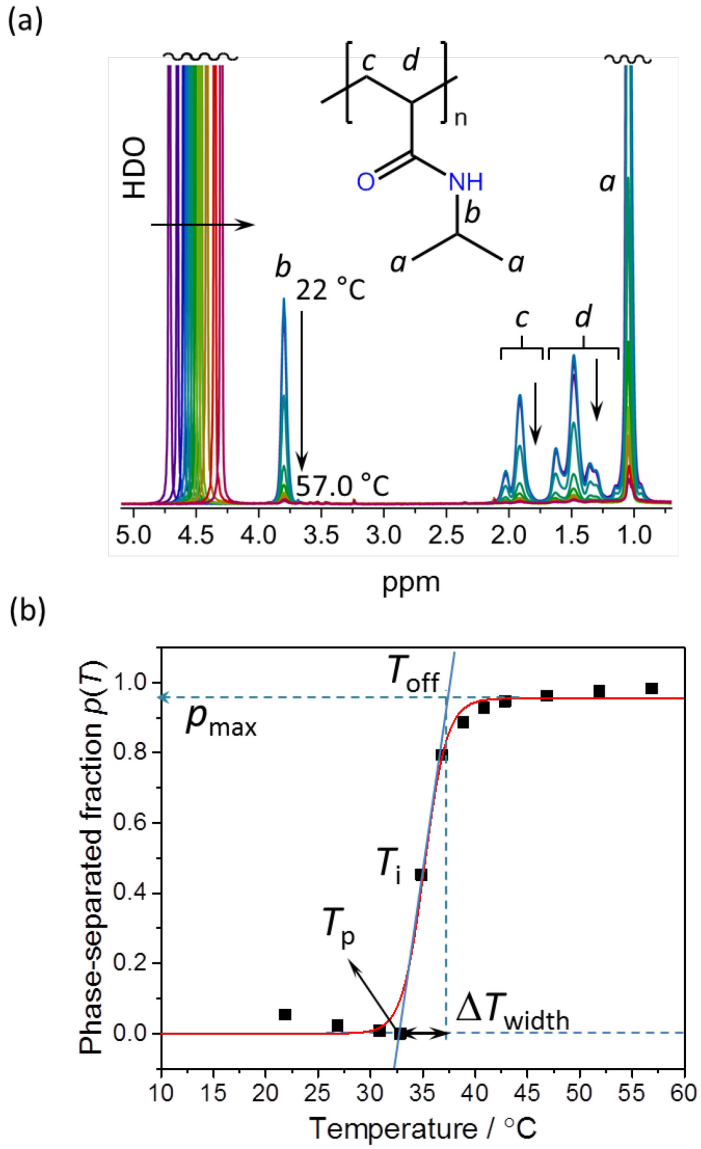

Figure 1.8. (a) Superimposed ^{1}H NMR spectra of PNIPAM (w_p = 1 wt.%) in D_2O solution measured at different temperatures. The assignment of PNIPAM is shown. (b) Phase-separated fraction $p(T)$ of "*b*" resonance of PNIPAM polymer units (solid squares) as obtained from (a) using equation (6). The solid line is fit based on equation (11).

While temperature increases from 22 °C to 57 °C, a gradual decrease of PNIPAM resonance intensity was observed (Figure 1.8a). This decrease represents the restriction in mobility of PNIPAM chains related to phase separation of the polymer. In order to thoroughly describe the phase separation process, PNIPAM signals (here CH signal of a pendant group or resonance "*b*") are integrated and the obtained intensities are then used in the equation (6) to

calculate the value of the phase-separated fraction of PNIPAM units $p(T)$[21,74] using this equation:

$$p(T) = 1 - \frac{T}{T_0}\frac{I(T)}{I_0(T_0)}, \tag{6}$$

where $I(T)$ and $I_0(T_0)$ are the temperature-dependent integrated intensity of the polymer resonance obtained from NMR measurements (here CH signal of PNIPAM pendant group) in partly phase-separated system (determined at $T > 22$ °C) and in a non-phase-separated system (determined at $T_0 = 22$ °C in case of PNIPAM, where $p(T_0) = 0$), respectively.

Dependence of phase-separated fraction on temperature (Figure 1.8b) provides insight into the phase separation process and yields basic parameter, such as the maximum fraction of polymer units participating in the phase separation p_{max}, width of phase separation ΔT_{width} (the difference between onset and offset temperatures) and phase separation temperature T_p at which phase separation starts to occur (also called the onset temperature of the $p(T)$ curve).

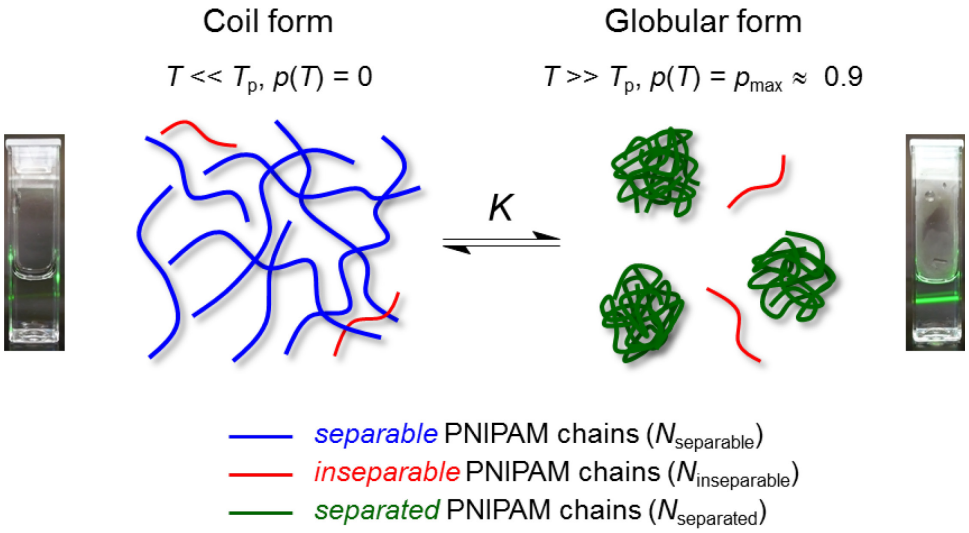

Figure 1.9. A schematically represented thermodynamic model of PNIPAM phase separation including three types of polymer units: separable, inseparable and separated. Photos of the solution below and above phase separation (irradiated by green light laser pointer, 532 nm) are included.

A thermodynamic model shown in Figure 1.9 illustrates a phase separation based on the equilibrium between two exchangeable states (two-state model of phase separation).[75]

State one consists of polymer molecules, which are generally present in solution in random-coil conformation and move freely.[76] The second state is represented by a rather compact globular-like rigid structures. A transition from state one to state two (called a coil–globule transition) is characterized by an equilibrium constant K, which is defined by equation (7) as:

$$K = \frac{N_{\text{separated}}}{N_{\text{separable}}}, \tag{7}$$

where $N_{\text{separated}}$ is a number of phase-separated PNIPAM units and $N_{\text{separable}}$ is a number of phase separable (but not separated yet) PNIPAM units. This model (Figure 1.9) takes into account that some part of PNIPAM chains remains not separable, due to the presence of low molecular weight fractions of the polymer[77], reflected by $N_{\text{inseparable}}$ (i.e. a number of inseparable polymer units). Then, the fraction of phase-separated PNIPAM units $p(T)$ is generally calculated in equation (8).

$$p(T) = \frac{N_{\text{separated}}}{N_{\text{separable}} + N_{\text{inseparable}} + N_{\text{separated}}}. \tag{8}$$

Combination of equations (7) and (8) provides a formula (9) for $p(T)$ as a function of K:

$$p(T) = \frac{p_{\max}}{1 + K^{-1}}, \tag{9}$$

where $p_{max} = (N_{\text{separable}} + N_{\text{separated}})/(N_{\text{separable}} + N_{\text{inseparable}} + N_{\text{separated}})$ is the maximum fraction of PNIPAM units which participate in the phase separation. Equation (10) is the Boltzmann factor connection between the equilibrium constant K and Gibbs free energy expressed in terms of standard enthalpy (ΔH) and entropy (ΔS) changes associated with phase separation of PNIPAM:

$$K = e^{-\frac{\Delta H - T\Delta S}{RT}}, \tag{10}$$

where R is the gas constant (8.314 J mol^{-1} K^{-1}) and T is the absolute temperature (K). Combining equations (9) and (10) gives a final formula for $p(T)$.[75]

$$p(T) = \frac{p_{\max}}{1 + e^{\frac{\Delta H}{RT} - \frac{\Delta S}{R}}}. \tag{11}$$

Equation (11) is used for fitting experimentally obtained NMR data for $p(T)$ as shown in Figure 1.8b and also allows to obtain the values of ΔH and ΔS associated with phase separation. Additionally, these thermodynamically important parameters can be obtained for variety of other polymeric systems exhibiting phase separation just by means of fitting the equation (11) into experimental data (as shown later in this work).

Another significant parameter describing the phase separation is T_p, which is the phase separation temperature, determined from the fitting of the $p(T)$ curve as the onset temperature (see Figure 1.8b). The value of T_p is defined at the intersection point of the x-axis and the tangent at the inflexion point T_i of the $p(T)$ curve. The inflexion is the point where the curvature of the $p(T)$ function changes its sign, which yields the condition for the second derivative of $p(T)$ must equal to zero (i.e. $p''(T) = d^2p(T)/dT^2 = 0$). Performing the derivative and rearrangement of the latter equation gives the following equation (12) for T_i:

$$2T_i\left(1 + e^{\frac{\Delta H}{RT_i} - \frac{\Delta S}{R}}\right) + \frac{\Delta H}{R}\left(1 - e^{\frac{\Delta H}{RT_i} - \frac{\Delta S}{R}}\right) = 0. \tag{12}$$

Equation (12) does not have an analytical solution in the closed-form. However, a solution of excellent accuracy can be found using the following approximations. The equation (12) can be rearranged into equation (13).

$$\frac{2RT_i}{\Delta H} = \frac{e^{\frac{\Delta H}{RT_i} - \frac{\Delta S}{R}} - 1}{e^{\frac{\Delta H}{RT_i} - \frac{\Delta S}{R}} + 1} = \tanh\left[\frac{1}{2}\left(\frac{\Delta H}{RT_i} - \frac{\Delta S}{R}\right)\right] \approx \frac{1}{2}\left(\frac{\Delta H}{RT_i} - \frac{\Delta S}{R}\right). \tag{13}$$

The term including exponentials can be represented as the tanh(x) function, which is then approximated by the first term of its Taylor expansion (where $\tanh(x) \approx x$). Subsequently, equation (14) for T_i is obtained in the form of the quadratic equation:

$$4R^2T_i^2 + \Delta H\Delta ST_i - \Delta H^2 = 0. \tag{14}$$

Physically meaningful solution of equation (14) is represented by equation (15):

$$T_i = \frac{\Delta H\Delta S}{8R^2}\left(\sqrt{1 + \left(\frac{4R}{\Delta S}\right)^2} - 1\right). \tag{15}$$

Herein, second Taylor expansion is used, for up to the second order term (i.e. $\sqrt{1+x} \approx 1 + \frac{1}{2}x - \frac{1}{8}x^2$). Applied approximation yields to the formula (16) for the temperature at inflexion point T_i:

$$T_i = \frac{\Delta H}{\Delta S}\left(1 - \frac{4R^2}{\Delta S^2}\right), \tag{16}$$

Subsequently, knowing the T_i, phase separation temperature T_p can be calculated from the mathematical definition of the tangent line at the inflexion point intersecting the x-axis. This yields the equation (17):

$$T_{\mathrm{p}} = -\frac{p(T_{\mathrm{i}})-p\prime(T_{\mathrm{i}})\times T_{\mathrm{i}}}{p\prime(T_{\mathrm{i}})} = T_{\mathrm{i}} - \frac{RT_{\mathrm{i}}^2}{\Delta H}\left(1 + e^{-\frac{\Delta H}{RT_{\mathrm{i}}}+\frac{\Delta S}{R}}\right), \tag{17}$$

where $p'(T_{\mathrm{i}})$ indicates the first derivative of $p(T)$ function at the inflexion point T_{i}. Then, using a similar procedure an offset temperature T_{off}, a temperature at which phase separation is almost finished can be obtained (Figure 1.8b). At this point, T_{off} is found as an intersection point of the tangent line to $p(T)$ curve at the inflexion point T_{i} with line $y = p_{\mathrm{max}}$:

$$T_{\mathrm{off}} = \frac{p_{\mathrm{max}}-p(T_{\mathrm{i}})+p\prime(T_{\mathrm{i}})\times T_{\mathrm{i}}}{p\prime(T_{\mathrm{i}})} = T_{\mathrm{i}} + \frac{RT_{\mathrm{i}}^2}{\Delta H}\left(1 + e^{\frac{\Delta H}{RT_{\mathrm{i}}}-\frac{\Delta S}{R}}\right). \tag{18}$$

Finally, knowing phase separation temperature T_{p} and offset temperature T_{off}, the width of the phase separation $\Delta T_{\mathrm{width}}$ is obtained using equation (19):

$$\Delta T_{\mathrm{width}} = T_{\mathrm{off}} - T_{\mathrm{p}} = \frac{2RT_{\mathrm{i}}^2}{\Delta H}\left[1 + \cosh\left(\frac{\Delta H}{RT_{\mathrm{i}}} - \frac{\Delta S}{R}\right)\right]. \tag{19}$$

In summary, the equation (11) was used for fitting of experimental data and provided us values of ΔH, ΔS and p_{max} associated with a PNIPAM phase separation. Equations (17) and (19) allowed us to calculate T_{p} and $\Delta T_{\mathrm{width}}$. Another important aspect to notice is that the above-mentioned approximations introduce only negligible errors into the determination of T_{i}, T_{p}, T_{off} and $\Delta T_{\mathrm{width}}$ values.[74] This can be illustrated on a comparison of the exact numerical solution of equation (12) (denoted as $T_{\mathrm{i}}^{\mathrm{exact}}$) with approximate solution described by equation (16) (denoted as $T_{\mathrm{i}}^{\mathrm{approx}}$), which shows that for $\Delta H \geq 10^5$ J·mol^{-1} and $\Delta S \geq 200$ J·mol^{-1}·K^{-1}, the error is $|T_{\mathrm{i}}^{\mathrm{exact}} - T_{\mathrm{i}}^{\mathrm{approx}}| < 0.04$ K. The lower boundary of ΔH and ΔS is chosen as an extreme case far from usually obtained values in order to cover all possible experimentally obtainable situations. For higher values of ΔH and ΔS, the error further decreases. Subsequently, errors calculated (using exact and approximate values of T_{i}) for the phase separation temperature T_{p} (equation (18)) and the width of the phase separation $\Delta T_{\mathrm{width}}$ (equation (19)) are $|T_{\mathrm{p}}^{\mathrm{exact}} - T_{\mathrm{p}}^{\mathrm{approx}}| < 10^{-4}$ K and $|\Delta T_{\mathrm{width}}^{\mathrm{exact}} - \Delta T_{\mathrm{width}}^{\mathrm{approx}}| < 10^{-4}$ K, respectively. Therefore, the approximations used during the derivation process introduce negligible errors.

This approach improved the way of extracting the phase separation parameters from NMR data. The parameters of phase separation, such as T_{p}, T_{off}, $\Delta T_{\mathrm{width}}$ as well as ΔH and ΔS provide profound insight into phase separation phenomena. The approach could be also suggested for other phase-separable systems with similar NMR spectral patterns. More details about applicability of this approach can be found in our work.[74]

1.2.3 Relaxation techniques: T_2 relaxation time

Relaxation phenomenon is a process by which a nuclear spin system returns to thermal equilibrium after RF pulse perturbation. Two types of relaxation can be distinguished by NMR spectroscopy: spin-lattice (longitudinal) relaxation and spin-spin (transverse) relaxation. Spin-lattice relaxation is characterised by exponential time constant T_1, which results in the establishment of an equilibrium value of the net nuclear magnetization with the surroundings (the 'lattice') along the external magnetic field axis z. Spin-spin relaxation is characterised by exponential time constant T_2, which measures how fast the spin systems exchange energy in the transverse (xy) plane. Both T_1 and T_2 relaxation times provide information about the dynamical properties of an investigated spin system. T_2 relaxation times are frequently used for characterization of dynamics in systems with high mobility, like liquids, whereas T_1 times are generally applied for the description of solid or highly viscous samples. As in this work, we studied liquid samples, T_1 will not be discussed in detail.

The relaxation time that will be frequently addressed in this work is the transverse or spin-spin relaxation time T_2 that is an exponential signal decay of the transverse component of the magnetization vector $M_{xy,}$ which is related to the initial value of net magnetization M_0 immediately before the RF pulse with the following relation:

$$M_{xy} = M_0 e^{-t/T_2}, \tag{20}$$

Transverse relaxation time T_2 is measured by the use of a spin-echo Carr–Purcell–Meiboom–Gill (CPMG) sequence (Figure 1.10). CPMG employs a single 90^{o}_{x} pulse followed by multiple 180^{o}_{y} pulses, separated by the same spin-echo time τ_E. The application of an initial 90^{o}_{x} pulse is followed by 180^{o}_{y} pulses that refocus the dephasing of spins due to field inhomogeneities and thus forms an echo. The echo amplitude reduction is determined only by the transversal relaxation processes.

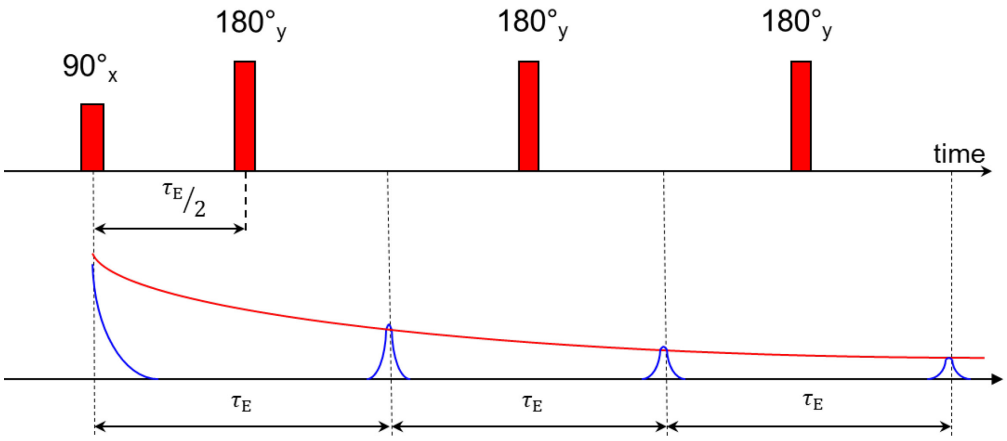

Figure 1.10. The Carr–Purcell–Meiboom–Gill (CPMG) pulse sequence for measuring T_2 relaxation time.

T_2 relaxation time is inversely proportional to the widths of NMR resonances. Short T_2 corresponds to a faster disappearance of the transverse magnetisation, which in the NMR spectrum is represented by a broader Lorentzian line. Approximate T_2 values can be determined from the full width at half-height $\Delta\nu_{1/2}$ of the resonance signal using the following equation (21):

$$\Delta\nu_{1/2} = \frac{1}{\pi T_2^*}, \tag{21}$$

where T_2^* refers to transverse relaxation time with contribution from the magnetic field inhomogeneity. Due to this inhomogeneous line broadening the T_2 values obtained using formula (21) are shorter compare to the actual T_2 values obtained by the CPMG method. As a result, for further rigorous analysis of phase separation phenomenon T_2 values obtained by the CPMG method were used.[78] For polymer solutions T_2 relaxation time is usually in the range of hundreds of ms.

1.2.4 Other physico-chemical methods: DSC, DLS, SAXS, OM, UV-Vis and PL

Differential Scanning Calorimetry (DSC) is a thermo-analytical method suitable for studying thermal transitions in pure polymers or polymer solutions. Phase separation of solutions of temperature-sensitive polymer is routinely studied using DSC. During the phase separation (demixing) or mixing the amount of heat absorbed or released by polymer solution is monitored. Generally, changes in the sample heat capacity are monitored in terms of change in the heat flow and compared with the reference (empty pan) during heating-cooling cycles. Importantly, the sample and the reference are both kept at the same temperature. Then, a signal proportional to the difference between the heat flow input to the sample and the reference is recorded and the DSC curve is obtained. Further integration of peaks on the DSC curve provides information on enthalpies of the polymer phase separation.[79]

Dynamic Light Scattering (DLS) is one of the most common methods for the determination of hydrodynamic diameter and size distribution of polymeric aggregates, nanoparticles and colloidal dispersions.[80] DLS of a polymer solution is based on the fluctuations of scattered light intensity due to Brownian motion of the polymer particles in solution. The intensity of scattered light from particles with a higher value of a translational diffusion coefficient has faster fluctuations in time in comparison with the particles with a lower value of a diffusion coefficient. Quantitate analysis of scattered intensity time fluctuations is done using the mathematical apparatus of the autocorrelation function, which provides the translational diffusion coefficient of particles - D_t. Consequently, D_t is used in the Stokes-Einstein equation for determination of the hydrodynamic diameter D_h of non-interacting spheres:

$$D_h = \frac{k_B T}{3\pi\eta D_t}, \tag{22}$$

where k_B is the Boltzmann constant, T is the absolute temperature and η is the solvent dynamic viscosity. Hydrodynamic diameter is the diameter of an equivalent hard sphere with the same diffusion coefficient as the particle under observation including the solvation shell. DLS yields the z-average hydrodynamic diameter $D_{h,z}$, later in the text referred as D_z.

Small Angle X-Ray Scattering (SAXS) is a technique, which besides the determination of a nanoparticle size and shape provides valuable information on nanoparticle's internal structure (presence of a core, shell, or domains). The wavelength of X-rays is 0.01-10 nm which is much shorter in comparison with visible light, 400-700 nm, therefore, SAXS is able to provide structural information on the submicron level. Another difference from visible light is that X-ray scattering occurs on the electronic shells of atoms. When X-rays are passing through a sample, one part of X-rays could be absorbed and converted into other forms of energy (heat, fluorescence, etc); the rest is either transmitted or scattered from the electrons of an atomic shell.[81] Spherically averaged scattered intensity I_s of X-rays is registered by detector as a temporal average of squared norm of scattering amplitude E_s (equation 23).

$$I_s(q) = \langle |E_s(q)|^2 \rangle. \tag{23}$$

Here, q is the scattering vector that is represented by the relation (24):

$$q = \frac{4\pi}{\lambda} sin\frac{\theta}{2}, \tag{24}$$

where θ is the scattering angle, λ is the wavelength of the applied radiation. The X-rays scattered from all atoms in a nanoparticle interfere with each other providing information about the shape of the particle, a so-called form factor $P(q)$. For very low scattering angles, $qR_g < 1$, and for diluted systems, $P(q)$ can be approximated by Guinier law:

$$P(q) = e^{(-\frac{q^2 R_g^2}{3})}, \tag{25}$$

where R_g is the radius of gyration of a particle, mass-weighted distance from the centre of mass of the particle to each mass element in the particle.

To get detailed information on nanoparticles, an experimental form factor is fitted with a theoretical model including spherical, ellipsoidal, cylindrical, micellar and many more structures.[82] In order to adequately evaluate SAXS experimental data, one should put into the consideration other factors, such as chemical structure of the molecule, optical micrographs of aggregates, NMR, etc.

Optical Microscopy (OM) is an experimental technique that uses visible light and a system of lenses in order to study polymer's morphology. An OM can study objects of size between 0.2 and 200 μm with a maximum possible magnification of an object about 1000×.

The morphology development (polymer globules formation) can be observed for a thin layer of polymer solution placed between a support glass slide and a coverslip and inserted into a temperature-controlled environment of a hot stage.[83]

UV-Vis Spectrophotometry (UV-Vis) is an absorption spectroscopy technique used for the quantitative determination of conjugated molecules by ultraviolet and visible light irradiation. It is based on atoms and molecules electronic transitions from the ground state to the excited state. The more easily the electrons in the molecule get excited the longer the light wavelength they absorb. There are four possible types of molecular transition and can be ordered in the way from higher to lower excitation energy: $\sigma \rightarrow \sigma^* > n \rightarrow \sigma^* > n \rightarrow \pi^* > \pi \rightarrow \pi^*$. $\sigma \rightarrow \sigma^*$ and $n \rightarrow \sigma^*$ are transition in the ultraviolet region exhibited by saturated organic compounds. $n \rightarrow \pi^*$ and $\pi \rightarrow \pi^*$ are transitions in unsaturated compounds which require less energy and occur at a longer wavelength in comparison with transitions to σ^* orbitals. The UV-Vis spectrophotometry is a useful technique for studying of the host-guest binding process, protonation process, etc.[84]

Photoluminescence (PL) is a spectroscopic technique based on the absorption and emission of a photon by a molecule. After the absorption of a photon, an electron moves from the electronic ground state to certain vibrational levels of excited state and then relaxes back to the ground state. The PL technique detects photons transmitted by the molecule during the relaxation process, i.e. the electronic transitions from the excited (higher energy) state to the ground (lower energy) state. Photoluminescence spectroscopy provides important information on photochemical and optical properties of conjugated molecules, semiconductors, etc. This method is contactless and non-destructive, therefore it can be applied for studying solutions, solids and gaseous samples.[85]

2 Aims of the thesis

The main goal of this thesis is an investigation of phase separation phenomena in solutions of temperature-responsive macromolecular systems using NMR spectroscopy and other complementary experimental techniques (DSC, DLS, SAXS, UV-VIS, etc). There are many examples of additives (often salts or alcohols) used for tuning the phase separation of polymers. Here, we have selected additives bearing structural similarities with the polymers and which contain different functional groups (amine, alcohol, ether and ketone) in order to alter phase separation parameters, such as phase separation temperature, width of phase separation, fraction of phase separable polymer units, enthalpy change, etc. of PNIPAM and PVME polymers. Special emphasis has been placed on the dynamics of the phase separation process, the formation of hydrogen bonds between polymer-water and polymer-additive. In order to extend the functionality of polymers, a novel porphyrin-PNIPAM conjugates have been prepared. The effects of the presence of porphyrin unit on PNIPAM phase separation have been investigated. These conjugates present extra responsivity to pH and solvent composition which has been probed in detail using various experimental techniques (e.g. NMR, DSC, DLS, etc.). Also, special effort has been made to develop a general phase separation model based on a thermodynamic approach for a physically meaningful description of phase separable systems.

The specific aims of the thesis are:

1) An investigation of the influence of *t*-butanol, *t*-butylamine, *t*-butyl methyl ether, and *t*-butyl methyl ketone on phase separation and interactions in PVME solutions.

2) A study the influence of *t*-butanol, *t*-butylamine, *t*-butyl methyl ether, and *t*-butyl methyl ketone on phase separation and polymer interactions in PNIPAM solutions.

3) A study of the phase behaviour of novel star-like shape porphyrin-PNIPAM conjugates.

4) A thermodynamic description of NMR results of phase separable systems as a two-state process with the use of physically meaningful parameters (such as enthalpy and entropy changes connected with the phase separation).

The findings presented in this thesis should broaden the knowledge of multi-responsive polymeric systems applicable in the field of material science including for potential biomedical purposes.

3 Experimental part

3.1 Samples preparation

3.1.1 PVME with additives

PVME was purchased from Sigma-Aldrich (St. Louis, MO, USA) with M_w = 60500, $M_w/M_n \approx 3$ (see Figure 1.3 for the structure). *t*-BuAM, *t*-BuOH, *t*-BuME and *t*-BuMK (see Figure 3.1 for the structures) were purchased from Sigma-Aldrich and used as received. After drying, solutions with appropriate PVME (w_p = 0.5-10 wt %), D_2O (99.9 % of deuterium) and additive concentration ($w_{additive}$ = 0-10 wt %) were prepared. All the PVME/D_2O samples were placed in 5 mm NMR tubes, degassed and sealed under argon. The weight fraction of PVME in the binary solvent D_2O/additive was calculated as $w_p = m_p/(m_p+m_{D2O}+m_{additive}) \times 100\%$ (in wt.%), where m_p, m_{D2O}, and $m_{additive}$ are masses of PVME polymer, D_2O and additive, respectively. The composition of the binary solvent D_2O/additive was determined by the weight fraction of an additive in D_2O/additive solution as $w_{additive} = m_{additive}/(m_{D2O} + m_{additive}) \times 100\%$ (in wt.%).

Figure 3.1. Chemical structures of the additives used in this research: (from left to right) *t*-BuAM, *t*-BuOH, *t*-BuME and *t*-BuMK.

3.1.2 PNIPAM with additives

PNIPAM (M_w = 19000−26000 g/mol) (see Figure 1.4 for the structure) was purchased from Sigma-Aldrich and used as received. Solutions with appropriate PNIPAM (w_p = 5-10 wt %), D_2O (99.9 % of deuterium) and additive concentration ($w_{additive}$ = 0-7 wt %) were prepared. A similar preparation procedure as described for PVME was used for PNIPAM solutions.

3.1.3 Porphyrin-PNIPAM conjugates

5,10,15,20-Tetrakis(4-(α-methyltrithiocarbonate-(*S*)-phenylacetoxy)phenyl)-21H,23H-porphine (TPP-CTA) was synthesized as previously described.[86] *N*-Isopropylacrylamide (NIPAM) and 2,2'-azobis(2-methylpropionitrile) (AIBN) (both Aldrich Chemical Co.) were recrystallized before use from *n*-hexane and acetone, respectively. Using the standard reversible addition-fragmentation transfer (RAFT) polymerization protocol. NIPAM (2 g, 17.7 mmol), TPP-CTA (484 mg, 0.29 mmol for **PP**$_{8.4}$ or 145 mg, 88.4 μmol for **PP**$_{22.7}$), AIBN (molar ratio of TPP-CTA:AIBN = 8:1) were dissolved in 1,4-dioxane (11 mL). The polymerization vessel was then degassed by three freeze-pump-thaw cycles, purged with dry argon, sealed and stirred at 70°C for 8 h. The polymer was subsequently precipitated in cold diethyl ether, filtered and dried. The crude polymer was dissolved in cold water and dialyzed against water at 4°C for 48 h (molecular weight cut-off of the dialysis membrane was 3.5 kDa for **PP**$_{8.4}$ and 12-14 kDa for **PP**$_{22.7}$) and recovered by freeze-drying as purple solid. A chemical structure of **PP** conjugate is shown in Figure 3.2. For the purposes of this work, two conjugates with number molecular weight 8.4 kDa and 22.7 kDa denoted as **PP**$_{8.4}$ and **PP**$_{22.7}$, respectively, were synthesised.

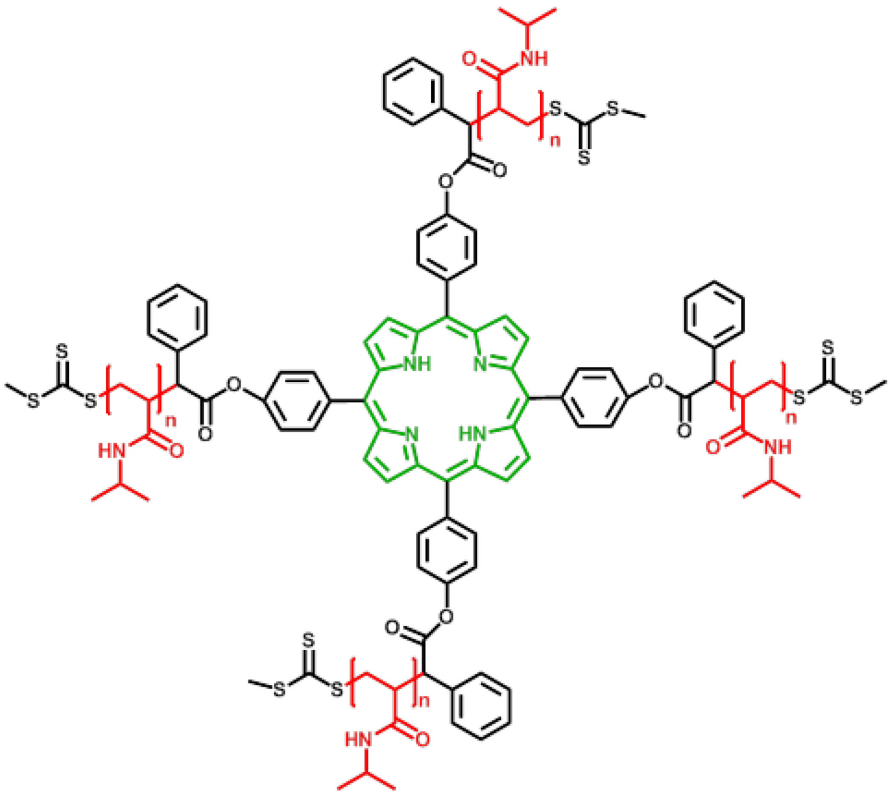

Figure 3.2. A chemical structure of tetraphenylporphyrin-PNIPAM conjugate (**PP**).

Characterization of PP conjugates. The mass-averaged molecular weight M_w, number-averaged molecular weight M_n and dispersity $Đ = M_w/M_n$ of the **PP** conjugates were determined by size exclusion chromatography (SEC) using an HPLC Ultimate 3000 system (Dionex, USA) equipped with a SEC column (TSKgel SuperAW3000 150 × 6 mm, 4 μm). Three detectors, UV-Vis, refractive index (RI) Optilab rEX and multi-angle light scattering (MALS) DAWN EOS (Wyatt Technology Co., USA) were employed with a methanol and sodium acetate buffer (0.3 M, pH 6.5) mixture (80:20 vol%, a flow rate of 0.5 mL/min) as mobile phase. To determine the average degree of polymerization of PNIPAM arms, these were cleaved off the porphyrin center by hydrolysis of TPP-PNIPAM in 0.1 M aqueous NaOH for 6 h at room temperature. Alternatively, the average degree of polymerization of PNIPAM arms was estimated by UV-VIS spectrophotometry in methanol (ε = 5 900 l·mol^{-1}·cm^{-1}, λ = 518 nm) assuming one TPP molecule per conjugate. Due to the interference of **PP** absorption with the wavelength of the MALS laser (λ = 658 nm), the molecular weight and polydispersity of the **PP** conjugates were estimated by SEC using poly(ethylene oxide) (PEO) standards. A number average molecular weight of $\mathbf{PP}_{8.4}$ and $\mathbf{PP}_{22.7}$ were 8.4 kDa and 22.7 kDa, respectively (Table 1).

Table 1. Characterization of **PP** conjugates.

Conjugate	$[NIPAM]_0/[TPP\text{-}CTA]_0$[a]	DP[b] of one arm (SEC)[c]	DP[b] of one arm (UV-VIS)	M_n (kDa)[c]	M_w/M_n[d]
$\mathbf{PP}_{8.4}$	60/1	14	14	8.4	1.09
$\mathbf{PP}_{22.7}$	200/1	44	40	22.7	1.15

[a]Initial feed molar ratio. [b]Degree of polymerization. [c]Determined by SEC-MALS after hydrolysis of the ester groups. [d]Estimated by SEC using PEO standards.

Preparation of PP solutions. The weight fraction of **PP** in binary solvent D_2O/MeOD is denoted as $w_{PP} = m_{PP}/(m_{PP} + m_{D2O} + m_{MeOD}) \times 100\%$ (in wt.%), where m_i , i = **PP**, D_2O, MeOD, is the mass of each component. The composition of the binary solvent D_2O/MeOD, determined by the volume fraction of MeOD in D_2O/MeOD, is denoted as $\phi_{MeOD} = V_{MeOD}/(V_{D2O} + V_{MeOD}) \times 100\%$ (in vol.%), where V_i, i = D_2O, MeOD, is the volume of

each component. The same formulas were used for preparation of **PP** in binary solvent H_2O/MeOH.

3.2 Methods of measurements

3.2.1 ^{1}H and ^{1}H spin-spin relaxation time T_2

High-resolution ^{1}H NMR spectra were recorded using a Bruker Avance III 600 spectrometer operating at 600.2 MHz. All experiments were performed at the same experimental conditions. Measurement conditions were as follows: 90° pulse width 18 μs, relaxation delay 10 s, spectral width 6602 Hz, acquisition time 4.96 s and 64 scans. The ^{1}H spin-spin relaxation times T_2 were measured using a CPMG pulse sequence of $90^o_x - (t_d - 180^o_y - t_d)_n$ – acquisition with a half-echo time t_d = 5 ms. Each experiment was performed over 4 scans with a relaxation delay between scans of 120 s. The resulting T_2 relaxation curves are mono-exponential. The fitting process made it possible to determine consistently a single value of the relaxation time. The relative error of T_2 values of the HDO and the additive $(CH_3)_3$ groups did not exceed ±8%. During measurement, the temperature was maintained constant within ±0.2 K using a BVT 3000 temperature unit. Before each measurement samples were equilibrated for about 15 min at the measurement temperature. The resulting spectra were processed using Topspin 4.0.5 software.

3.2.2 DSC measurements

DSC measurements were performed using a DCS 3100S calorimeter (Mac Science Co., Ltd.) on samples prepared in deuterated water (D_2O). Four complete heating/cooling cycles with rates of 10 °C/min over a range of 10°C – 90°C were performed. Samples of approximately 10 mg were dissolved in D_2O and then encapsulated in aluminium pans. The characteristic phase-separation temperature (T_p^{DSC}) was determined from DSC thermograms as the endotherm onset temperature. The transition was further characterized by the calculation of the enthalpy changes per mol of monomeric units of polymer through the integration of the endotherm.

3.2.3 DLS measurements

The hydrodynamic diameter D_z (z-average) of **PP** assemblies during the investigation of pD ("pH" in D_2O) effects on the phase separation were measured in heavy water (D_2O) at

20°C and 50°C using a ELSZ-2000S particle size analyzer (Otsuka Electronics Co., Ltd.). The samples were prepared with constant **PP** fraction of w_{PP} = 0.013 wt.% (in D_2O) and pD of D_2O solvent was changed in the range from 3.0 to 12.0 using (*S*)-CSA acid and pyridine base. The D_z values during the investigation of co-nonsolvency effects in binary H_2O/MeOH solvent at 20°C and 50°C were obtained using ZEN 3600 Zetasizer Nano Instrument (Malvern Instruments, Inc.). The **PP** samples were prepared with a constant concentration of w_{PP} = 0.011 wt.%. Prior to any measurement, samples were filtered using a 0.45 μm PVDF filter to remove any interfering dust particles. Each measurement consisted of an average of five scans.

3.2.4 SAXS measurements

SAXS experiments were performed on a beamline BM29 BIOSAXS at ESRF (Grenoble, France) using a pixel detector (Pilatus 1M). The X-ray scattering images were recorded at a sample−detector distance 2.867 m, using a monochromatic incident X-ray beam with an energy E = 12.5 keV, covering the range of scattering vectors 0.025 $nm^{-1} < q < 5$ nm^{-1} (q =4π sin θ/λ, where 2θ is the scattering angle). No measurable radiation damage was detected in analysed samples, as determined by comparing 10 successive time frames that had 50 ms exposure time. In all cases reported in this paper, the two-dimensional scattering patterns were isotropic. The patterns were azimuthally averaged to determine the dependence of the scattered intensity $I_s(q)$ on the scattering vector q. The solvent (D_2O) scattering was subtracted prior to the fitting analysis. All data manipulations were performed using SASfit software.

3.2.5 OM measurements

OM measurements were carried out under a nitrogen atmosphere with a Nikon Eclipse 80i equipped with a PixeLINK PL-A662 camera and a Linkam LTS350 temperature cell. All micrographs were taken from samples prepared in aqueous (H_2O, three-stage purification system (Millipore); resistivity ≥ 18 MΩ cm) solutions. The morphology was observed in a thin sample layer placed between a support glass slide and a cover slip with 50× magnification. Before each snapshot, the sample was maintained at a constant temperature for about 1 min.

3.2.6 UV-Vis measurements

UV-Vis spectra were measured using a JASCO V-570 ultraviolet-visible (UV-Vis)/near-infrared (NIR) spectrophotometer. Heavy water (D_2O) solutions of **PP**$_{8.4}$ (0.0025 wt.%, 3.3×10^{-6} M) and **PP**$_{22.7}$ (0.0027 wt.%, 1.3×10^{-6} M) in a 1 cm quartz cell with screw cap were prepared. The UV-Vis spectra were recorded at 20°C and 55°C and pD ("pH" in D_2O) effects were investigated by titration with (*S*)-CSA (dropped into quartz cell from a D_2O stock solution using a micro-syringe).

3.2.7 PL measurements

PL measurements were performed at room temperature using a FS5 spectrofluorometer (Edinburgh Instruments, Ltd.) for **PP**$_{22.7}$ (0.011 wt.%, 5.5×10^{-6} M) in quartz cuvette of 1 cm path length and excitation wavelength λ_{ex} = 420 nm.

4 Results and discussion

4.1 Influence of additives on phase separation of poly(vinyl methyl ether)

In this chapter of the thesis influence of *t*-BuOH and *t*-BuAM on phase separation of poly(vinyl methyl ether) (PVME) as well as their comparative analysis with the influence of *t*-BuMK and *t*-BuME will be discussed.[87] This study was done using ^{1}H NMR and time-resolved ^{1}H NMR spin-spin relaxation time T_2 experiments. These results were fully reported in publications 1 and 2 (see Appendix).

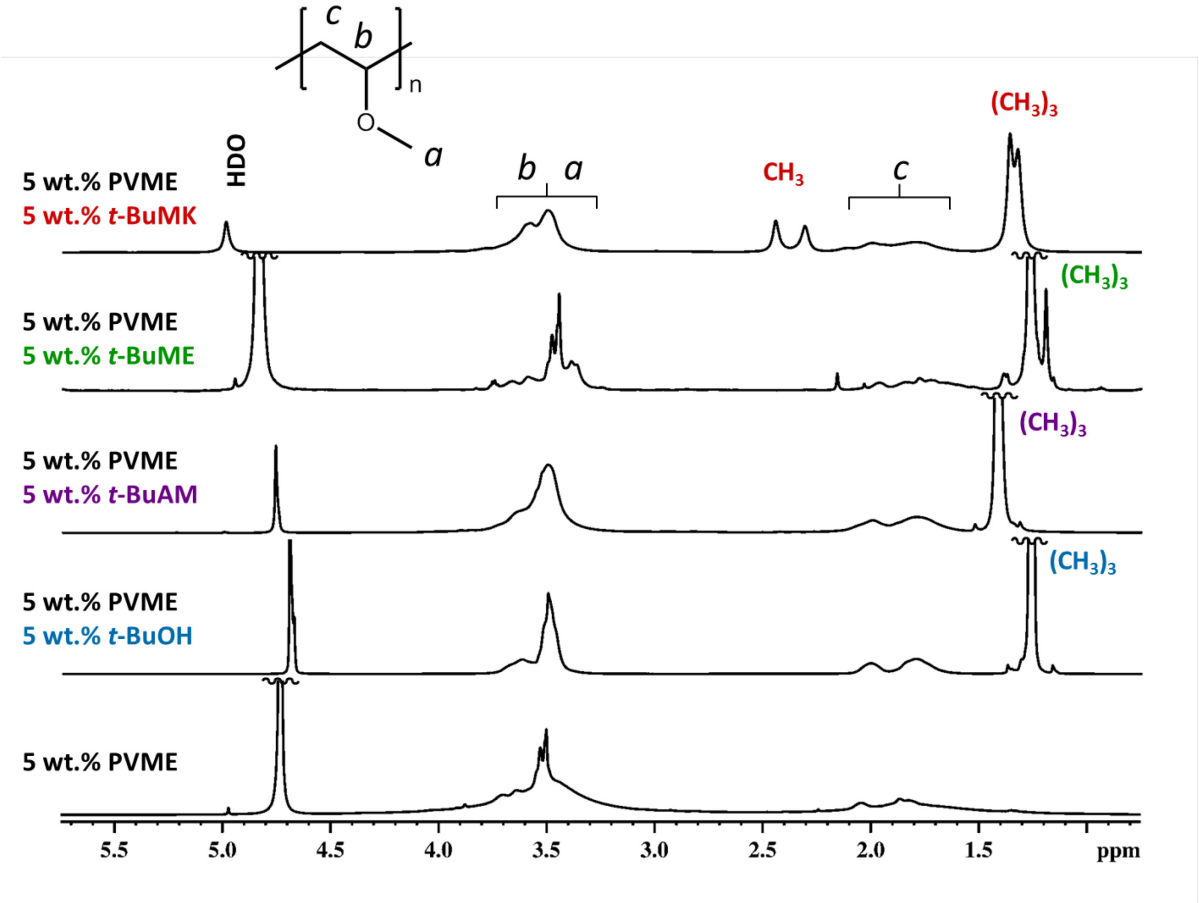

Figure 4.1.1. High-resolution ^{1}H NMR spectra of D_2O solutions of neat PVME (w_p = 5 wt.%) and solutions with additives *t*-BuOH, *t*-BuAM, *t*-BuME, and *t*-BuMK (w_p = 5 wt.%, $w_{additive}$ = 5 wt.%) measured at temperatures above the phase separation for each particular system.

Figure 4.1.1 show high-resolution ^{1}H NMR spectra of D_2O solutions of neat PVME (w_p = 5 wt.%) and PVME solutions with four additives: *t*-BuOH, *t*-BuAM, *t*-BuME, and *t*-BuMK (w_p = 5 wt.%, $w_{additive}$ = 5 wt.%) measured at temperatures above the phase separation for each particular system. The assignment of resonances to various proton types is shown directly in the spectra. The "*a*" resonance corresponds to OCH_3 group of PVME side chain, while signals "*b*" and "*c*" are related to CH and CH_2 protons from the main chain of PVME. Hydroxyl and amine signals from *t*-BuOH and *t*-BuAM, respectively are found in the water signal at ≈ 4.7-4.8 ppm. Additives' methyl and *tert*-butyl signals are assigned as CH_3 and $(CH_3)_3$ respectively. It can be seen in Figure 4.1.1 that the presence of additives influences the shape of polymer signals and thus, two types of polymer signals can be distinguished. For the polymer signals "*a*" and "*b*", a broad part of these signals corresponds to highly immobilized polymer chains and covers area from 3.0 to 4.0 ppm on the ^{1}H NMR spectrum. Whereas, the narrow part of the same signals corresponds to flexible polymer chains which does not participate in the phase separation. This effect occurs most prominently for PVME with *t*-BuME additive. In order to avoid overlapping of methyl signal of *t*-BuME with "*a*" and "*b*" signals from PVME, *t*-BuME was used with deuterated methyl groups. This was done in order to obtain a more precise value of the phase-separated fraction $p(T)$.

A series of variable temperature ^{1}H NMR spectra of PVME (w_p = 5 wt.%) in the presence of *t*-BuOH ($w_{t\text{-BuOH}}$ = 2 wt.%) are shown in Figure 4.1.2. As mentioned above, extraction of the broad part of PVME "*a*" and "*b*", signals (using fitting procedure) was used for calculation of $p(T)$ fraction. The ^{1}H NMR spectra show that the intensity and shape of polymer, water and *t*-BuOH signals vary with temperature. While temperature increases, the intensity of non-phase separated PVME signals ("*a*", "*b*", "*c*") decreases while broad phase-separated signals becoming more intensive. This behaviour is caused by the restricted mobility of polymer segments and the formation of polymer globules. The beginning of phase separation is around 308 K (≈ 35 °C) with the maximum fraction of phase-separated units reaching 0.9. Meanwhile, a signal from $(CH_3)_3$ group of *t*-BuOH just slightly broadens which indicates a rather weak association with PVME. This is the result of a rather fast chemical exchange between free and bound *t*-BuOH molecules to PVME globular structures.

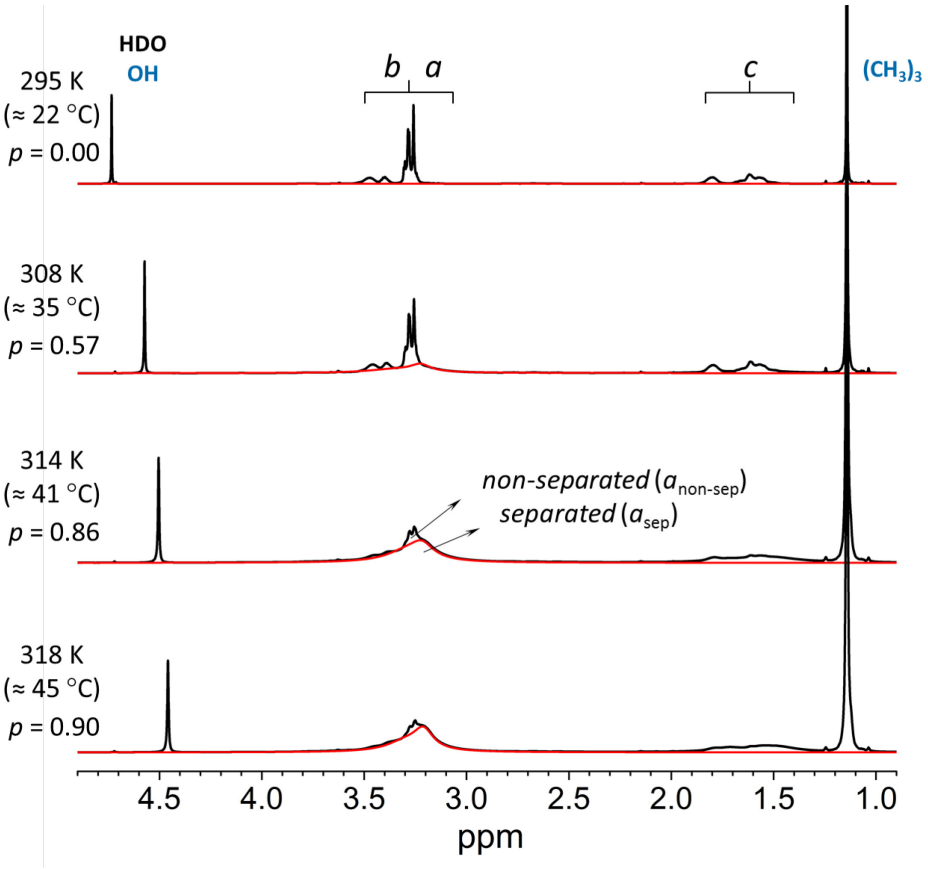

Figure 4.1.2. High-resolution ^{1}H NMR spectra of PVME (w_p = 5 wt.%) in binary *t*-BuOH/D_2O solvent ($w_{t\text{-BuOH}}$ = 2 wt.%) measured from 295 K to 318 K. Assignment of PVME and *t*-BuOH signals is the same as for Figure 4.1.1. Key: Black line = spectrum, red line = fit of broad phase-separated parts of PVME CH_3 and CH groups. The value of phase-separated fraction *p* is given for each spectrum.

The procedure of determining phase-separated fraction $p(T)$ and fitting $p(T)$ curve, as well as obtaining physico-chemical characteristics of the phase separation process is extensively explained in the Part 1.2.2 of the thesis.

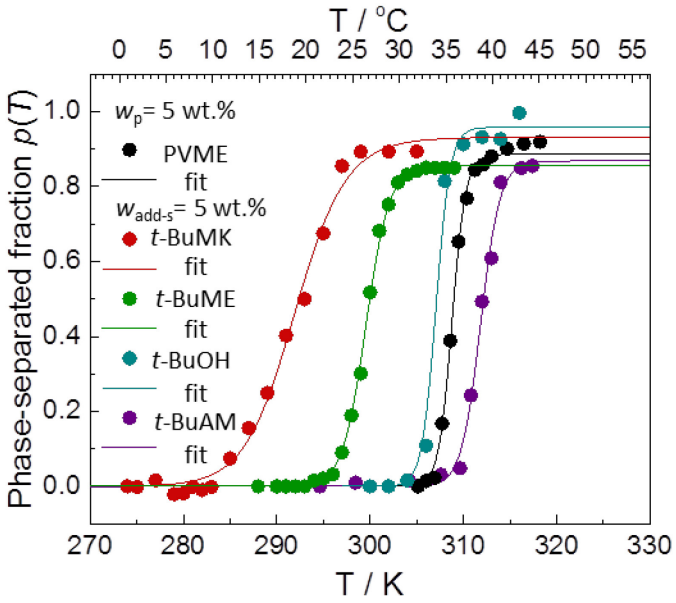

Figure 4.1.3. Temperature dependences of $p(T)$ fraction as obtained from integrated intensities of "*a*" and "*b*" resonances of PVME in neat PVME solution in D_2O (w_p = 5 wt.%) and PVME/additives solutions in D_2O (w_p = 5 wt.%, $w_{additive}$ = 5 wt.%). The solid lines are fits based on equation (11).

The analysis of PVME phase separation in the presence of additives is done by the determination of $p(T)$ fraction of the PVME units with significantly reduced mobility. Phase-separated fractions $p(T)$ were calculated using equation (11) and are represented in Figure 4.1.3 for PVME with each additive. Due to the overlapping of CH and O–CH_3 polymer signals, $p(T)$ fractions of these signals were taken as a whole. The presence of *t*-BuMK, *t*-BuME and *t*-BuOH additives shift phase separation temperature T_p of PVME to lower values due to hydrophobic association with the polymer. Contrary, *t*-BuAM has the opposite influence on T_p and acts as a good solvent for PVME, which reinforces polymer-solvent interactions. Moreover, the presence of additives extends the width of the phase separation region compare to neat PVME. The most notable influence from all additives has *t*-BuMK ($\Delta T_{width} \approx 15$ °C). The presence of *t*-BuMK, *t*-BuME, *t*-BuAM or *t*-BuOH additive results in p_{max} about 0.8-0.9 which is comparable to neat PVME. Presumably, the remaining ~ 0.1 fraction of mobile PVME units comes from short oligomer chains that do not undergo phase separation.[27]

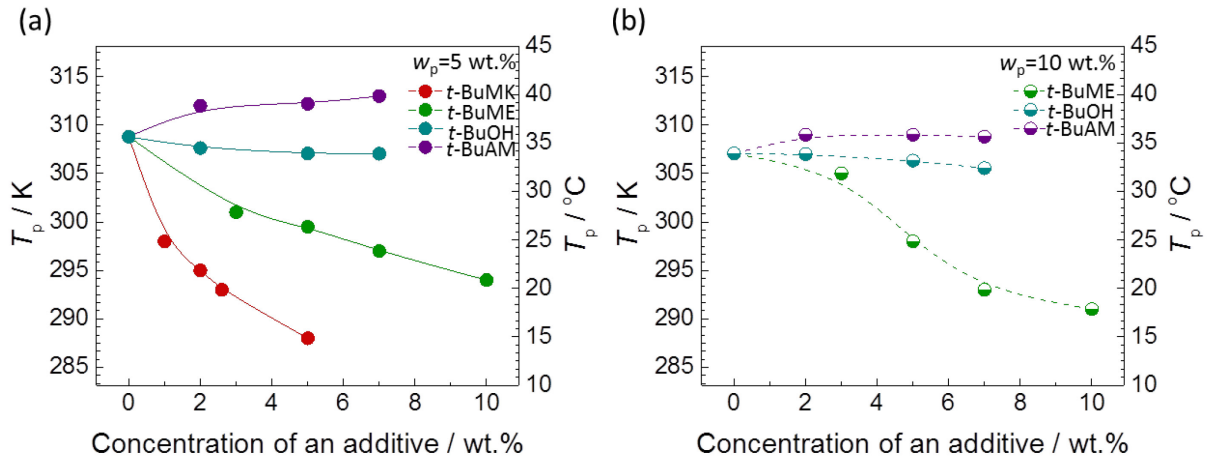

Figure 4.1.4. Concentration dependence of the phase separation temperature T_p for PVME/additives solutions in D_2O (a) w_p = 5 wt.% and (b) w_p = 10 wt.%.

In Figure 4.1.4 are shown T_p dependences on the additive concentration for two PVME concentrations (5 wt.% and 10 wt.%) in the presence of four additives: *t*-BuAM, *t*-BuOH, *t*-BuME and *t*-BuMK at concentrations 0 wt.%, 2 wt.%, 5 wt.% and 7 wt.%. A rather slight influence of PVME concentration (5 wt.% or 10 wt.%) on the phase separation temperature was observed (Figure 4.1.4a,b). For 10 wt.% PVME concentration the T_p is shifted about 2 °C lower compared to 5 wt.% PVME solutions. This is attributed to a greater number of polymer-polymer contacts and stronger hydrophobic interactions. Phase separation temperature T_p decreases with increasing the fraction of *t*-BuOH, *t*-BuME and *t*-BuMK, which means that higher additive concentration initiates polymer-polymer interactions at a lower temperature. *t*-BuMK has the biggest effect on T_p of PVME (decrease of ca. 15 °C – 20 °C), due to the hydrophobic nature of their interactions. Similar influence on the phase separation temperature was observed for aqueous solutions of PNIPAM in the presence of hydrophobic benzaldehydes, which besides lowering T_p extended the phase separation interval.[88] Meanwhile, *t*-BuAM shows a stabilizing effect on phase separation of PVME and increases T_p of PVME for ca. 2 °C – 4 °C. *t*-BuAM behaves as a good solvent and promotes interactions between PVME and water. Most probably it is the interaction between NH_2 group of *t*-BuAM and etheric oxygen from PVME.

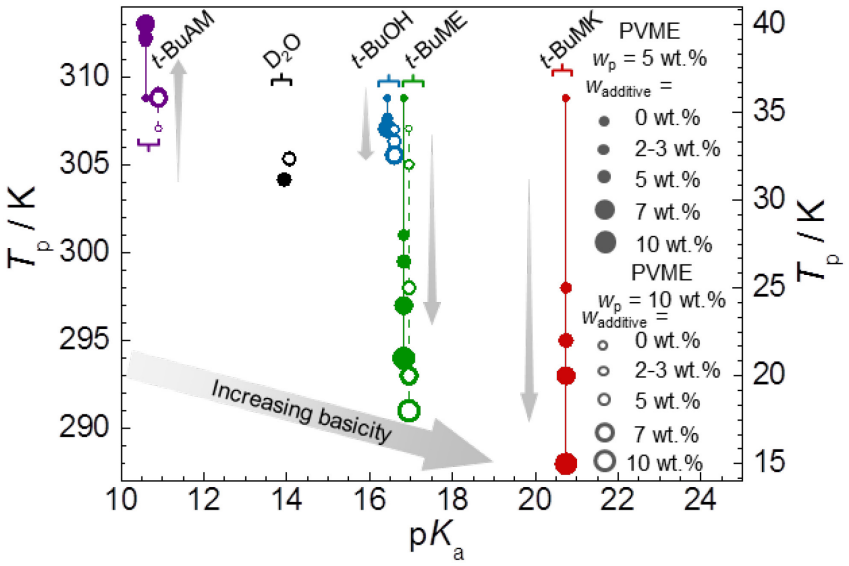

Figure 4.1.5. Plot of phase separation temperature T_p of PVME (data from Figure 4.1.4a,b) as a function of pK_a of the studied additives and their content ($w_{additive}$ = 0-10 wt %) for w_p = 5 wt.% and w_p = 10 wt.%.

Additives and their influence on phase separation of the polymer can be characterized by their acidity/basicity. In Figure 4.1.6 is shown a plot of phase separation temperature of PVME/additive system depending on the pK_a of each additive. The pK_a values were obtained from literature; *t*-BuAM (pK_a = 10.68)[89], *t*-BuOH (pK_a = 16.54)[90], *t*-BuME (pK_a = 16.89)[91], and *t*-BuMK (pK_a = 20.8).[92] The pK_a value of neat D_2O was set to 14. Values for pK_a of 5 wt.% and 10 wt.% of PVME were slightly shifted for clarity. Basicity of studied additives increases in the following order: *t*-BuAM > *t*-BuOH > *t*-BuME > *t*-BuMK. Higher basicity of additive (higher pK_a) lowers the phase separation temperature T_p. As a result, PVME phase separation temperature T_p correlates with the pH of D_2O/additive solution.

Time-resolved ^{1}H NMR spin-spin relaxation time T_2 experiments were used in order to examine the mobility of water and additive molecules in globular structures. Values of T_2 relaxation times were acquired from HDO (together with OH from *t*-BuOH or NH_2 from *t*-BuAM) signal at 4.7-4.8 ppm and $(CH_3)_3$ groups of the additive at 1.1-1.4 ppm (Figure 4.1.1). Changes of polymer conformation (i.e. coil–globule transition) are often accompanied by reduced mobility of solvent molecules if trapped in mesoglobular structures. This is well-demonstrated by lower values of T_2 for both HDO and $(CH_3)_3$ (from *t*-BuOH) resonances at temperatures above T_p (Table 2) as obtained 10 min after the heating. This effect is more

pronounced in samples with higher 10 wt.% PVME content. On the other hand, for PVME in D_2O/*t*-BuAM binary mixtures, the T_2 values of both HDO and *t*-BuAM molecules increase above T_p temperature. Therefore, weaker interactions of *t*-BuAM additive than *t*-BuOH molecules with PVME can be presumed. Therefore, based on the T_2 values, we can assume that in the phase-separated state of PVME some part of HDO and *t*-BuOH molecules are inside or on the surface of polymer globules. Whereas in the case of *t*-BuAM additive, HDO and *t*-BuAM molecules interact only very weakly with PVME, which indicates no substantial binding to polymer globules.

Table 2. Values of ^{1}H NMR spin-spin relaxation time T_2 for PVME in D_2O/*t*-BuOH solution ($w_{t\text{-BuOH}}$ = 5 wt.%) and in D_2O/*t*-BuAM solution ($w_{t\text{-BuAM}}$ = 5 wt.%) below and above phase separation temperature as obtained 10 min after heating.

Temperature	Spin-spin relaxation time T_2 / s							
	t-BuOH (5 wt.%)				*t*-BuAM (5 wt.%)			
	PVME concentration				PVME concentration			
	5 wt.%		10 wt.%		5 wt.%		10 wt.%	
	HDO	$(CH_3)_3$	HDO	$(CH_3)_3$	HDO	$(CH_3)_3$	HDO	$(CH_3)_3$
Below T_p (22 °C)	1.0	1.7	0.9	1.6	1.3	2.2	1.5	2.1
Above T_p (39 °C)	0.38	1.47	0.16	0.8	2.5	3.0	3.1	3.6

Two different type of solvent release behaviour were observed from PVME globular structures with *t*-BuAM and *t*-BuOH (Figure 4.1.6). T_2 values of HDO and $(CH_3)_3$ (from *t*-BuAM molecules) in PVME/*t*-BuAM/D_2O system are time-independent within the time scale of 1.5~3 days for both PVME concentrations (Figure 4.1.6a,b). This means that formed globules are rather rigid and stabilized by the presence of *t*-BuAM. On the other hand, time-dependent release behavior was observed for PVME/*t*-BuOH/water system. Above phase separation temperature of PVME, the T_2 values of HDO and $(CH_3)_3$ (from *t*-BuOH molecules)

resonance are gradually increasing with time (see Figure 4.1.6c,d). For 5 wt.% PVME concentration the release ceases after about 1 day leaving globular structures rather more compact. For this system, the T_2 evolution curve has an exponential-like decay, whereas for 10 wt.% of PVME the T_2 evolution curve is more sigmoidal-like. Note that the concentration of *t*-BuOH was kept the same for both concentrations of PVME. The release of water and *t*-BuOH molecules from globular structures starts after about ~2 days and reaches the plateau in about ~5 days. This delay in release behavior can be explained by rather denser and bigger aggregated structures compare to the lower polymer concentration.

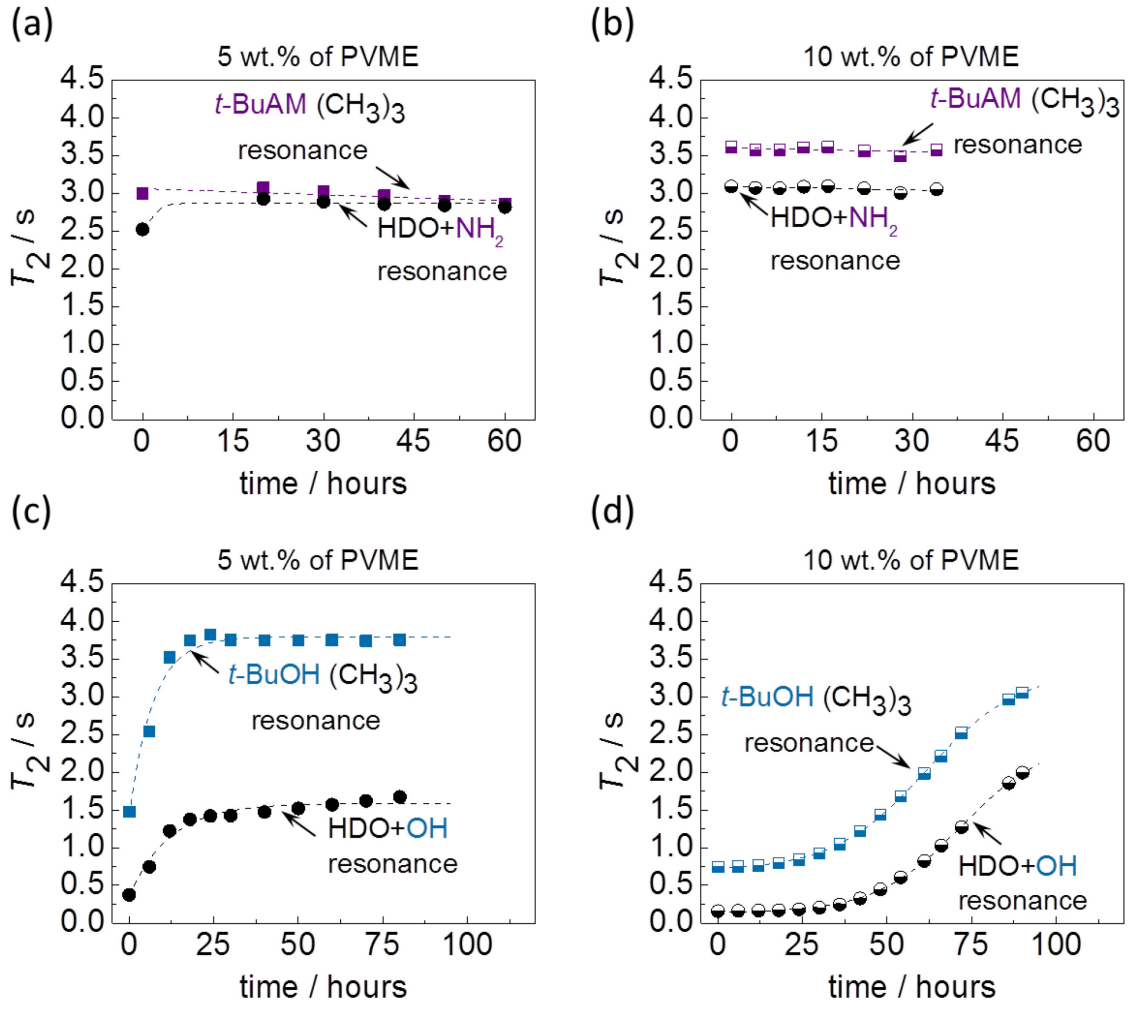

Figure 4.1.6. Time dependences of spin-spin relaxation time T_2 of $(CH_3)_3$ resonances of additives ($w_{additive}$ = 5 wt.%) and HDO resonance above phase separation temperature of PVME with *t*-BuAM (a) w_p = 5 wt.% and (b) w_p = 10 wt.% and PVME with *t*-BuOH (c) w_p = 5 wt.% and (d) w_p = 10 wt.%.

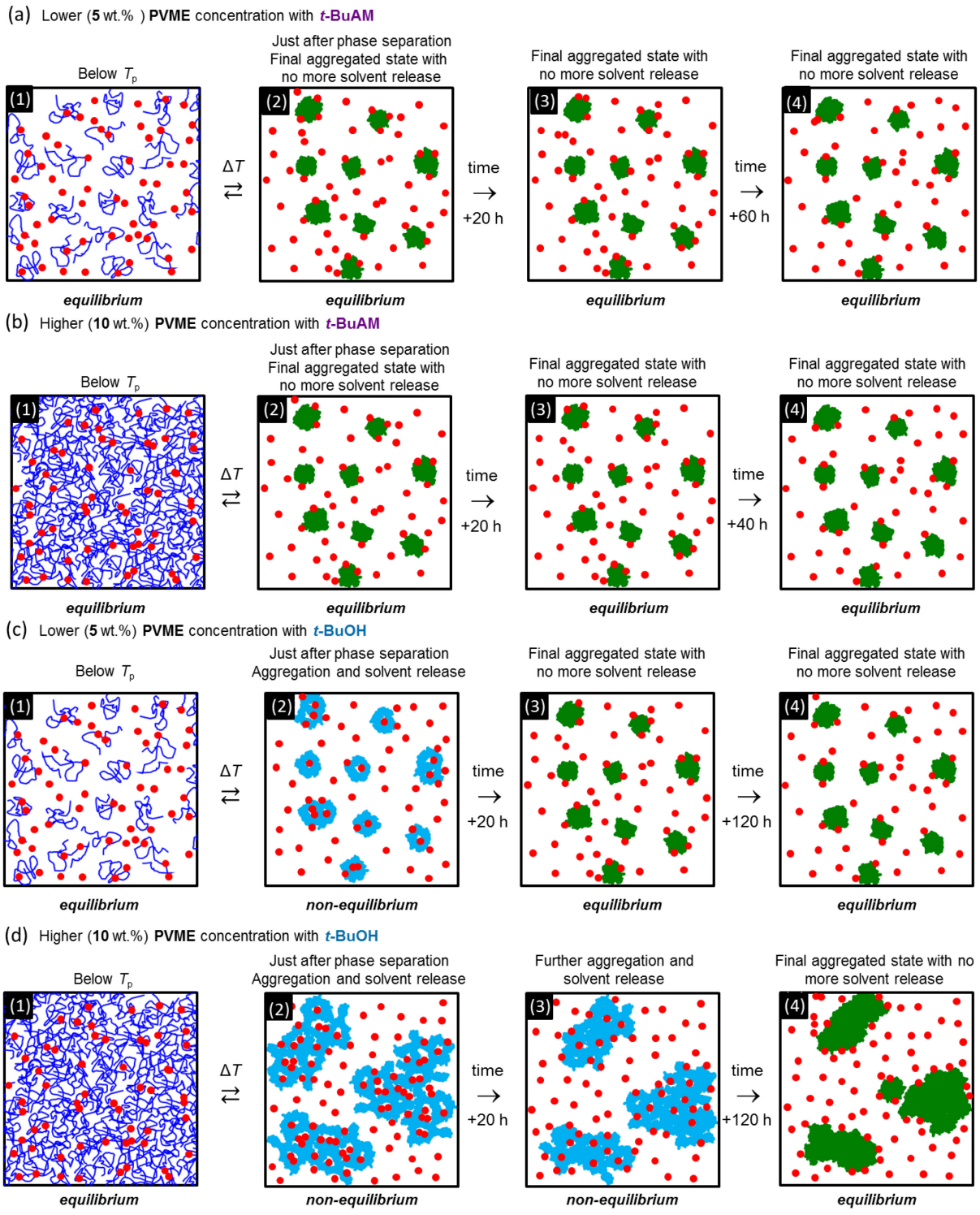

Figure 4.1.7. Model of PVME phase separation based on T_2 relaxation time measurements for (a) w_p = 5 wt.% and (b) w_p = 10 wt.% in the presence of *t*-BuAM and (c) w_p = 5 wt.% and (d) w_p = 10 wt.% in the presence of *t*-BuOH.

Based on time-dependent NMR relaxation measurements phase separation process of PVME in the presence of *t*-BuAM and *t*-BuOH additives can be visually depicted in the following way (Figure 4.1.7). For both PVME concentrations with *t*-BuAM, immediately after the phase separation, the equilibrium state is reached with no water or *t*-BuAM release (Figure 4.1.7a,b). The surface of polymer globules is stabilized by *t*-BuAM molecules. For PVME with *t*-BuOH different behavior is observed. At lower polymer concentration, immediately after the T_p is achieved, the system is in a non-equilibrium state with solvent and *t*-BuOH molecules readily escaping polymer globules. In about 20-24 h the system becomes stable (time unchangeable) and more compact (Figure 4.1.7c). At higher PVME content, non-equilibrium sponge-like structures are formed after phase separation with solvent molecules trapped inside. With time, the system slowly releases solvent and additive molecules and moves towards the equilibrium (Figure 4.1.7d).

In summary, phase separation of PVME in the presence of four additives (*t*-BuAM, *t*-BuOH, *t*-BuME, *t*-BuMK) has been studied by high resolution NMR spectroscopy. Polymer concentration has a rather minor influence on the phase separation temperature T_p compare to the additives concentration. T_p of PVME decreases with the increase of additive concentration as well as additive type in the following way: *t*-BuOH > *t*-BuME > *t*-BuMK. Such behaviour is attributed to hydrophobic association with PVME and is more pronounced for PVME with *t*-BuMK (decrease of T_p ca. 15–20 °C). On the other hand, the presence of *t*-BuAM shows a rather stabilizing effect on T_p of PVME and shifts its T_p to the higher values. This is probably due to the interactions between NH_2 group of *t*-BuAM and etheric oxygen from PVME. For all studied samples, about 80 to 90% of polymer groups undergo phase separation. Additives promote the extension of the phase separation interval which is most pronounced in the case of *t*-BuMK (up to ca. 15 °C). NMR relaxation experiments were used in order to study the dynamics of water and additive molecules before and after phase separation. Two different models of phase separation were proposed based on spin-spin relaxation time T_2 measurements. The presence of *t*-BuAM stabilizes PVME globules and thus, no water or additive release is observed in the timescale of 1.5~3 days leaving formed globules rather rigid. Whereas, in the presence of *t*-BuOH or *t*-BuMK[87] over time some part of water and additive molecules are released from formed PVME globules leaving formed globules rather sponge-like.

4.2 Influence of additives on phase separation of poly(*N*-isopropylacrylamide)

In this chapter of the thesis influence of *t*-BuOH, *t*-BuAM, *t*-BuMK and *t*-BuME on phase separation of PNIPAM will be discussed. This study was done using ^{1}H NMR and time-resolved ^{1}H NMR spin-spin relaxation time T_2 experiments. These results were fully reported in publication 3 (see Appendix).

^{1}H NMR spectra of PNIPAM in D_2O (w_p = 5 wt.%) measured below (at 22 °C) and above phase separation temperature (at 41 °C) in the presence of four additives: *t*-BuAM, *t*-BuOH, *t*-BuME and *t*-BuMK ($w_{additive}$ = 2 wt.%) are shown in Figure 4.2.1. These spectra display that after phase separation the peaks assigned to PNIPAM ("*a*", "*b*", "*c*" and "*d*" peaks in Figure 4.2.1) vanish from high resolution NMR spectra. The cause of this behaviour is the low mobility of PNIPAM chains in globular structures above the phase separation temperature.[93] Lower mobility of polymer chains is reflected by the shorter T_2 relaxation time of proton signals of polymer groups and thus they are displayed by wider peaks in the ^{1}H NMR spectrum. Likewise, for methyl signals corresponding to additives ("*x*" and "*y*"), one can see resonance broadening and intensity decrease with increasing temperature. These changes in the spectra indicate that additives participating in phase separation.

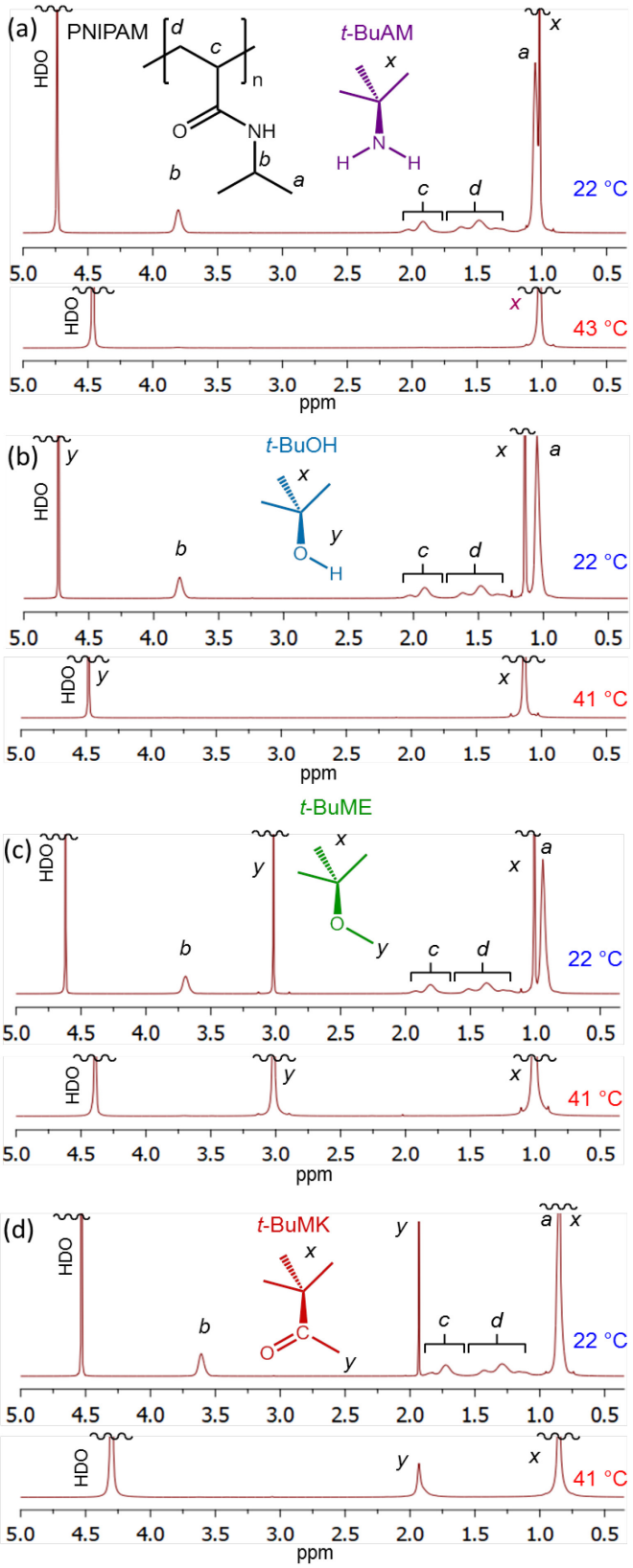

Figure 4.2.1. ^{1}H NMR spectra of PNIPAM (w_p = 5 wt.%) in D_2O below (at 22 °C) and above (at ca. 41 °C) phase separation temperature in the presence of $w_{additive}$ = 2 wt.% of each of the additive: (a) *t*-BuAM, (b) *t*-BuOH, (c) *t*-BuME and (d) *t*-BuMK.

The procedure of determining phase-separated fraction $p(T)$ and fitting $p(T)$ curve, as well as obtaining physico-chemical characteristics of the phase separation process was explained in detail in Part 1.2.2 of the thesis. Further analysis of $p(T)$ fraction was done similarly to the PVME system.

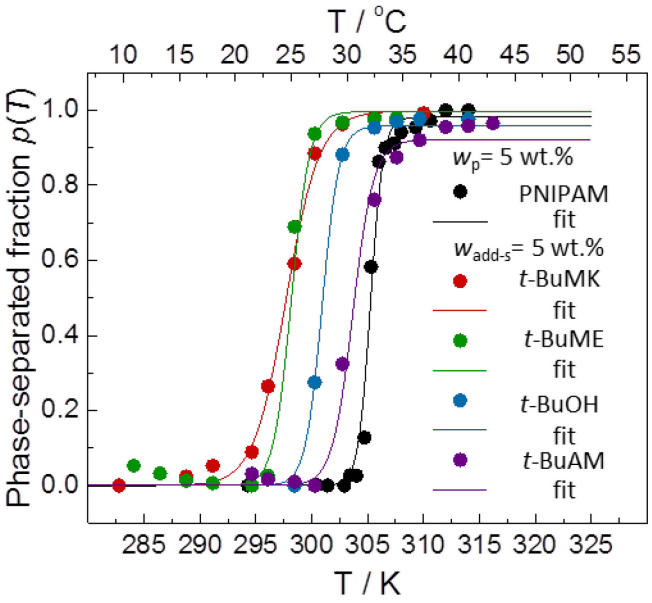

Figure 4.2.2. Temperature dependences of phase-separated fraction $p(T)$ of w_p = 5 wt.% of PNIPAM in D_2O as obtained from the "*b*" resonance of PNIPAM in the presence of additives ($w_{additive}$ = 5 wt.%). The solid lines are fits based on equation (11).

The Figure 4.2.2 shows how phase separation fractions $p(T)$ of "*b*" resonance of PNIPAM (w_p = 5 wt.%) change in the presence of *t*-BuAM, *t*-BuOH, *t*-BuME and *t*-BuMK ($w_{additive}$ = 5 wt.%). Two-state thermodynamic model of phase separation (equation (11)) was used for fitting $p(T)$ curves. The phase separation temperatures T_p of PNIPAM is strongly influenced by the presence of additives and is decreasing in the following manner: neat PNIPAM > *t*-BuAM > *t*-BuOH > *t*-BuME > *t*-BuMK (Figure 4.2.3). This behaviour was observed for both polymer concentrations 5 wt.% and 10 wt.%. For all studied additives more than 90% (p_{max}) of PNIPAM chains transit to globular state at temperatures higher than their phase separation temperature. All studied systems showed a relatively narrow width of phase separation (ΔT_{width}) up to 5 °C. From obtained results, T_p of studied systems is rather independent of polymer concentration but strongly dependent on the type of additive. In these PNIPAM /D_2O/additive systems, no precipitation (sedimentation) was observed even after a long time in the order of days. Note, in the presence of additives protons from the main and

side chains of PNIPAM undergo phase separation at the same time, as it was reported previously for the neat PNIPAM/D_2O and PVME/D_2O solutions.[94,95]

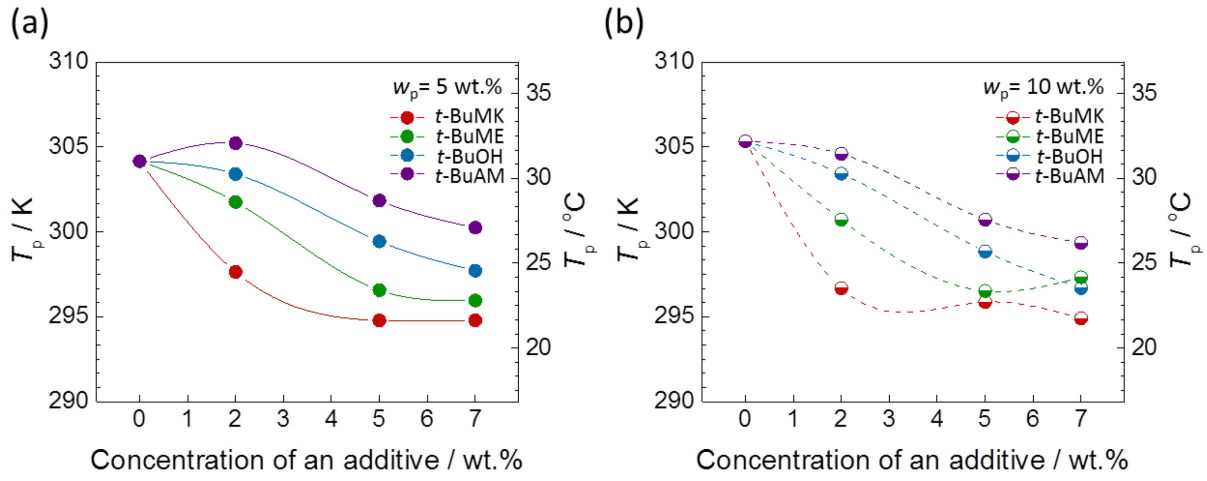

Figure 4.2.3. Influence of additives concentration on phase separation temperatures T_p of PNIPAM (a) w_p = 5 wt.% and (b) w_p = 10 wt.%.

Figure 4.2.3 shows T_p dependences on the concentration of *t*-BuAM, *t*-BuOH, *t*-BuME and *t*-BuMK additives for two PNIPAM concentrations (5 wt.% and 10 wt.%). Rather small influence of PNIPAM concentration (compare 5 wt.% and 10 wt.%) on its phase separation temperature was observed (Figure 4.2.3a,b). Phase separation temperature T_p decreases with increasing fraction of additive (independent of the type), which means that higher additive concentration initiates the hydrophobic association of polymer chains at a lower temperature. T_p is highly affected by additive presence and decrease in the following way: *t*-BuAM > *t*-BuOH > *t*-BuME > *t*-BuMK. *t*-BuMK has the biggest effect on T_p of PNIPAM (decrease of ca. 10 °C), due to the hydrophobic nature of their interactions. We supposed that $(CH_3)_3$ groups of *t*-BuMK form a cage around hydrophobic groups of PNIPAM, and as a result, remove water molecules from the vicinity of polymer chains and initiate phase separation at a lower temperature.

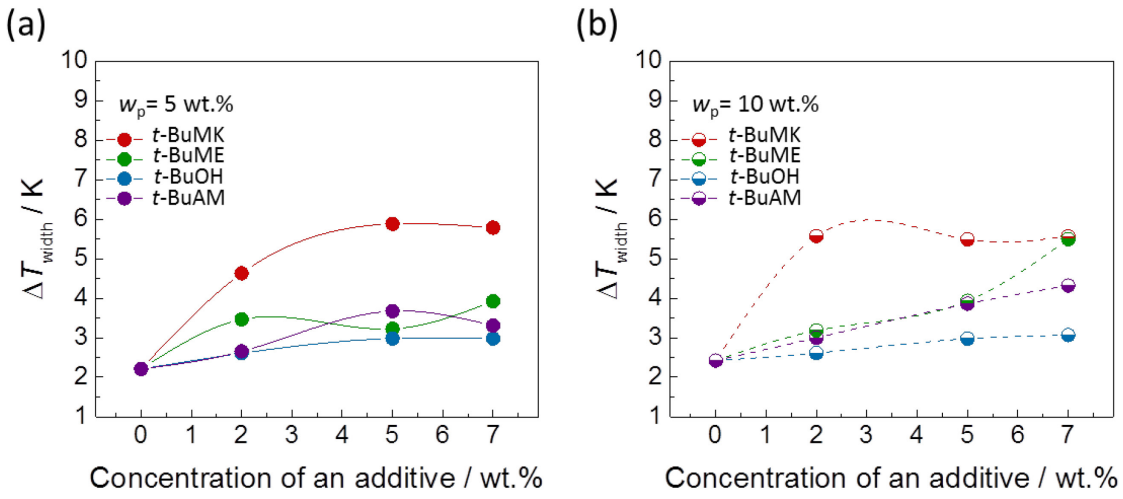

Figure 4.2.4. Influence of additives concentration on width of phase separation ΔT_{width} of PNIPAM at (a) w_p = 5 wt.% and (b) w_p = 10 wt.%.

ΔT_{width} is independent of PNIPAM concentration and just depends on the additives type. Furthermore, rising the additive fraction in the polymer solution slightly broadens the phase separation interval (ΔT_{width}; Figure 4.2.4a,b). The most pronounced effect with 5 °C width of phase separation interval was detected for *t*-BuMK. The extended phase separation temperature interval is associated with a slightly prolonged reorganization of polymer chains during phase separation.

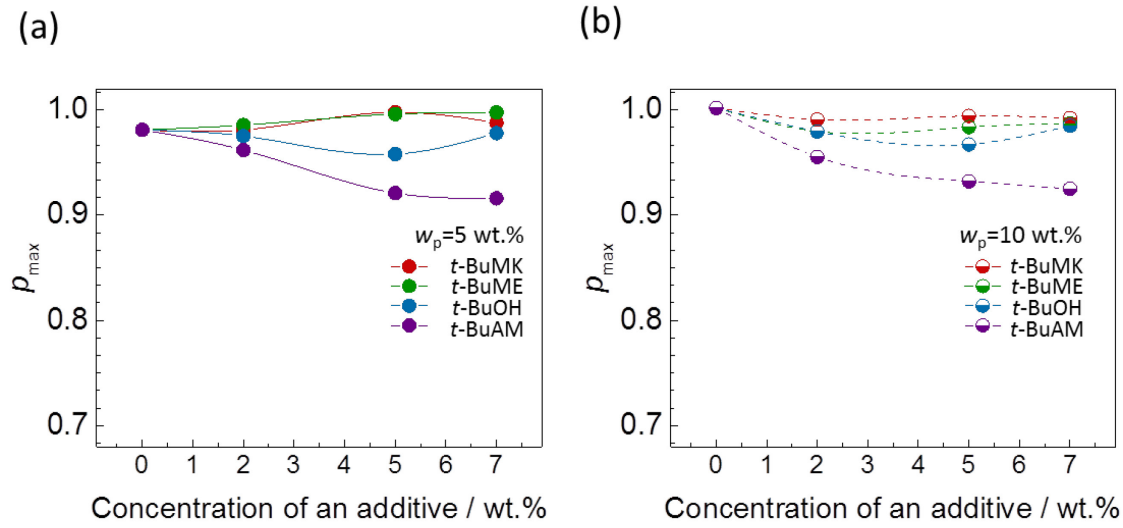

Figure 4.2.5. Influence of additives concentration on the maximum fraction of phase-separated PNIPAM units p_{max} of PNIPAM (a) w_p = 5 wt.% and (b) w_p = 10 wt.%.

The effect of additive concentration on the amount of polymer chain participating in phase separation for both polymer concentrations is shown in Figure 4.2.5a,b. For all studied additives values of p_{max} are more than 0.9, thus more than 90% of polymer chains are restricted in mobility above the phase separation temperature. This confirms the formation of highly rigid globular structures with just a small portion of mobile PNIPAM chains (Figure 4.2.5).

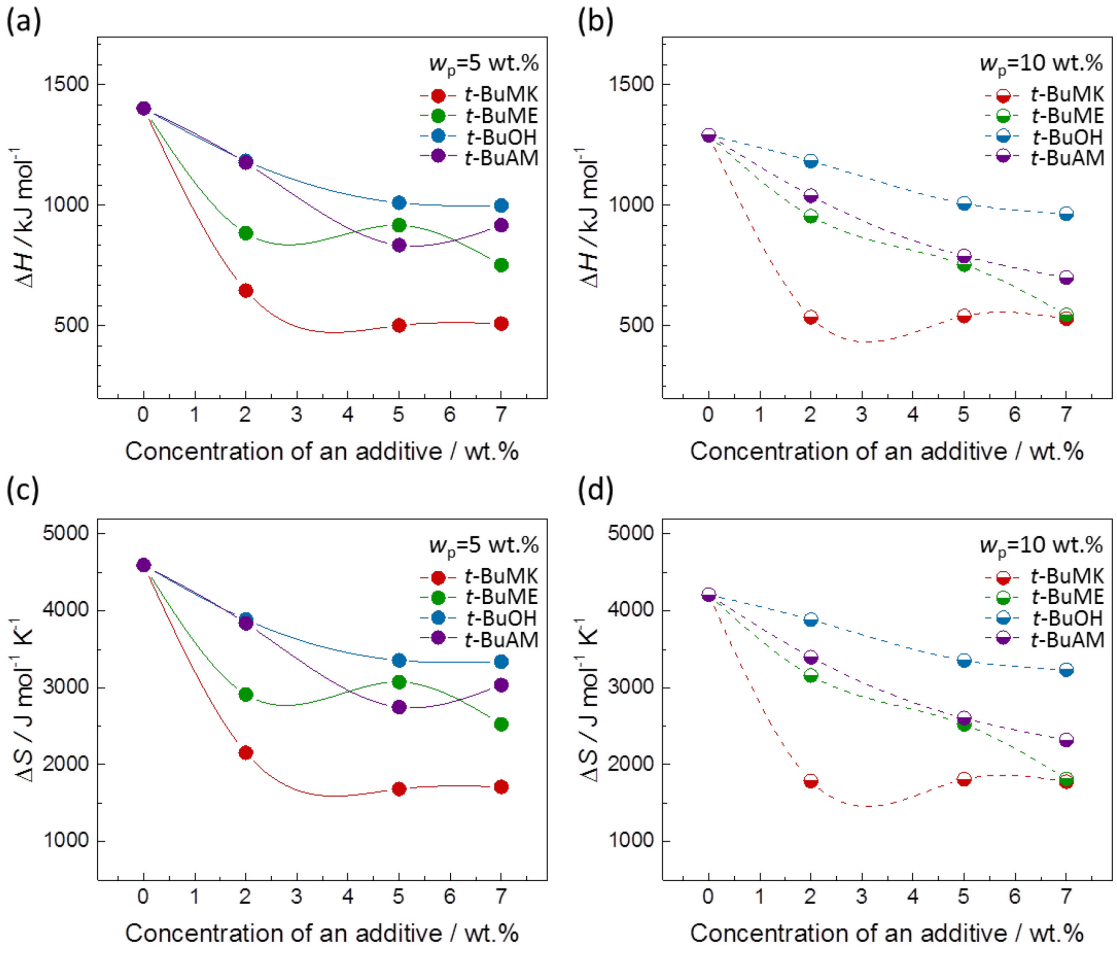

Figure 4.2.6. Phase separation parameters of PNIPAM (w_p = 5 wt.% and w_p = 10 wt.%) in the presence of the additives. (a, b) Variations in standard enthalpy, ΔH. (c, d) Variations in standard entropy, ΔS.

Additionally, enthalpy and entropy changes were extracted from NMR data by fitting procedure using equation (11), as seen for example in Figure 4.2.2. Increasing the fraction of any additive decreases both enthalpy (ΔH; Figure 4.2.6a,b) and entropy change (ΔS; Figure 4.2.6c,d) associated with phase separation of PNIPAM. In order to evaluate the nature of

molecular interactions between additives with the polymer, the value of additive's relative hydrophobicity was calculated. It was done using HSPiP software[96] and is represented in the following order starting from least to most hydrophobic: *t*-BuAM (0.3) > *t*-BuOH (0.5) > *t*-BuME (0.9) > *t*-BuMK (1.2). Therefore, *t*-BuAM affects the phase separation of PNIPAM the least, whereas *t*-BuMK hydrophobically associates with PNIPAM the most and shifts its T_p for about 10 °C (Figure 4.2.4a,b). This hydrophobic interaction with the polymer has a pronounced influence on the enthalpy of phase separation. The presence of a hydrophobic additive removes water molecules from the proximity of polymer chains, resulting in fewer hydrogen bonds between water and polymer chains. As a consequence, ΔH for systems with additives is lower; polymer undergoes phase separation earlier because of lower energy barrier needed for breaking hydrogen bonds between water and polymer molecules.

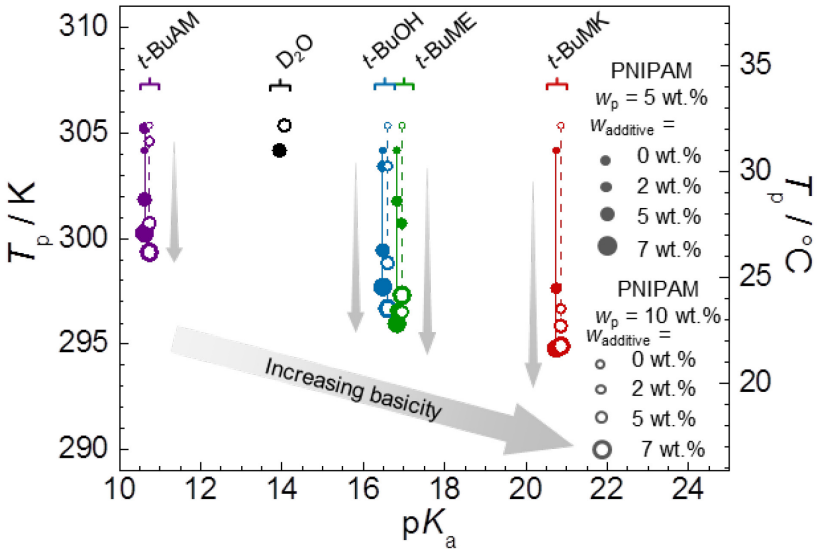

Figure 4.2.7. Plot of phase separation temperature T_p of PNIPAM (data from Figure 5a,b) as a function of pK_a of the studied additives and their content ($w_{additive}$ = 0-7 wt %) for w_p = 5 wt.% and w_p = 10 wt.%.

As in the PVME system, the influence of additives on phase separation of the polymer was characterized from the pH point of view. In Figure 4.2.7 is shown a plot of phase separation temperature of PNIPAM/additive system depending on pK_a for each of the studied additives. Likewise to PVME, basicity as well as hydrophobicity of PNIPAM increases in the following order: *t*-BuAM > *t*-BuOH > *t*-BuME > *t*-BuMK. Higher basicity (same as higher

pK_a) lowers the phase separation temperature T_p. Therefore, PNIPAM phase separation temperature T_p is related to the pH, which is tuned by the concentration of additive.

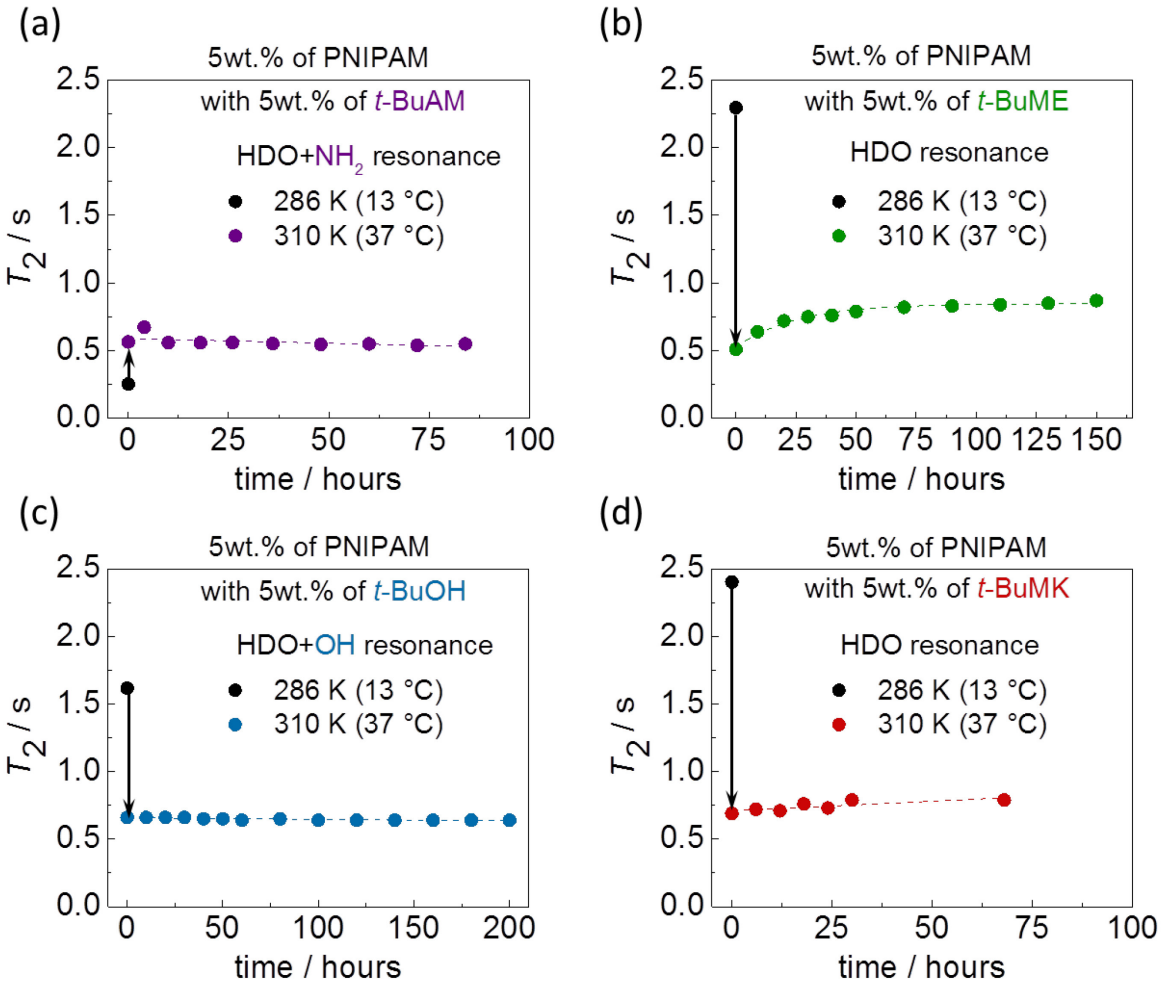

Figure 4.2.8. Time dependency of spin-spin relaxation time T_2 of HDO resonances of additive ($w_{additive}$ = 5 wt.%) below (T = 286 K = 13 °C) and above (T = 310 K = 37 °C) phase separation temperature of PNIPAM (w_p = 5 wt.%). T_2 values measured in the presence of (a) *t*-BuAM, (b) *t*-BuME, (c) *t*-BuOH and (d) *t*-BuMK.

In order to obtain information about the mobility of water and additive molecules during temperature-induced phase separation, a series of time-dependent ^{1}H spin-spin relaxation times T_2 were measured (Figure 4.2.8 and 4.2.9). T_2 values of residue HDO and $(CH_3)_3$ protons of *t*-BuAM, *t*-BuOH, *t*-BuME and *t*-BuMK were acquired below and above separation temperature for PNIPAM/D_2O solution (w_p = 5 wt.%). From the data shown in Figure 4.2.8 and 4.2.9 follow that T_2 values above phase separation temperature (T = 37 °C) are significantly shorter than those below phase separation temperature (T = 13 °C) for both

HDO and *t*-butyl $(CH_3)_3$ signals. This finding indicates that both water and additive molecules show spatially restricted mobility due to phase separation of PNIPAM. The only exception is extremely low mobility of HDO molecules at low temperature for PNIPAM/*t*-BuAM system (Figure 4.2.8a). The unusually low T_2 of HDO molecules in sample with *t*-BuAM at 13 °C is due to strong interaction between primary anime NH_2 group of *t*-BuAM and water molecules (which also includes chemical exchange of protons). This effect is also manifested by considerable increase of viscosity of water/*t*-BuAM binary mixture which is strongly dependent on *t*-BuAM content and moderately on temperature.[97] These interactions are known to significantly contribute to relaxation processes and thus reducing T_2 relaxation time of residual HDO molecules.

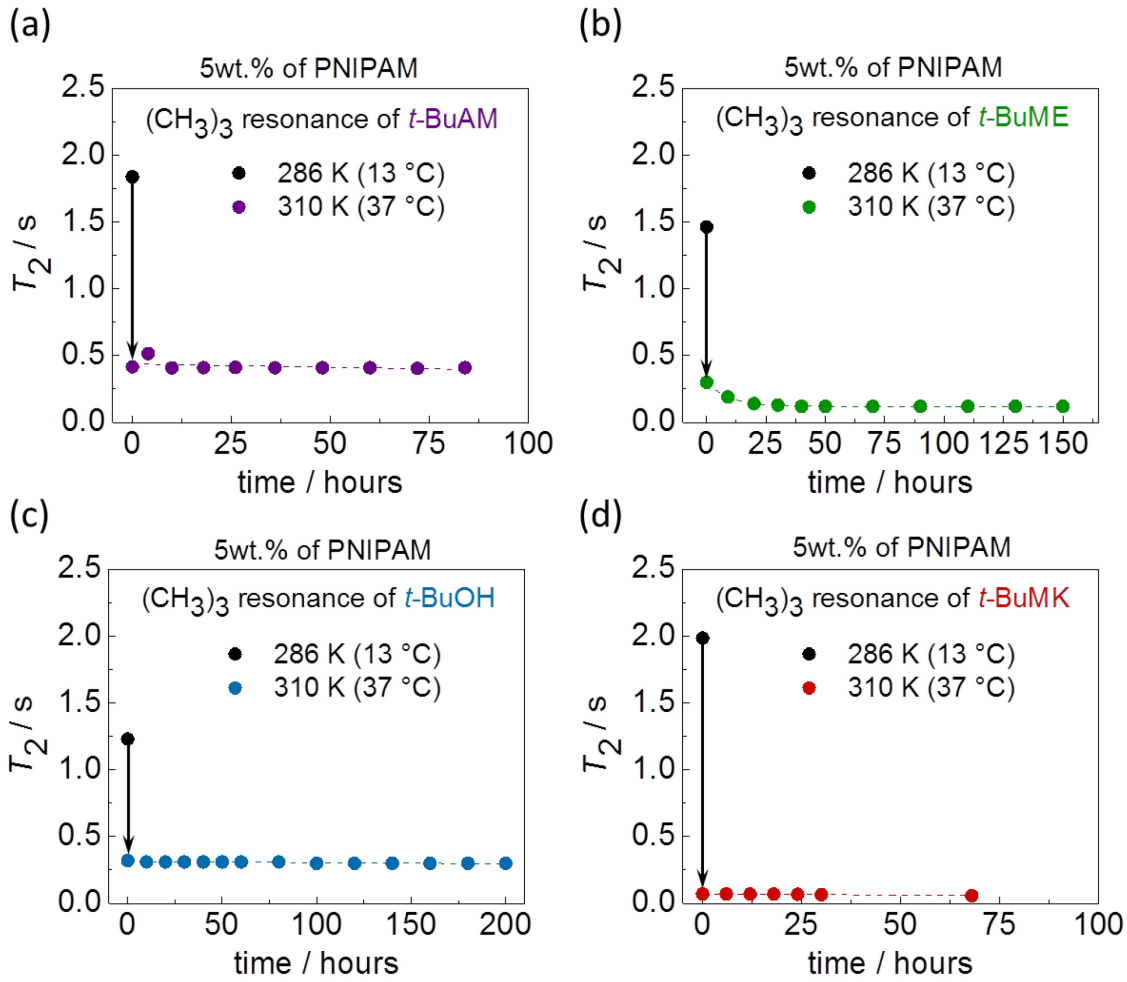

Figure 4.2.9. Time dependency of spin-spin relaxation time T_2 of $(CH_3)_3$ resonances of additive ($w_{additive}$ = 5 wt.%) below (at T = 286 K = 13 °C) and above (at T = 310 K = 37 °C) phase separation temperature of PNIPAM (w_p = 5 wt.%). T_2 values measured in the presence of (a) *t*-BuAM, (b) *t*-BuME, (c) *t*-BuOH and (d) *t*-BuMK.

In all cases, single resonance for both HDO and $(CH_3)_3$ signals were observed in the ^{1}H NMR spectrum and all T_2 curves had mono-exponential character. The observed T_2 values at temperatures above T_p correspond to a weighted average of free and bound T_2 values. Afterwards, in order to evaluate the dynamics and stability of polymer globules time dependence of spin-spin relaxation times T_2 were measured. After reaching an elevated temperature (T = 37 °C) studied samples were kept in the NMR magnet for a few days (Figure 4.2.8 and 4.2.9a-d). No changes in T_2 values over time were observed for HDO ($T_2 \approx 0.7$ s) and $(CH_3)_3$ groups of additives ($T_2 \approx 0.2$ s). Therefore, no solvent molecules releasing process was detected for the bound solvent molecules, which suggests that the presence of additives stabilize mesoglobular structures. This further indicates that these systems are colloidally stable solutions, such that the phase-separated particles do not aggregate and precipitate. In contrast, the T_2 relaxation time of water in a neat PNIPAM/D_2O system shows slow recovery to its original value within 130 hours (5.5 days).[10] This finding corresponds to the very slow release of water from polymer mesoglobules, thus making these structures more compact and rigid. On the other hand, the presence of studied additives demonstrates stabilizing effect on PNIPAM globules, since no water and/or the additives are released from mesoglobular structures within 3-8 days (Figure 4.2.8 and 4.2.9). These findings suggest that hydrophobic association of additives with PNIPAM, create somewhat a shell, which restricts aggregation and precipitation of polymer globules.

In summary, phase separation of PNIPAM in the presence of four additives (*t*-BuAM, *t*-BuOH, *t*-BuME, *t*-BuMK) has been studied by NMR. After fitting procedure, T_p, p_{max}, ΔT_{width}, ΔH and ΔS values connected with phase separation were extracted. Polymer concentration has an insignificant influence on the phase separation temperature T_p compare to additive effect. T_p decreases with an increase of additive concentration as well as additive type in the following way: *t*-BuAM > *t*-BuOH > *t*-BuME > *t*-BuMK. This behaviour is attributed to hydrophobic association with PNIPAM and is strongest for PNIPAM with *t*-BuMK additive (ca. 10 °C decrease of T_p). For all studied samples, more than 90% of polymer groups undergo phase separation with a rather narrow phase separation temperature interval (up to ca. 5 °C). The dynamics of water and additive molecules before and after phase separation was studied by NMR relaxation experiments. Spin-spin relaxation time T_2 measurements revealed that water and additive molecules are spatially restricted in the globular state. The presence of additives shows a stabilizing effect on PNIPAM globules.

4.3 Study of the phase behaviour of porphyrin-PNIPAM conjugates

Novel porphyrin-PNIPAM conjugates demonstrate both properties of porphyrin (J-/H-aggregates formation, pH sensitivity) and the polymer (phase separation and co-nonsolvency effects). In this part of the thesis, a systematic study of novel tetraphenylporphyrin with a four-arm star-shaped poly(*N*-isopropylacrylamide) (PNIPAM) polymer is described. This study was done using ^{1}H NMR, DSC, SAXS, UV-Vis, PL, DSL and OM. Currently, a manuscript containing our findings in this topic is under preparation for publication.

4.3.1 The phase separation phenomenon

The phase separation phenomenon was studied in D_2O solution using high resolution NMR spectroscopy. ^{1}H NMR spectra were acquired at different temperatures. The typical behaviour of **PP**$_{22.7}$ (ϕ_{PP} = 1.48 vol.%) is demonstrated in Figure 4.3.1. The spectra show a clear onset of the phase separation around 27 °C. Note, peaks from porphyrin core are very broad and undetectable in water solution due to its hydrophobic nature. While temperature increases from 18 °C to 45 °C, a gradual decrease of PNIPAM resonance intensity is observed ("*a*", "*b*", "*c*", "*d*" and "*e*" resonances in Figure 4.3.1), due to the restricted mobility of polymer chains. The "*b*" resonance of the CH pendant group of PNIPAM does not overlap with other signals in the ^{1}H NMR spectrum, thus it was chosen for further quantitative characterization of PNIPAM units participating in the phase separation. The "*b*" signal was integrated and obtained intensities were used in equation (6) to calculate the value of the phase-separated fraction of PNIPAM units $p(T)$.[21,74]

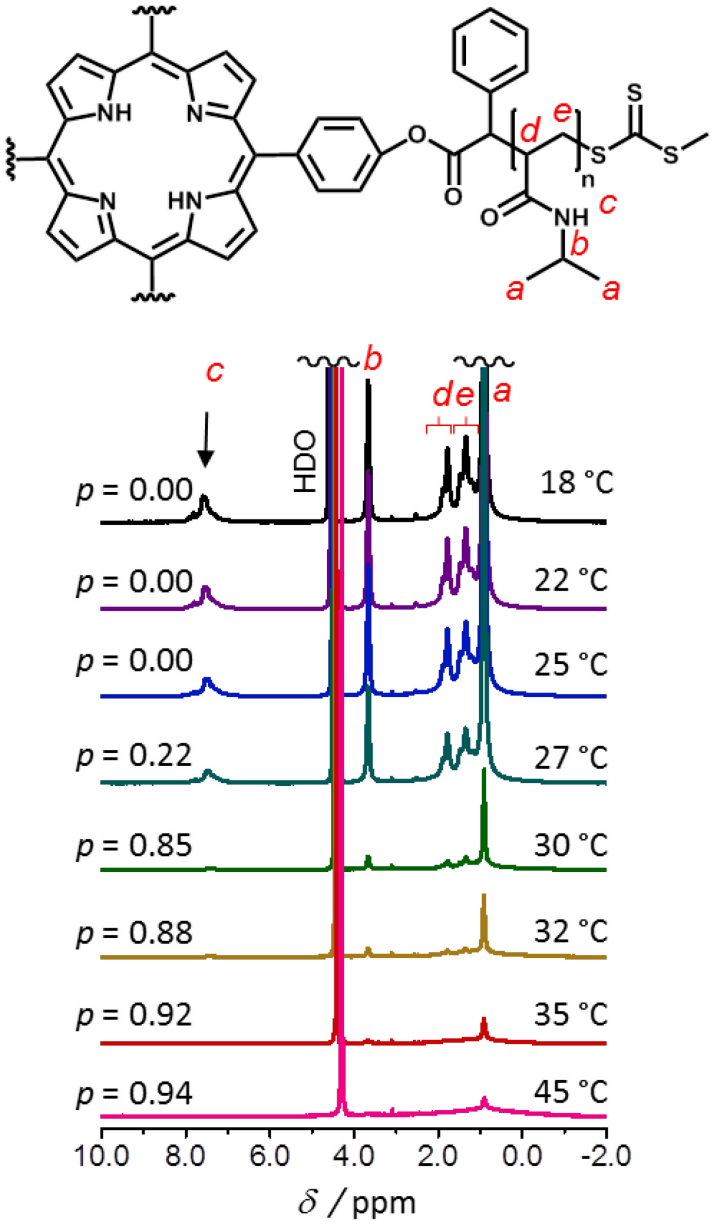

Figure 4.3.1. ^{1}H NMR spectra of **PP**$_{22.7}$ (ϕ_{PP} = 1.48 vol.%) in D_2O solvent measured from 18 to 45 °C at pD = 7.4, where pD = pH + 0.4. An assignment of **PP** signals is shown at the top spectrum. The value of phase-separated fraction p is given for each spectrum.

Figure 4.3.2 shows phase-separated fractions $p(T)$ calculated from NMR experimental data of **PP**$_{8.4}$ and **PP**$_{22.7}$ conjugates in D_2O at different concentrations of **PP**. **PP**$_{8.4}$ was studied in the concentration range of 0.033-8.2 vol.% and **PP**$_{22.7}$ was studied in the concentration range of 0.031-5.9 vol.%. It can be seen that the phase separation temperature T_p decreases with increasing sample concentration for both **PP** conjugates. It is also evident that T_p of **PP**$_{8.4}$ is a few degrees lower than T_p of **PP**$_{22.7}$, which means that **PP** with shorter

PNIPAM chains phase separates at lower temperature. This behaviour is opposite to usual LCST type behaviour of polymers, where higher molecular weight lowers the T_p. The **PP** conjugate behaviour can be attributed to the hydrophobic effect of porphyrin core. The hydrophobic core experience less screening in **PP** conjugates with shorter PNIPAM chains and thus is less soluble, which results in lower T_p. We also suppose that the phase separation starts from polymer units close to porphyrin hydrophobic core and then proceed along the polymer chains. For both types of conjugates more than 90% (p_{max}) of polymer chains appears in globular state at temperatures higher than the phase separation temperature. Two-state model of phase separation was used for both **PP** conjugates. One- and two-component model (consisting of one or two curves with equation (11)) of phase separation were used for fitting experimental $p(T)$ curves of $\mathbf{PP}_{8.4}$ and $\mathbf{PP}_{22.7}$, respectively. This was done in order to fit accurately $p(T)$ of $\mathbf{PP}_{8.4}$ and $\mathbf{PP}_{22.7}$ conjugates with slightly different molecular weight distribution, (dispersity $Đ_M$ = 1.09 and 1.15 for $\mathbf{PP}_{8.4}$ and $\mathbf{PP}_{22.7}$, respectively). $\mathbf{PP}_{8.4}$ showed wider phase separation interval (ΔT_{width}) compared to $\mathbf{PP}_{22.7}$ (Figure 4.3.2). Higher dispersity value might be the reason for presence of a "shoulder" on $p(T)$ curve of $\mathbf{PP}_{22.7}$ conjugate above $p(T) > 0.8$. Our results indicate that T_p of the porphyrin-PNIPAM conjugates can be tuned by **PP** concentration and by changing the length of PNIPAM chains in opposite manner then usually observed in LCST systems. The values of T_p as obtained from NMR are plotted in T-ϕ_{PP} phase diagram as shown in Figure 4.3.5a.

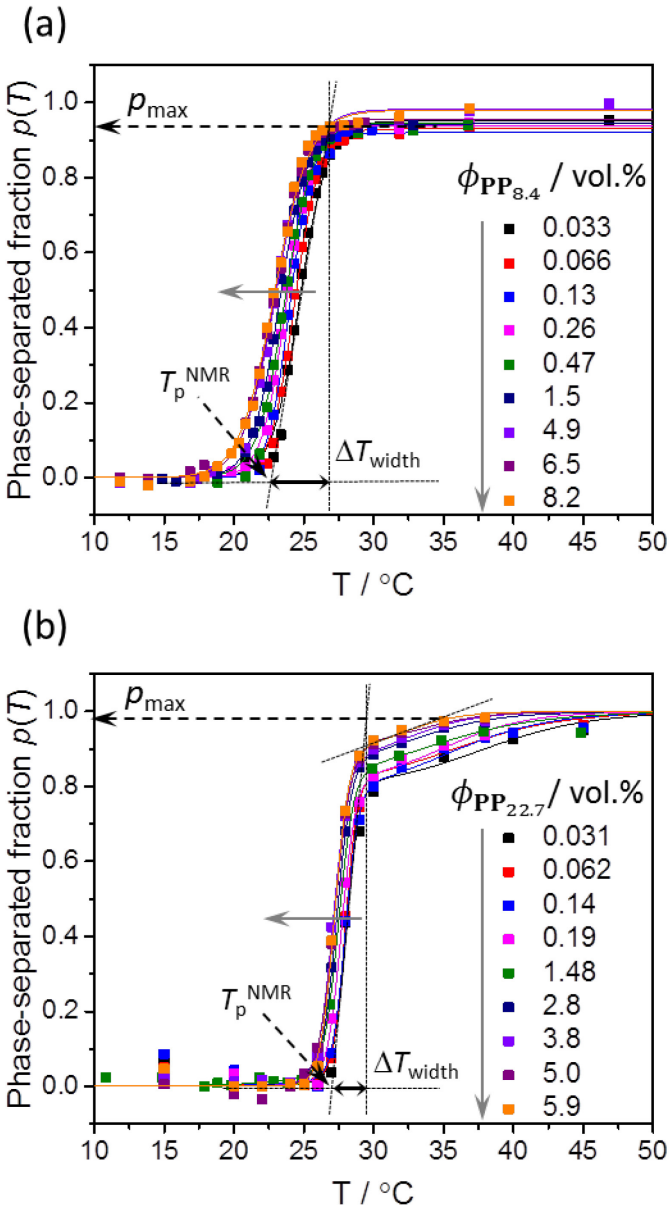

Figure 4.3.2. Temperature dependences of phase-separated fraction $p(T)$ of **PP** (in D_2O) as obtained from the "*b*" resonance of PNIPAM for (a) $\mathbf{PP}_{8.4}$ and (b) $\mathbf{PP}_{22.7}$. Samples with different volume fractions ϕ_{PP} were dissolved in D_2O and measured from 11 to 45 °C. Key: Full squares = experimental points, Solid lines = fits according to equation (11).

DSC is a complementary method to NMR and provides additional information about the phase separation phenomenon. In Figure 4.3.3 are shown selected concentration dependent DSC thermograms for both **PP** conjugates. The thermograms provide information about phase separation temperature (T_p) and enthalpy of the phase separation (ΔH_{DSC}). In Figure 4.3.3, the phase separation of PNIPAM is represented by endothermic peak upon

heating.[6,12,98] Increasing **PP** concentration decreases the phase separation temperature (Figure 4.3.5b), which is in agreement with NMR data as seen in Figure 4.3.5a. The DSC data also display higher T_p values for **PP** with longer PNIPAM chains.

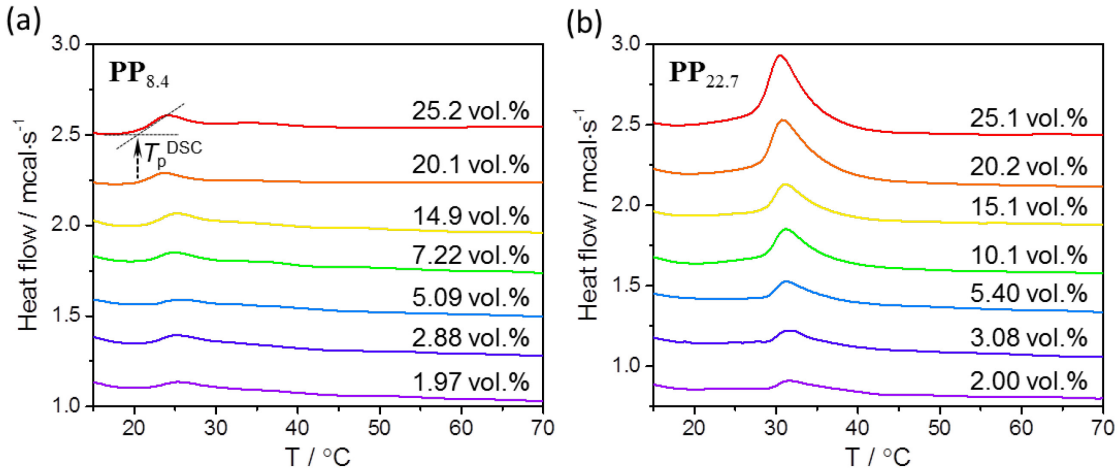

Figure 4.3.3. DSC heating scans at different concentrations for (a) **PP**$_{8.4}$ and (b) **PP**$_{22.7}$ solutions in D_2O.

The enthalpy changes as obtained from NMR (ΔH_{NMR}) using fitting procedure applied on experimental data and enthalpy changes from DSC (ΔH_{DSC}) analysis provide together additional information about the cooperativity of **PP** phase separation process. Assuming that the phase separation is a cooperative process, where the polymer chains (or their parts) undergo a transition as a whole by forming cooperative domains (coop. domains). The dimensional analyses of equation (11) together with the nature of NMR observed quantity (i.e. decrease of intensity of **PP** resonances) as obtained during the phase separation indicate that the ΔH_{NMR} enthalpy values are related to mol of cooperative units.[98] Thus, the comparison of ΔH_{NMR} with ΔH_{DSC} provides an important insight into the polymer cooperativity during the phase separation process. The ratio $\Delta H_{NMR}/\Delta H_{DSC}$ represents the average number of monomer units in one cooperative domain and quantitatively represents the degree of cooperativity.

$$number\ of\ monom.units\ in\ coop.\ domain = \frac{\Delta H_{NMR}(\mathrm{J/mol}\ of\ coop.\ domains)}{\Delta H_{DSC}(\mathrm{J/mol}\ of\ monom.\ unit)} \quad (26)$$

For further calculations, measured DSC values of ΔH_{DSC} in J/g of polymer were recalculated to mol of monomeric units (J/mol of monom. units):

$$\Delta H_{\mathrm{DSC}}(\mathrm{J/mol}\ of\ monom.\ unit) = \Delta H_{DSC}(\mathrm{J/g}\ of\ polymer) \times M_w, \qquad (27)$$

where M_w is the molecular weight in g/mol.

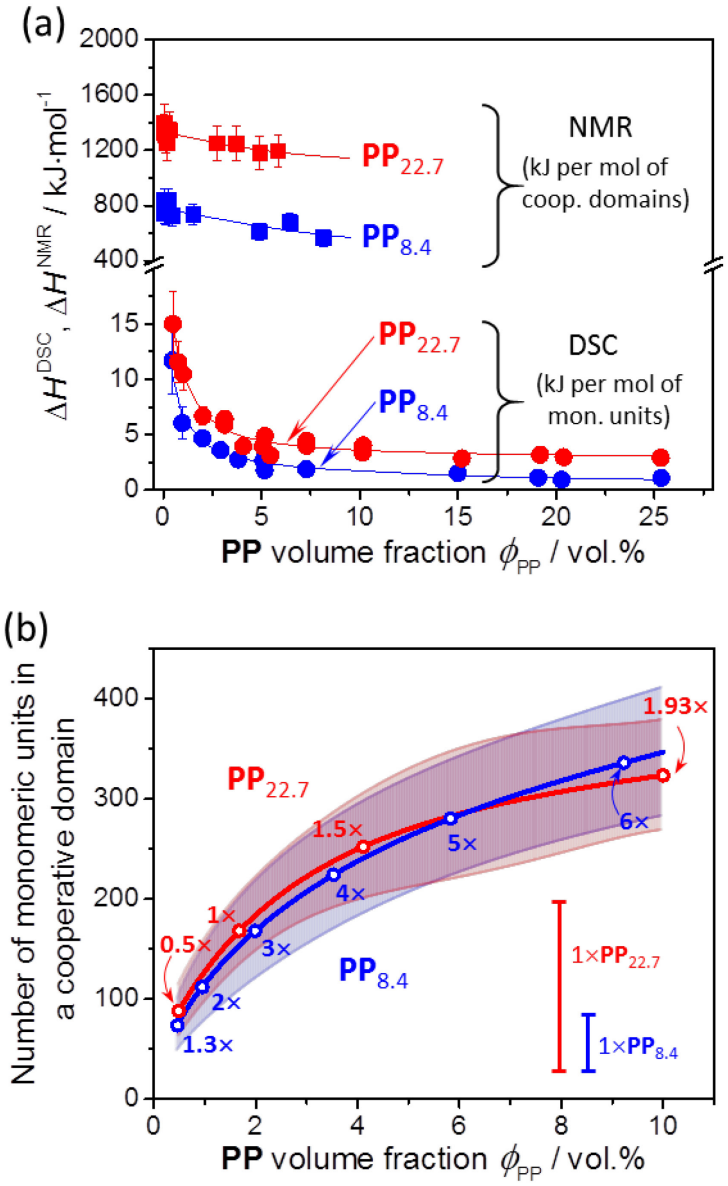

Figure 4.3.4. (a) **PP** volume fraction (in D_2O) dependence of enthalpy changes as obtained from NMR and DSC. (b) **PP** volume fraction (in D_2O) dependence of number of monomer units in a cooperative domain for both **PP** conjugates.

The results obtained from both NMR and DSC techniques show that the enthalpy change (at particular **PP** vol. fraction) is lower for **PP**$_{8.4}$ compare to **PP**$_{22.7}$ and monotonically decreases with concentration (Figure 4.3.4a). Furthermore, increasing the concentration of both **PP**$_{8.4}$ and **PP**$_{22.7}$ leads to an increase in number of monomer units in a cooperative

domain (Figure 4.3.4b). One molecule of **PP**$_{8.4}$ consists on average about 56 NIPAM monomeric units, whereas one molecule of **PP**$_{22.7}$ contains 168 NIPAM units. At the concentration around 2 vol.%, in the case of both **PP**$_{8.4}$ and **PP**$_{22.7}$ conjugates, 168 monomer units of NIPAM form a cooperative domain. It is fairly difficult to estimate whether (at ϕ_{PP} = 1.8 vol.%) the domain is formed by one **PP**$_{22.7}$ molecule or rather by a group of PNIPAM chains from different molecules (the same consideration applies to ca. three molecules of **PP**$_{8.4}$). One can see that at the same concentration roughly the same number of monomeric units form cooperative domain for both **PP** conjugates (Figure 4.3.4b). Thus, despite the different molecular weight of two conjugates, they form cooperative domains consisting of approximately the same number of monomeric units and this number is solely dependent on the weight fraction of conjugate in water.

Figure 4.3.5 shows phase diagrams for **PP**$_{8.4}$ and **PP**$_{22.7}$ as constructed from NMR and DSC data. Theoretical binodal and spinodal curves were derived using the Flory–Huggins (F–H) theory[99-102] and subsequently were used to fit the experimental data.

The F–H mean-field lattice theory provides an expression for the Gibbs free energy of mixing of solvent molecules (D_2O) and **PP** conjugates (treated as star-shaped polymers) in the following form:

$$\Delta G_{\mathrm{mix}} = NRT\left(\phi_1 ln\phi_1 + \frac{1}{r}\phi_2 ln\phi_2 + \chi(T,\phi_2)\phi_1\phi_2\right), \tag{28a}$$

$$\phi_1 = \frac{N_1}{N_1 + rN_2}, \tag{28b}$$

$$\phi_2 = \frac{rN_2}{N_1 + rN_2}, \tag{28c}$$

$$N = N_1 + rN_2, \tag{28d}$$

where N is the number of lattice cells, R is the gas constant, T is the absolute temperature, ϕ_1 and ϕ_2 are the volume fraction of water (D_2O) and **PP** conjugate, respectively, and $\phi_1 + \phi_2 = 1$. Coefficient $r = V_{PP}/V_{D2O}$ is the ratio of volumes of one **PP** conjugate molecule ($V_{PP8.4}$ = 12680 Å^3, $V_{PP22.7}$ = 34267 Å^3) and one D_2O molecule (V_{D2O} = 30.04 Å^3). N_1 and N_2 are the numbers of solvent molecules and **PP** conjugate molecules, respectively. The $\chi(T,\phi_2)$ is the generalized Flory-Huggins interaction parameter dependent on T and also on ϕ_2 in the form of equation (29)[103]:

$$\chi(T,\phi_2) = \alpha T^{-1} + \beta + \gamma\phi_2, \tag{29}$$

where α, β and γ are experimentally determined enthalpy (α) and excess entropy (β and γ) coefficients. The phase behaviour can be derived from equations (28) with the F-H interaction parameter defined in equation (29) based on the criteria for equilibrium (binodal) and limit of stability (spinodal) evaluated at constant temperature and pressure. The conditions for the coexistence of phases (binodal curve) require equality of chemical potentials $\Delta\mu_i$ of both components (i = 1, 2) in both phases (usually called solvent-rich phase I and polymer-rich phase II) which are expressed in equations (30):

$$\Delta\mu_1\left(\phi_2^{\mathrm{I}}\right) = \Delta\mu_1\left(\phi_2^{\mathrm{II}}\right), \tag{30a}$$

$$\Delta\mu_2\left(\phi_2^{\mathrm{I}}\right) = \Delta\mu_2\left(\phi_2^{\mathrm{II}}\right), \tag{30b}$$

where chemical potential $\Delta\mu_i$ is defined as

$$\Delta\mu_i = \left[\frac{\partial\Delta G_{\mathrm{mix}}}{\partial N_i}\right]_{T,p}. \tag{31}$$

Evaluation of equations (30) yields after some rearrangement two non-linear equations which need to be solved simultaneously:

$$\ln\left(\frac{1-\phi_2^{\mathrm{I}}}{1-\phi_2^{\mathrm{II}}}\right) + \left(1-\frac{1}{r}\right)\left(\phi_2^{\mathrm{I}} - \phi_2^{\mathrm{II}}\right) + \left(\frac{\alpha}{T} + \beta - \gamma\right)\left(\phi_2^{\mathrm{I}^2} - \phi_2^{\mathrm{II}^2}\right) + 2\gamma\left(\phi_2^{\mathrm{I}^3} - \phi_2^{\mathrm{II}^3}\right) = 0, \tag{32a}$$

$$\ln\left(\frac{\phi_2^{\mathrm{I}}}{\phi_2^{\mathrm{II}}}\right) + (r-1)\left(\phi_2^{\mathrm{I}} - \phi_2^{\mathrm{II}}\right) + r\left(\frac{\alpha}{T} + \beta\right)\left[\left(1-\phi_2^{\mathrm{I}}\right)^2 - \left(1-\phi_2^{\mathrm{II}}\right)^2\right] + 2r\gamma\left[\phi_2^{\mathrm{I}}\left(1-\phi_2^{\mathrm{I}}\right)^2 - \phi_2^{\mathrm{II}}\left(1-\phi_2^{\mathrm{II}}\right)^2\right] = 0. \tag{32b}$$

It is possible to express T from equation (32a) in the following form (this value is denoted as T_{p} for consistency with experimental data):

$$T_{\mathrm{p}} \equiv T = \frac{-\alpha\left(\phi_2^{\mathrm{I}^2} - \phi_2^{\mathrm{II}^2}\right)}{\ln\left(\frac{1-\phi_2^{\mathrm{I}}}{1-\phi_2^{\mathrm{II}}}\right) + \left(1-\frac{1}{r}\right)\left(\phi_2^{\mathrm{I}} - \phi_2^{\mathrm{II}}\right) + \beta\left(\phi_2^{\mathrm{I}^2} - \phi_2^{\mathrm{II}^2}\right) - \gamma\left(\left(1-2\phi_2^{\mathrm{I}}\right)\phi_2^{\mathrm{I}^2} - \left(1-2\phi_2^{\mathrm{II}}\right)\phi_2^{\mathrm{II}^2}\right)} \tag{33}$$

and it can be substituted into equation (32b) yielding the equation (34):

$$\left(\phi_2^{\mathrm{I}}+\phi_2^{\mathrm{II}}\right)\ln\left(\frac{\phi_2^{\mathrm{I}}}{\phi_2^{\mathrm{II}}}\right)-r\left(\phi_2^{\mathrm{I}}+\phi_2^{\mathrm{II}}-2\right)\ln\left(\frac{1-\phi_2^{\mathrm{I}}}{1-\phi_2^{\mathrm{II}}}\right)+2(r-1)\left(\phi_2^{\mathrm{I}}-\phi_2^{\mathrm{II}}\right)+$$

$$r\gamma\left(\phi_2^{\mathrm{I}}-\phi_2^{\mathrm{II}}\right)^3=0. \quad (34)$$

Equation (34) can be solved using the numerical bisection method in the following manner. We set volume fraction of **PP** conjugate ϕ_2^{I} (which can be also denoted as $\phi_{\mathrm{PP}} \equiv \phi_2^{\mathrm{I}}$ also for consistency with experimental data) as a constant parameter and obtain numerically the solution ϕ_2^{II} of equation (34) in the interval $\phi_2^{\mathrm{II}} \in (0,1)$. The ϕ_2^{I} ($\equiv \phi_{\mathrm{PP}}$) and ϕ_2^{II} values are then input into equation (33), which gives the phase separation temperature T_{p}. By using this approach, we can construct a theoretical binodal curve dependent on r, α, β and γ parameters. These parameters (except r, which is already defined above by volumes of D_2O and **PP** molecules) are determined when the theoretical binodal is fitted to experimental data as seen in Figure 4.3.5 with values of r, α, β and γ showed in Table 3.

The enthalpic parameter α is negative in all cases studied implying a net attractive interaction between D_2O and **PP** molecules (mediated through hydrogen bonds). This is fully consistent with the LCST-type phase diagram.[104] The β and γ parameters are connected with the mechanism of intermolecular packing. Their values are both positive therefore decreasing entropic contribution to the Gibbs free energy of mixing ΔG_{mix}. The value of γ is greater than 0.25 (Table 3) in all the cases studied here, which is consistent with Type II phase diagram typical for PNIPAM polymer.[103,105,106] The Type II phase diagram (with necessary condition $\gamma > 1/6 \approx 0.17$)[107] has off-zero and polymer chain length (almost) independent positioning of critical point.[103,105-107] The positions of critical points ($\phi_{\mathrm{PP}}^{\mathrm{LCST}}$ and T^{LCST}) for each **PP** conjugate obtained using both NMR and DSC methods are shown in Table 3.

In order to calculate the spinodal phase boundary we use the stability condition in the form:

$$\left[\frac{\partial^2 \Delta G_{\mathrm{mix}}}{\partial \phi_2^2}\right]_{T,p}=0. \quad (35)$$

Evaluation of the second derivative and rearrangement gives the spinodal boundary $T_{\mathrm{spin}}(\phi_2)$ in the closed-form expression as:

$$T_{\mathrm{spin}}=\frac{2\alpha r(1-\phi_2)\phi_2}{1+(r-1)\phi_2+2r[\gamma(1-3\phi_2)-\beta](1-\phi_2)\phi_2}. \quad (36)$$

For correspondence with experimental results, note that $\phi_2 \equiv \phi_{\mathrm{PP}}$. The α, β and γ coefficients are those obtained from fitting of binodals (see Table 3) and actual spinodals are plotted in Figure 4.3.6 as dashed lines.

Table 3. Phase diagram parameters as obtained from fitting of Flory–Huggins theory

	PP$_{8.4}$		**PP$_{22.7}$**	
Parameter	DSC	NMR	DSC	NMR
ϕ_{PP}^{LCST} / (vol.%)	20.8	20.8	19.2	19.2
T^{LCST}/ °C	20.4	19.9	26.9	25.5
r	422.1	422.1	1140.7	1140.7
α / K	-936.7	-1118.2	-442.0	-1131.9
β	3.92	4.55	2.20	4.52
γ	0.26	0.26	0.25	0.25

As expected, both DSC and NMR methods provide comparable position of LCST critical point (ϕ_{PP}^{LCST}, T^{LCST}) for each **PP** conjugate. The higher molecular weight **PP**$_{22.7}$ has T^{LCST} about 6 °C higher than **PP**$_{8.4}$, which (as mentioned above) is contrary to expectations for LCST behaviour polymers. Slight differences exist between the LCST (i.e. T^{LCST}) position obtained by NMR and DSC data for each particular **PP** conjugate, with the DSC values being higher. The effect of heating rate (in our case 10 °C/min) during DSC measurements is likely to be responsible for this since it is known that greater heating rates can lead to an increase in the onset temperature of endothermic peaks in DSC. Note that the porphyrin-PNIPAM solution changes its opaque state from transparent red to turbid red upon heating while transitioning from coil to globule state (pictures of vials are shown in Figure 4.3.5a,b).

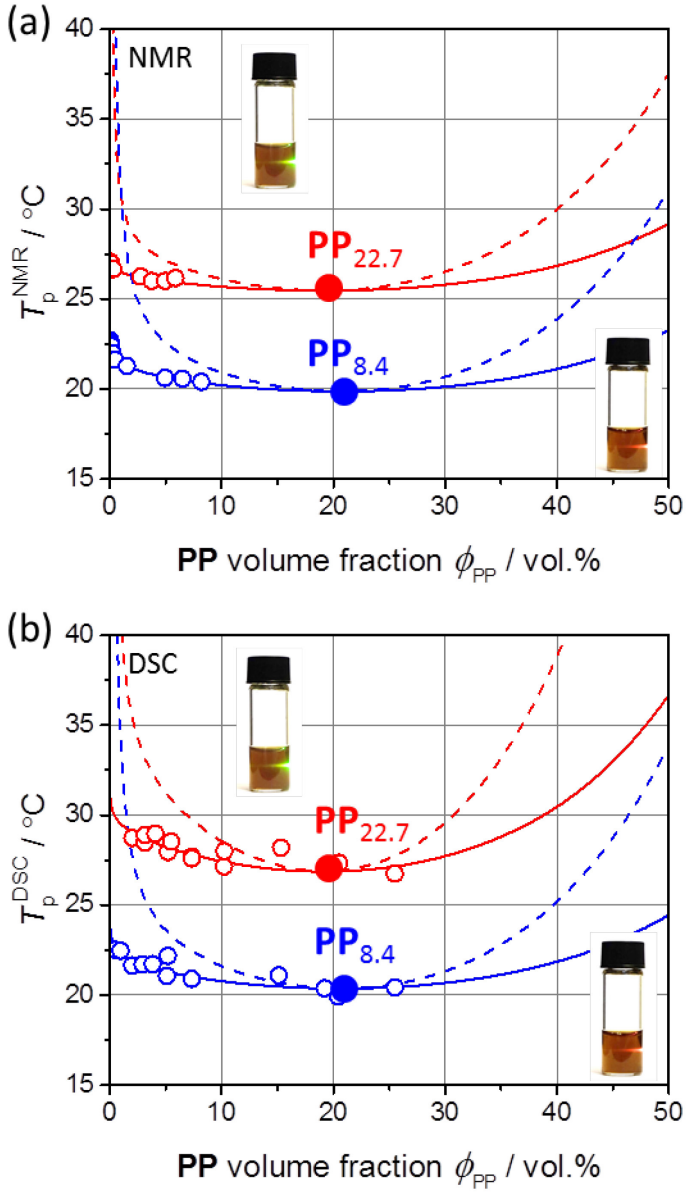

Figure 4.3.5. Phase diagrams of **PP**$_{8.4}$ and **PP**$_{22.7}$ in D_2O from (a) NMR and (b) DSC. Binodal and spinodal curves fitted using Flory–Huggins theory. Photos of **PP**$_{8.4}$ (ϕ_{PP} = 0.45 vol.%) in H_2O at 20 °C (red colour) and 50 °C (turbid red colour). A green light laser pointer (532 nm) is directed (from right side) through the solution to illustrate turbidity.

In order to gain more information about the internal structure of porphyrin-PNIPAM conjugates in D_2O (i.e. sizes and shapes) a SAXS technique was applied. A series of samples at different concentrations of **PP** were measured. **PP**$_{8.4}$ was studied in the concentration range of 0.14-1.44 wt.% and **PP**$_{22.7}$ was studied in the concentration range of 0.13-4.31 wt.%. Obtained data were fitted using SASFit software.[82] The scattering curves of **PP** conjugates

were fitted using two different form factor models, namely: polydisperse spheroids (i.e. ellipsoids with two equal minor axes) at low temperatures ($T < T_p$) and polydisperse spheres at high temperatures ($T > T_p$) with the Schulz-Zimm polydispersity applied to both models. To improve quality of fits, the contribution from large aggregates was added to both models. It should be noted that the scattering data at low temperatures ($T < T_p$) were fitted with a hard sphere model as the first step. However, this model was abandoned due to unrealistically high Schulz-Zimm polydispersity value (0.8-0.9), which was in disagreement with other experimental data.

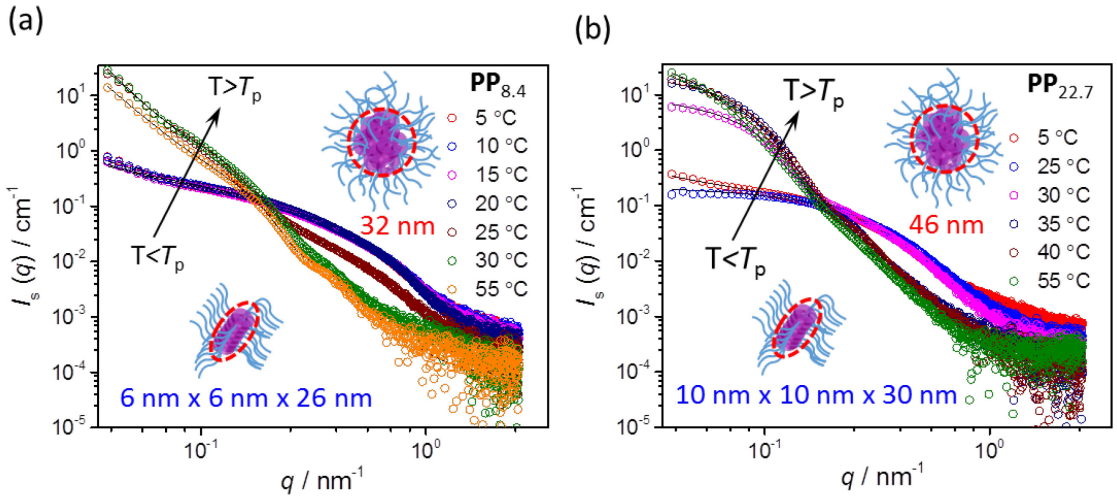

Figure 4.3.6. Scattered intensity I_s as a function of the scattering vector q for (a) $\mathbf{PP}_{8.4}$ (w_{PP} = 0.46 wt.%) and (b) $\mathbf{PP}_{22.7}$ (w_{PP} = 0.43 wt.%) measured at different temperatures. The dimensions of spheroids (ellipsoids with two equal minor axes) at 5 °C and diameter for spheres at 55 °C are calculated according to the SAXS data. Solid lines are fits of SAXS data as obtained from SASFit software.

The scattering curves for $\mathbf{PP}_{8.4}$ at temperatures 5–20 °C have similar shape, which means that the particles are similar in size and structure (Figure 4.3.6a). The $\mathbf{PP}_{8.4}$ molecules in the solution at 5 °C form prolate spheroids with dimensions of 6 nm × 6 nm × 26 nm and a modest polydispersity value of 0.22. However, the scattering curves at elevated temperatures differed from the one at lower temperatures reflecting the change in shape or/and size of the nanostructure. At 25 °C (above T_p) and 30 °C two types of particles were found: prolate spheroids and spheres. Further temperature increase to 55 °C led to the formation of spheres with 32 nm in diameter and a rather low polydispersity value of 0.11. Similar data were obtained for $\mathbf{PP}_{22.7}$: prolate spheroids at $T < T_p$ (10 nm × 10 nm × 30 nm and polydispersity

0.18), prolate spheroids and spheres at 25 °C (close to the phase separation temperature), and spheres at $T > 35$ °C (above T_p) (46 nm and polydispersity 0.45) as seen in Figure 4.3.6b. It is worth to mention that the dimensions of **PP**$_{8.4}$ nanoparticles are generally smaller than **PP**$_{22.7}$ (at the same weight concentration). This molecular weight dependence can be rationalized in terms of higher chance of physical entanglements of **PP** molecules with longer PNIPAM chain.

To summarise, the phase separation phenomenon of porphyrin-PNIPAM conjugates was studied by means of NMR, DSC and SAXS. LCST of **PP** conjugates can be tuned by sample concentration and by changing the length of PNIPAM chains in the opposite manner that is usually expected for LCST-type polymers. Despite the different molecular weight of the two conjugates, they form cooperative domains consisting of approximately the same number of monomeric units and this number is solely dependent on the volume fraction of **PP** conjugate in water. Below phase separation the **PP** conjugates form prolate spheroids, while above the phase separation spheres are formed.

4.3.2 Stacked structures and pH responsiveness (protonation) phenomenon

Small angle X-Ray scattering (SAXS) technique was used for the detection of sizes and shapes of **PP** stacked structures in D_2O at temperature $T = 5$ °C (below T_p). It can be seen that the major axis of prolate spheroids increases with increasing **PP** concentration while the minor axis remains independent of **PP** concentration (Figure 4.3.7a). The minor axes as obtained from SAXS (ca. 6 nm and 9 nm for **PP**$_{8.4}$ and **PP**$_{22.7}$, respectively) are shorter than the diameter across one extended star-shape **PP** conjugate molecule (end-to-end distance) as estimated from its structure (ca. 9 nm and 23 nm for **PP**$_{8.4}$ and **PP**$_{22.7}$, respectively). This is in good agreement since the PNIPAM chains are flexible and tend to form polymer coil structure with shorter average end-to-end distance. Thus, the increase in the size of the major axis indicates that porphyrin cores form aggregates due to π-stacking.[108] The dimensions as obtained from SAXS also allow to estimate number of **PP** molecules in one aggregate. For example, at $w_{PP} = 0.45$ wt.% (Figure 4.3.7), the aggregates formed by **PP**$_{8.4}$ and **PP**$_{22}$ contain about 310 and 370 molecules, respectively. However, their precise structure (J- or H-aggregate) cannot be unambiguously determined from SAXS data. In order to determine the type of aggregated structure absorption (UV-Vis) and emission (PL) spectra of **PP**$_{22.7}$

conjugate in D_2O were measured (Figure 4.3.7b). Soret band in the UV-Vis spectrum is located at 418 nm and maximum of emission in PL spectrum is at 650 nm. This difference, called Stokes shift, is remarkably large and typical for H-aggregates.[109]

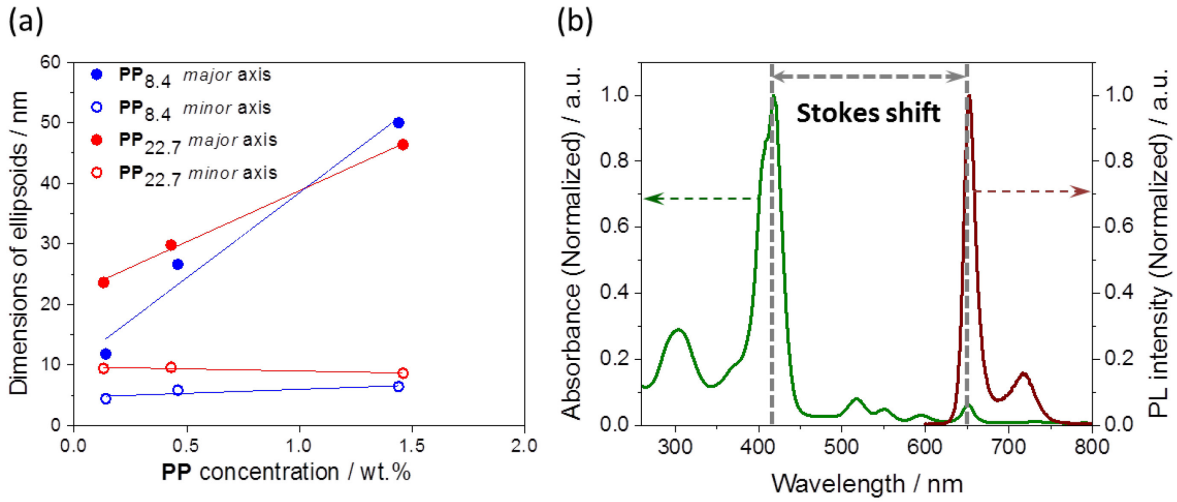

Figure 4.3.7. (a) **PP** stacked structures dimensions as obtained by SAXS: concentration dependence of major and minor axes (i.e. major and minor diameters) of prolate spheroids formed at 5 °C ($T < T_p$) in D_2O. (b) UV-Vis spectrum of $\mathbf{PP}_{22.7}$ (w_{PP} = 0.0027 wt.%) in D_2O at 20 °C (green spectrum). Photoluminescence spectrum (λ_{ex} = 420 nm) of $\mathbf{PP}_{22.7}$ (w_{PP} = 0.011 wt.%) in H_2O at 25 °C (brown spectrum).

Protonation (or equivalently pH responsiveness) of **PP** conjugates was studied by UV-Vis spectrophotometry. The protonation of porphyrin core in the presence of an acid is typically represented by shift of Soret band to the higher wavelength.[55] This behaviour was observed for both **PP** conjugates when the Soret band shifted in the absorption spectrum from about 406-418 nm to 440 nm (Figure 4.3.8). At 20 °C this spectral variation is accompanied with colour change from red to green (Figure 4.3.8a). Furthermore, porphyrin core stays protonated even at 55 °C, when phase separation is already has taken place and the solution colour changed from turbid red to turbid green (Figure 4.3.8b).

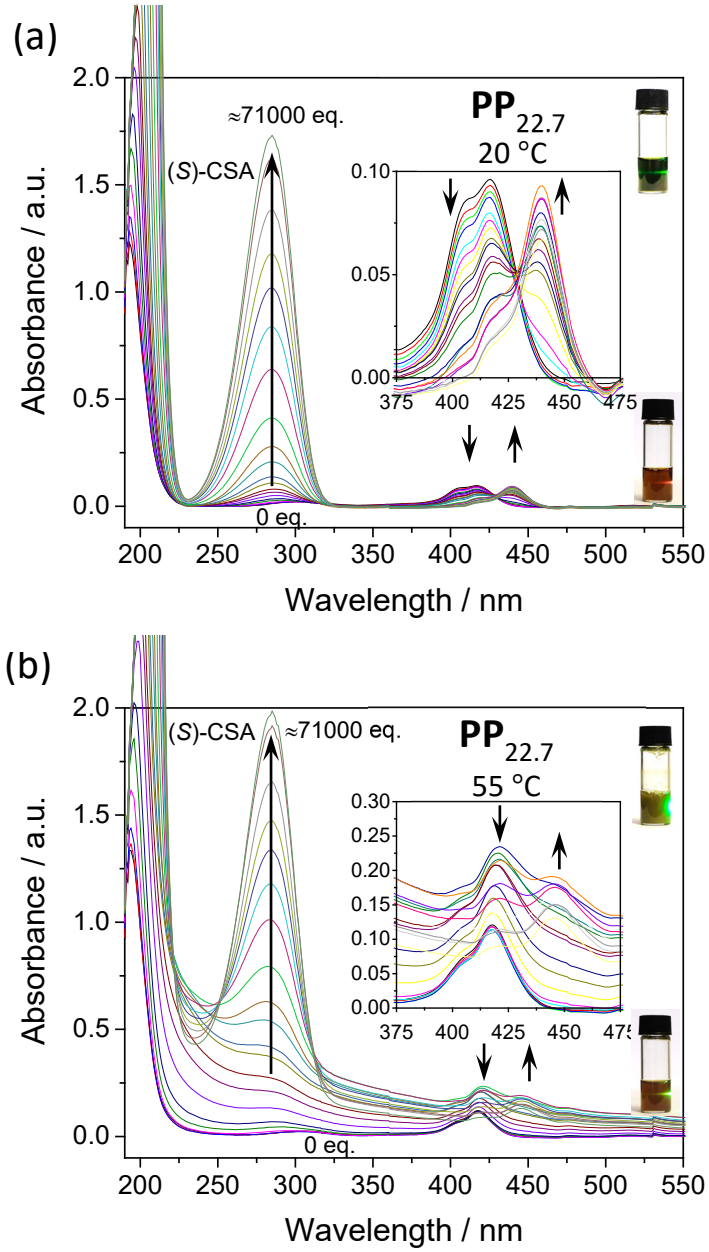

Figure 4.3.8. UV-Vis titration of **PP**$_{22.7}$ in H_2O (w_{PP} = 0.0027 wt.%, c_{PP} = 1.3 μM) with (*S*)-CSA acid at (a) 20 °C and at (b) 55 °C. Final concentration of [(*S*)-CSA] = 111.9 mM. Note that the band at 280 nm corresponds to (*S*)-CSA. The Soret band of porphyrin moiety is located at 420 nm where the protonation effects can be seen. Photos of vials with **PP** (w_{PP} = 0.5 wt.%, c_{PP} = 0.7 mM) solution in H_2O: (a) at 20 °C without acid (red solution; at the bottom) and in the presence of 22 equiv. of (*S*)-CSA acid (15 mM) (green solution; at the top); (b) at 50 °C without acid (turbid red solution; at the bottom) and in the presence of 22 equiv. of (*S*)-CSA acid (15 mM) (turbid green solution; at the top). All vials are irradiated by green light laser pointer (532 nm) from right side.

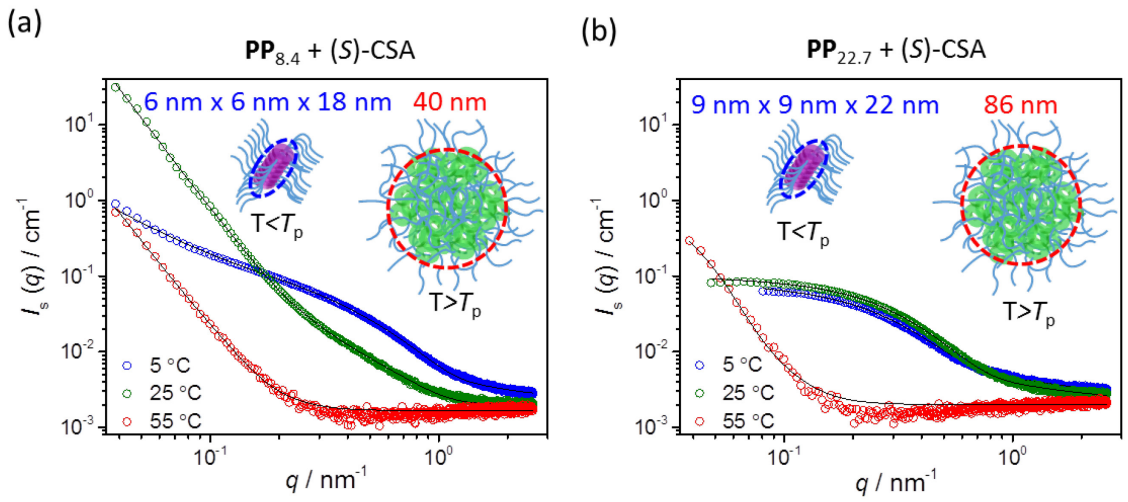

Figure 4.3.9. Scattered intensity I_s as a function of the scattering vector q for (a) **PP**$_{8.4}$ (w_{PP} = 0.46 wt.%) in D_2O at pH ≈ 1.25 ((*S*)-CSA) and (b) **PP**$_{22.7}$ (w_{PP} = 0.43 wt.%) in D_2O at pH ≈ 1.25 ((*S*)-CSA) measured at different temperatures.

Additionally, the pD (equivalent of pH in D_2O) sensitivity of **PP** conjugates in D_2O was confirmed using SAXS technique. Figure 4.3.9 shows the fits of the form factor by the models described in the previous section. These models are in a very good agreement with the experimental data. **PP**$_{8.4}$ and **PP**$_{22.7}$ samples were measured in the presence of (*S*)-CSA, at pD ≈ 1.25. The results obtained for acidic pD are qualitatively similar to neutral pD. In **PP**$_{8.4}$ solution at acidic pD at 5 °C prolate spheroids with the dimensions of 6 nm × 6 nm × 18 nm and polydispersity 0.15 were formed. Close to the phase separation temperature (25 °C) two types of particles were present in the solution: prolate spheroids and spheres. At 55 °C (above T_p) spheres with 40 nm in diameter and a rather low polydispersity value of 0.19 were detected. Similar structures were obtained for **PP**$_{22.7}$ conjugate: prolate spheroids at $T < T_p$ (9 nm × 9 nm × 22 nm and polydispersity 0.19) and spheres both at 25 °C and 55 °C (above T_p) (86 nm in diameter and polydispersity 0.33). Below T_p, rather comparable sizes of prolate spheroids for unprotonated and protonated porphyrin conjugates were observed (Figure 4.3.6a,b with Figure 4.3.9a,b). Whereas above T_p, **PP** conjugates undergo both the phase separation and protonation. The sizes of nanostructures grow from 32 nm to 40 nm for **PP**$_{8.4}$ and from 46 nm to 86 nm for **PP**$_{22.7}$.

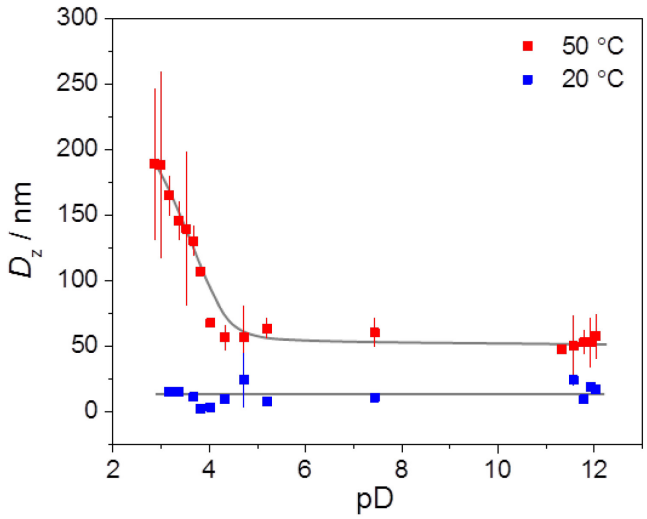

Figure 4.3.10. pD dependence of *z*-average hydrodynamic diameter (D_z) of **PP**$_{22.7}$ (ϕ_{PP} = 0.01 vol.%) solution in D_2O solution at 20 °C and 50 °C. (*S*)-CSA acid and pyridine base were used to set required pD value.

pD dependence of *z*-average hydrodynamic diameter D_z of **PP**$_{22.7}$ at 20 °C and 50 °C was measured by DLS (Figure 4.3.10). Below the phase separation temperature (at 20 °C) the diameter of **PP** structures varies only slightly around 18 nm independently of pD value. While in the phase-separated solution (at 50 °C) the pD has significant effect on the aggregates diameter. At 50 °C and pD > 4 the diameter is about 60 nm, which is consistent with SAXS observations. In more acidic conditions at pD < 4 the hydrodynamic diameter starts rise up to 180 nm. This seems to be associated with protonation of porphyrin units in **PP** conjugates and formation of enlarged globules due to Coulombic repulsion with presumably extra content of water molecules within these globular structures. Thus, pD as well as temperature contribute to the dimensions of particles formed by **PP** conjugates. The pD effect seems to be present solely due to porphyrin core since there is no known strong effect of pD (or pH) on neat PNIPAM in water.

Besides SAXS and DLS, phase separation and protonation processes were also studied by ^{1}H NMR. Figure 4.3.11 shows ^{1}H NMR spectra of **PP**$_{22.7}$ in D_2O at various pD (regulated by (*S*)-CSA) values below (25 °C) and above (45 °C) the phase separation temperature. Narrow peaks from 0.5 to 3 ppm correspond to (*S*)-CSA and partially overlap with PNIPAM resonances. The influence of pD on the phase separation temperature and enthalpy change corresponding to phase separation of **PP** conjugate obtained from NMR are

shown in Figure 4.3.12. ΔH_{NMR} of phase separation and T_p of porphyrin-PNIPAM conjugate remain almost independent from pD. Previously, Kuckling et al. reported similar behaviour of the phase separation temperature of PNIPAM homopolymer at various pH values.[110] Hence, addition of an acid to the aqueous solution of **PP** conjugates protonates the porphyrin cores but interestingly has no influence on the phase separation temperature.

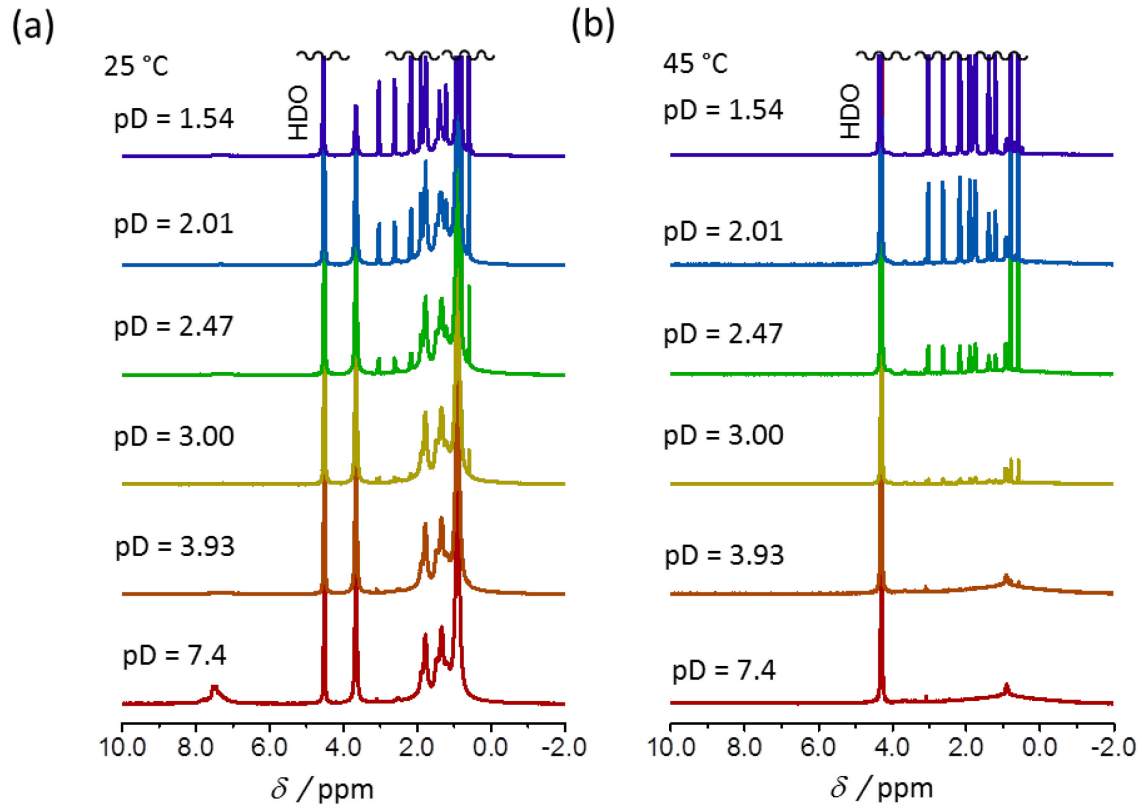

Figure 4.3.11. pD dependence of ^{1}H NMR of **PP**$_{22.7}$ (1.47 vol.%) solution in D_2O measured at (a) 25 °C and (b) 45 °C. pD was set by the addition of (*S*)-CSA acid. The value of pD is given for each spectrum.

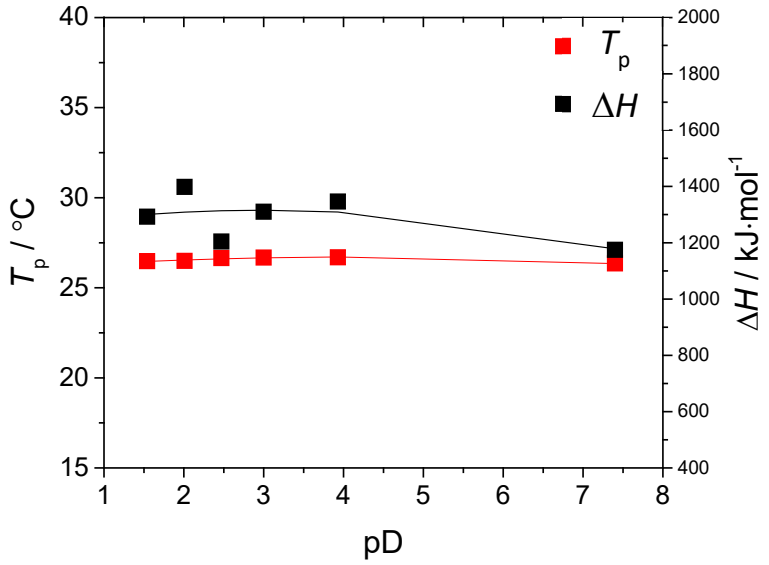

Figure 4.3.12. pD dependence of phase separation temperature T_p (red squares) and pD dependence of enthalpy changes (back squares) for **PP**$_{22.7}$ (ϕ_{PP} = 1.47 vol.%) in D_2O as obtained from NMR measurements. pD was achieved by the addition of (*S*)-CSA.

Figure 4.3.13 shows the temperature dependences of phase-separated fraction during gradual heating and cooling at pD 7.4 and pD 1.54. For both neutral and acidic pD the difference in phase separation temperatures T_p during heating and cooling cycles were about 0.3 °C. This difference is in the range of experimental error and can be considered as insignificant. No notable changes in the width of the phase separation interval during heating and cooling cycles or the number of PNIPAM units that participate in phase separation (p_{max}) were observed. In the literature, there are several cases of PNIPAM hysteresis of about 2 °C, which was found in high molecular weight (1-10 MDa) PNIPAM homopolymer solutions. This hysteresis is attributed to the formation of additional hydrogen bonds formed between carbonyl and amide groups in the globular state, which would behave somewhat like a crosslinker and making demixing (phase separation upon heating) and mixing (one phase formation upon cooling) rather unsymmetrical processes.[111-113] The absence of pronounced hysteresis of **PP** conjugate suggests the formation of relatively loose structures with fully reversible coil-to-globule transition of PNIPAM side-arms of **PP**.

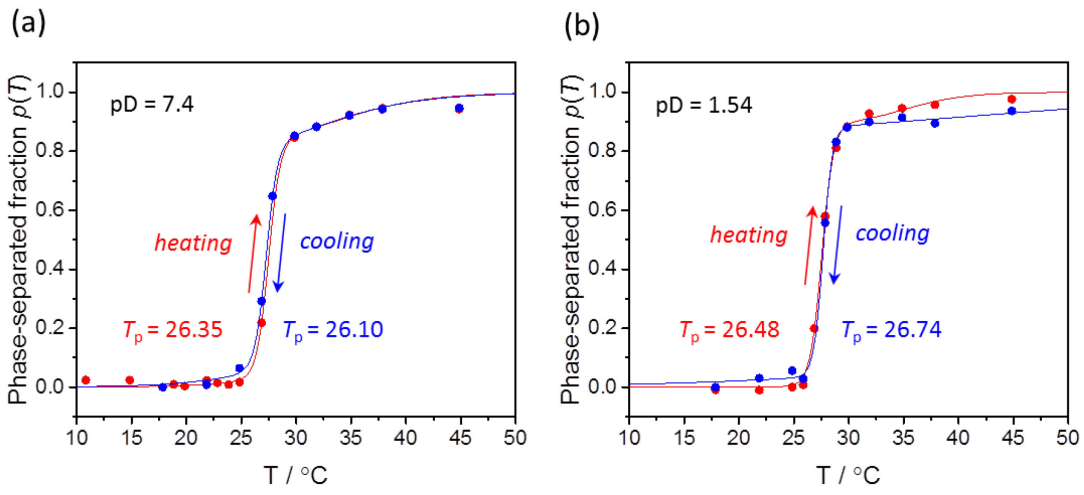

Figure 4.3.13. Temperature dependences of phase-separated fraction $p(T)$ of **PP**$_{22.7}$ (ϕ_{PP} =1.47 vol.%) in D_2O solvent during gradual heating and cooling measured at (a) pD = 7.4 and (b) pD = 1.54. Heating/cooling rate was 0.1 °C/min

In conclusion, pH (or pD) responsiveness and aggregation of **PP** conjugates were studied by UV-Vis, SAXS, NMR, DLS and photoluminescence. The **PP** conjugates form H-aggregates with high aspect ratio prolate spheroids below T_p. In the presence of an acid (below T_p), H-aggregation is slightly suppressed due to repulsion of protonated porphyrin cores. Above T_p, in acidic pH larger spherical particles are formed in comparison to neutral pH due to repulsion of porphyrin cores and phase separation of PNIPAM chains. Basic pH does not influence the size of nanostructures at given temperature. T_p is independent of pH. Thus, the addition of an acid protonates the porphyrin core but does not influence the phase separation temperature. Phase separation of **PP** conjugates is fully reversible both in acidic and neutral pH.

4.3.3 Co-nonsolvency effect

Apart from phase separation and pH responsivity, the co-nonsolvency effect of **PP** in binary mixture of D_2O/MeOH was examined using high resolution NMR spectroscopy. For this analysis **PP** conjugate was dissolved in D_2O/MeOD with different volume fractions ϕ_{MeOD} of MeOD (ranging from 0 to 1) and also measured at several temperatures (20, 30, 40

and 50 °C). Figure 4.3.14 shows phase-separated fraction $p(T)$ of **PP**$_{22.7}$ as a function of solvent composition ϕ_{MeOD}. The data were obtained from NMR spectra using the method as for processing of phase separation of **PP** in pure D_2O (i.e. integration and application of equation (6)).

There are several interesting features in the co-nonsolvency behaviour of **PP**$_{22.7}$ conjugate (Figure 4.3.14). If the MeOD volume fraction is up to 0.2 the **PP**$_{22.7}$ solution exhibits behaviour typical for LCST, i.e. with increasing temperature the fraction of phase-separated **PP**$_{22.7}$ units $p(T)$ increasing. Above 0.2 MeOD volume fraction the behavior is reversed and upon heating the fraction of phase-separated **PP**$_{22.7}$ units $p(T)$ decreasing, which is typical for upper critical solution temperature (UCST) behaviour. Yamauchi and Maeda previously reported the existence of both LCST and UCST behaviour for PNIPAM homopolymer in the co-solvent mixture of DMSO/H_2O.[114] Although, PNIPAM is linked to highly hydrophobic porphyrin unit we still observe typical co-nonsolvency effect similar to PNIPAM homopolymer in water with both LCST and UCST phase behaviours.

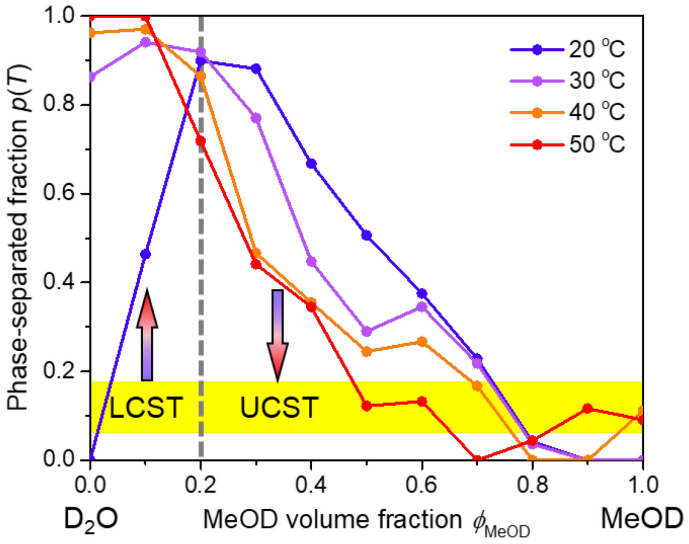

Figure 4.3.14. Dependence of phase-separated fraction $p(T)$ of **PP**$_{22.7}$ conjugate (2 mg/mL) on binary D_2O/MeOD solvent composition ϕ_{MeOD}. The blue-red arrows indicate the direction of heating.

The co-nonsolvatic formation of two phases is visible by the naked eye (see photos of NMR cuvettes in Figure 4.3.15a). The formation of globular structures can be also

observed at microscopic level (see optical micrographs in Figure 4.3.15b). The Figure 4.3.15 shows the co-nonsolvency at two temperatures 25 °C and 50 °C, below and above the phase separation temperature of **PP**$_{22.7}$ in neat water. It can be seen that, for example, at 25 °C the sample is phase-separated (and forms globular structures) in the solvent composition interval $0.2 \leq \phi_{MeOH} \leq 0.6$, which is depicted by enhanced scattering of laser light or by formation of globular structures in optical micrographs (Figure 4.3.15).

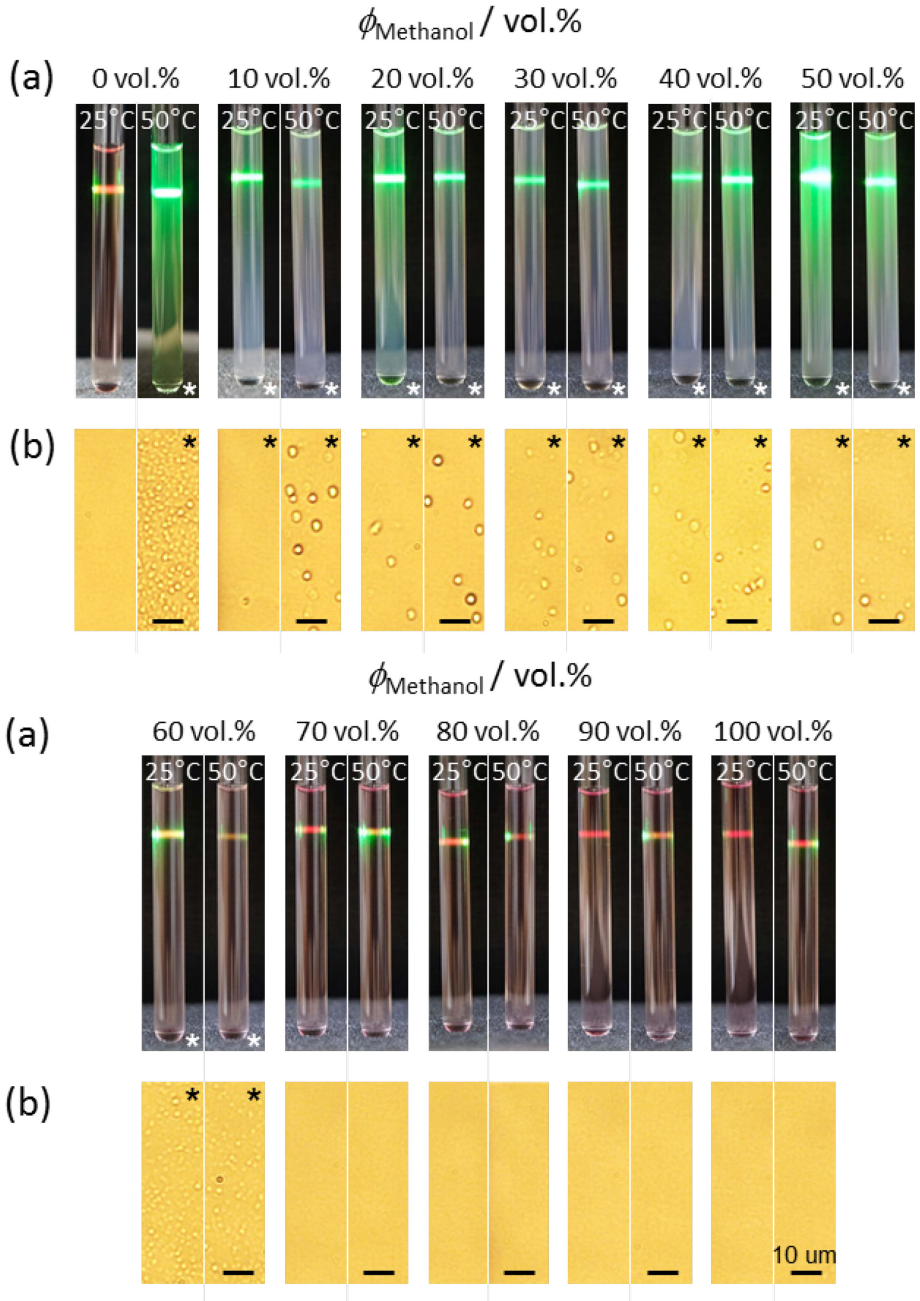

Figure 4.3.15. (a) Photographs of 5 mm NMR cuvettes containing 0.6 mL of **PP**$_{22.7}$ (ϕ_{PP} = 0.18 vol.%) in D_2O/MeOD solution at 25 °C and 50 °C irradiated by green light laser

pointer (532 nm). (b) Optical micrographs of **PP**$_{22.7}$ (ϕ_{PP} = 0.18 vol.%) in H_2O/MeOH mixtures at 25 °C and 50 °C. Partially as well as completely phase-separated samples are highlighted by (white or black) asterisks.

In addition, the co-nonsolvency of **PP**$_{22.7}$ was investigated by DLS at 20 °C and 50 °C (Figure 4.3.16). The dependence of average hydrodynamic diameter of **PP**$_{22.7}$ globules on ϕ_{MeOH} has surprisingly almost identical tendency for both temperatures investigated (20 °C and 50 °C). The only detectable deviation is at $\phi_{MeOH} = 0$ which is also observable in Figure 4.3.15. The diameter of particles (H-aggregates as identified in previous sections) in non-separated solutions is around 17 nm, which is in good agreement with results obtained from SAXS measurements. This value is quite surprisingly the same as in neat MeOH. The DLS analysis further confirms that at 25 °C the phase separation occurs only in the solvent composition interval $0.2 \leq \phi_{MeOH} \leq 0.6$ (Figure 4.3.16). Within this interval the diameter of particles grow monotonically up to about 220 nm (at $\phi_{MeOH} \approx 0.6$) followed by sudden drop back to single phase solution with particle size ca. 17 nm for $\phi_{MeOH} \geq 0.7$.

At constant temperature the change of solvent quality (transition from good to bad solvent and vice versa) is responsible for phase separation of **PP** conjugates. From the literature, the co-nonsolvency effect of PNIPAM in methanol/water mixture is caused by the competitive hydrogen bonding by water and methanol molecules onto the polymer chain.[38,115,116] In the standard formulation of co-nonsolvency theory there are three types of hydrogen bonding interactions: between PNIPAM–water, PNIPAM–methanol and water–methanol. If one interaction dominates the other two are relatively suppressed and phase separation occurs. The co-nonsolvency effect of PNIPAM is the strongest at 0.35 mole fraction of methanol in water, which converted to volume fraction is $\phi_{MeOH} \approx 0.55$, very close to the point where the larges **PP** particles are formed (Figure 4.3.16). At $\phi_{MeOH} \approx 0.55$ the interaction between methanol and water molecules is the strongest and in the same time the interaction between PNIPAM part of **PP** with water and methanol become the lowest, which results in phase separation. Further increase of ϕ_{MeOH} leads to **PP** mixing back into solution mainly due to increase of PNIPAM–methanol and decrease of water–methanol interactions. This is represented by abrupt decrease of particles diameter at $\phi_{MeOH} \geq 0.7$ (Figure 4.3.16).

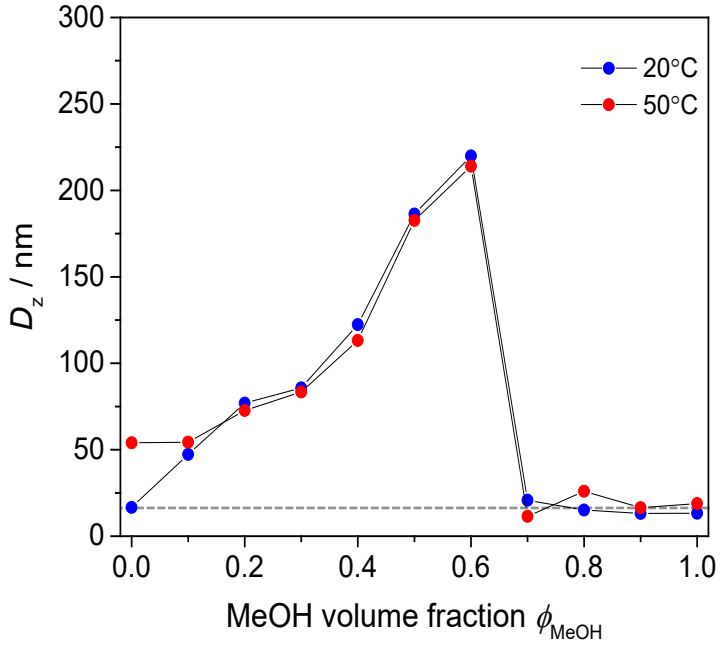

Figure 4.3.16. Dependence of hydrodynamic diameter D_z (*z*-average) of **PP**$_{22.7}$ (ϕ_{PP} = 0.01 vol.%) on MeOH volume fraction ϕ_{MeOH} in binary H_2O/MeOH solvent at 20 °C and 50 °C. Gray dashed baseline indicates diameter of particles in non-separated solutions ($D_z \approx 17$ nm).

In summary, the co-nonsolvency effect was studied by the means of NMR, DLS and optical microscope. The **PP** conjugate shows characteristic polymer property in water/methanol mixtures with both LCST and UCST behaviours. At methanol volume fraction of around ϕ_{MeOH} = 0.6 the interaction between the two solvent molecules is the strongest, thus observed dimensions of **PP** particles in the phase-separated solution are the biggest (ca. 220 nm) due to the strong co-nonsolvency effect which promotes the hydrophobic polymer-polymer interactions over the interactions polymer-solvent.

Conclusions

In this work, the phase separation phenomenon of temperature-sensitive polymers (PVME and PNIPAM) in the presence of additives (*t*-BuAM, *t*-BuOH, *t*-BuME, *t*-BuMK) has been investigated (chapters 4.1 and 4.2). Additionally, the phase behaviour of star-shaped porphyrin-PNIPAM conjugates was studied during variation of temperature, pH and composition of binary water/methanol solvent mixtures (chapter 4.3).

In Chapters 4.1 and 4.2, ^{1}H NMR and time-resolved ^{1}H NMR spin-spin relaxation time T_2 measurements were used for the characterization of structural changes at the molecular level and to determine the behaviour of water and additive molecules during the temperature-induced phase separation of PVME and PNIPAM in D_2O solutions. In the case of both PVME and PNIPAM polymers, concentration has a relatively unimportant effect on phase separation temperature T_p while the concentration of the additive has a modest effect on T_p. T_p of PVME and PNIPAM is influenced by the properties of additives (i.e. hydrophobicity and pK_a) and decreases in the following order: *t*-BuAM > *t*-BuOH > *t*-BuME > *t*-BuMK. This behaviour can be attributed to the hydrophobic association of the abovementioned additives with the polymer chains. Of the additives used here, *t*-BuMK has the strongest effect on T_p of PVME and PNIPAM with decreases in T_p of ca. 15–20 °C and T_p ca. 10 °C, respectively. There is also a notable stabilizing effect of *t*-BuAM on PVME with an increase in T_p of ca. 2–4 °C probably being due to the interaction of the NH_2 group of *t*-BuAM with the ether oxygen atoms of PVME. Moreover, the additives promote extension of the phase separation temperature interval of PNIPAM by up to ca. 5 °C (upon addition of *t*-BuMK) and of PVME by up to ca. 15 °C (upon addition of *t*-BuMK).

The dynamics of water and additive molecules below and above the phase separation temperature was studied in NMR relaxation experiments. Two different modes of phase separation could be identified from spin-spin relaxation time T_2 measurements. For the PNIPAM system with additives, spin-spin relaxation time T_2 measurements revealed that water and additive molecules are spatially restricted in the globular structures adopted by the polymer chains after phase separation. The presence of additives has a stabilizing effect on mesoglobular PNIPAM structures within 3-8 days, depending on the additive. A similar stabilizing effect was observed for the PVME system with *t*-BuAM. In that case, no solvent molecules were released over a timescale of 1.5~3 days leaving the thus formed globules rather rigid. However, in the presence of *t*-BuOH or *t*-BuMK some portion of water and

additive molecules were released over time from the resulting PVME globules leading to mesoglobules with a sponge-like structure. Therefore, the stabilizing effect is highly dependent on the balance of additive-polymer and additive-solvent interactions.

Chapter 4.3 presents a rigorous study of novel porphyrin-PNIPAM conjugates showing temperature, pH and binary solvent composition sensitivity. During phase separation, the opacity of the samples is changed from transparent red to turbid red. The temperature-induced phase separation phenomenon for porphyrin-PNIPAM (**PP**) conjugates was studied by using NMR, DSC and SAXS. We observed that LCST of **PP** conjugates can be weakly affected according to **PP** concentration while the length of appended PNIPAM chains at the periphery of the porphyrin unit has a large effect. This dependence on molecular weight is in contrast to that usually observed in LCST polymeric systems (where higher molecular weight lowers LCST). Despite the difference in molecular weight of the two conjugates, they both form cooperative domains consisting of approximately the same number of monomer units and this number is solely dependent on volume (weight) fraction of conjugate in water.

The aggregation state and its dependence on pH (or equivalently pD in D_2O) of **PP** conjugates was studied by means of UV-Vis, SAXS, NMR, DLS and photoluminescence spectroscopy. Below the phase separation temperature, **PP** conjugates form H-aggregates with prolate spheroidal shape, while at temperatures above the phase separation spheres are formed. In the presence of an acid, aggregation is suppressed slightly because of coulombic repulsion of porphyrin cores. Above T_p at acidic pH (< 4), spherical particles up to about 3× larger in diameter are formed than at neutral pH due to repulsion of protonated porphyrin cores and phase separation of PNIPAM chains. This effect seems to be present solely due to porphyrin core since there is no known strong effect of pH on neat PNIPAM in water.

Basic pH does not influence the dimensions of the nanostructures. T_p was found to be nearly independent of pH. Thus, the addition of an acid protonates the porphyrin core but does not influence the phase separation temperature. On addition of acid, the samples change colour from red to green accompanied by a variation in the geometry of the porphyrin core from flat to saddle-like shape. Phase separation of **PP** conjugates is fully reversible both under acidic or neutral pH conditions.

The co-nonsolvency effect was studied by NMR, DLS and optical microscopy. This effect manifests itself macroscopically as a change in turbidity of the solution from transparent red to opaque red. **PP** conjugates show characteristic PNIPAM properties in

binary water/methanol mixtures. LCST as well as UCST phase separation behaviour can be observed depending on the content of methanol in binary mixture (at constant temperature). The interaction between water and methanol molecules is the strongest at 0.6 volume fraction of methanol, which in turn leading to a relative suppression of the interactions between **PP** and both solvent molecules and results in formation of large **PP** aggregates.

References

1. Manouras T., Vamvakaki M., Field responsive materials: photo-, electro-, magnetic- and ultrasound-sensitive polymers. *Polym Chem*. **8**, 74-96 (2017)
2. Roy D, Brooks W.L.A, Sumerlin B.S., New directions in thermoresponsive polymers. *Chem Soc Rev.* **42**, 7214 (2013)
3. Liu F., Urban M.W., Recent advances and challenges in designing stimuli-responsive polymers. *Prog Polym Sci*. **35**, 3-23 (2010)
4. Schmaljohann D., Thermo- and pH-responsive polymers in drug delivery. *Adv Drug Deliv Rev*. **58**, 1655-1670 (2006)
5. Roy D., Cambre J.N., Sumerlin B.S., Future perspectives and recent advances in stimuli-responsive materials. *Prog Polym Sci.* **35**, 278-301 (2010)
6. Tiktopulo E.I., Uversky V.N., Lushchik V.B., Klenin S.I., Bychkova V.E., Ptitsyn O.B., "Domain" Coil-Globule Transition in Homopolymers. *Macromolecules*. **28**, 7519-7524 (1995)
7. Spěváček J., Hanyková L., Labuta J., Behavior of Water during Temperature-Induced Phase Separation in Poly(vinyl methyl ether) Aqueous Solutions. NMR and Optical Microscopy Study. *Macromolecules*. **44**, 2149-2153 (2011)
8. Starovoytova L, Spěváček J, Trchová M. ^{1}H NMR and IR study of temperature-induced phase transition of negatively charged poly(*N*-isopropylmethacrylamide-co-sodium methacrylate) copolymers in aqueous solutions. *Eur Polym J*. **43**, 5001-5009 (2007)
9. Müller A.H.E., Borisov O., *Self Oraganized Nanostructures of Amphiphilic Block Copolymers II*. Eds. Springer Berlin Heidelberg: **242** (2011)
10. Aseyev V., Tenhu H., Winnik F.M., Non-ionic Thermoresponsive Polymers in Water. *Romanian Reports of Physics*. **54**, 29-89 (2010)
11. Ward M.A., Georgiou T.K., Thermoresponsive Polymers for Biomedical Applications. *Polymers*. **3**, 1215-1242 (2011)
12. Aseyev V.O., Tenhu H., Winnik F.M., Temperature Dependence of the Colloidal Stability of Neutral Amphiphilic Polymers in Water. *Adv Polym Sci*. **196**, 1-85 (2006)
13. Filippov S.K., Verbraeken B., Konarev P.V., *et al*. Block and Gradient Copoly(2-oxazoline) Micelles: Strikingly Different on the Inside. *J Phys Chem Lett*. **8**, 3800-3804 (2017)
14. Bogomolova A., Filippov S.K., Starovoytova L., *et al*. Study of Complex Thermosensitive Amphiphilic Polyoxazolines and Their Interaction with Ionic Surfactants.

Are Hydrophobic, Thermosensitive, and Hydrophilic Moieties Equally Important? *J Phys Chem B*. **118**, 4940-4950 (2014)

15. Atkins P., de Paula J., *Physical Chemistry*. 9th ed. Oxford University Press, (2010)

16. Shiraga K., Naito H., Suzuki T., Kondo N., Ogawa Y., Hydration and Hydrogen Bond Network of Water during the Coil-to-Globule Transition in Poly(*N*-isopropylacrylamide) Aqueous Solution at Cloud Point Temperature. *J Phys Chem B*. **119**, 5576-5587 (2015)

17. Sood N., Bhardwaj A., Mehta S., Mehta A., Stimuli-responsive hydrogels in drug delivery and tissue engineering. *Drug Deliv*. **23**, 748-770 (2016)

18. Jeong B., Gutowska A., Lessons from nature: stimuli-responsive polymers and their biomedical applications. *Trends Biotechnol*. 20, 305-311 (2002)

19. Maharjan P., Woonton B.W., Bennett L.E., Smithers G.W., DeSilva K., Hearn M.T.W., Novel chromatographic separation — The potential of smart polymers. *Innov Food Sci Emerg Technol*. **9**, 232-242 (2008)

20. Aseyev V., Hietala S., Laukkanen A., *et al*. Mesoglobules of thermoresponsive polymers in dilute aqueous solutions above the LCST. *Polymer*. *46*, 7118-7131 (2005)

21. Hanyková L., Labuta J., Spěváček J., NMR study of temperature-induced phase separation and polymer–solvent interactions in poly(vinyl methyl ether)/D_2O/ethanol solutions. *Polymer*. **47**, 6107-6116 (2006)

22. Maeda Y., Yamamoto H., Ikeda I., Micro-Raman Spectroscopic Investigation on the Phase Separation of Poly(vinyl methyl ether)/Alcohol/Water Ternary Mixtures. *Langmuir*. **20**, 7339-7341 (2004)

23. Maeda Y., IR Spectroscopic Study on the Hydration and the Phase Transition of Poly(vinyl methyl ether) in Water. *Langmuir*. **17**, 1737-1742 (2001)

24. Yang H.E., Bae Y.C., Thermodynamic analysis of phase equilibrium and surface tension of ternary polymer solutions. *AIChE J*. **65**, 1-10 (2019)

25. Maeda Y., Yamamoto H., Ikeda I., The Association of Tetraalkylammonium Ions with Poly(vinyl methyl ether) in Water and its Effect on Phase-Separation Behavior as Studied by Micro-Raman Spectroscopy. *Macromol Rapid Commun*. **25**, 720-723 (2004)

26. Durme K. Van., Rahier H., Mele B. Van., Influence of Additives on the Thermoresponsive Behavior of Polymers in Aqueous Solution. **38**, 10155-10163 (2005)

27. Spěváček J., Hanyková L., ^{1}H NMR Relaxation Study of Polymer-Solvent Interactions during Thermotropic Phase Transition in Aqueous Solutions. *Macromol Symp*. **203**, 229-237 (2003)

28. Spěváček J., Hanyková L., ^{1}H NMR Study on the Hydration during Temperature-Induced Phase Separation in Concentrated Poly(vinyl methyl ether)/D_2O Solutions. *Macromolecules*. **38**, 9187-9191 (2005)

29. Philipp M., Aleksandrova R., Müller U., *et al*. Molecular versus macroscopic perspective on the demixing transition of aqueous PNIPAM solutions by studying the dual character of the refractive index. *Soft Matter*. **10**, 7297-7305 (2014)

30. Heskins M., Guillet J.E., Solution Properties of Poly(*N*-isopropylacrylamide). *J Macromol Sci Part A - Chem*. **2**, 1441-1455 (1968)

31. Lanzalaco S., Armelin E., Poly(*N*-isopropylacrylamide) and Copolymers: A Review on Recent Progresses in Biomedical Applications. *Gels*. **3**, 36 (2017)

32. Mano J.F., Stimuli-Responsive Polymeric Systems for Biomedical Applications. *Adv Eng Mater*. **10**, 515-527 (2008)

33. Dalgicdir C., Rodríguez-Ropero F., van der Vegt N.F.A., Computational Calorimetry of PNIPAM Cononsolvency in Water/Methanol Mixtures. *J Phys Chem B*. **121**, 7741-7748, (2017)

34. Dimitrov I., Trzebicka B., Müller A.H.E., Dworak A., Tsvetanov C.B., Thermosensitive water-soluble copolymers with doubly responsive reversibly interacting entities. *Prog Polym Sci*. **32**, 1275-1343 (2007)

35. Winnik F.M., Ringsdorf H., Venzmer J., Methanol-water as a co-nonsolvent system for poly(*N*-isopropylacrylamide). *Macromolecules*. **23**, 2415-2416 (1990)

36. Pica A., Graziano G., An alternative explanation of the cononsolvency of poly(*N*-isopropylacrylamide) in water–methanol solutions. *Phys Chem Chem Phys*. **18**, 25601-25608 (2016)

37. Xue N., Qiu X-P., Aseyev V., Winnik F.M., Nonequilibrium Liquid–Liquid Phase Separation of Poly(*N*-isopropylacrylamide) in Water/Methanol Mixtures. *Macromolecules*. **50**, 4446-4453 (2017)

38. Tanaka F., Koga T., Winnik F.M., Temperature-responsive polymers in mixed solvents: Competitive hydrogen bonds cause cononsolvency. *Phys Rev Lett.* **101**, 028302 (2008)

39. Zhang G., Wu C., The water/methanol complexation induced reentrant coil-to-globule-to-coil transition of individual homopolymer chains in extremely dilute solution. *J Am Chem Soc*. **123**, 1376-1380 (2001)

40. Zhang Y., Furyk S., Bergbreiter D.E., Cremer P.S., Specific Ion Effects on the Water Solubility of Macromolecules: PNIPAM and the Hofmeister Series. *J Am Chem Soc*. **127**, 14505-14510 (2005)

41. Costa M.C.M., Silva S.M.C., Antunes F.E., Adjusting the low critical solution temperature of poly(*N*-isopropylacrylamide) solutions by salts, ionic surfactants and solvents: A rheological study. *J Mol Liq*. **210**, 113-118 (2015)

42. Shechter I., Ramon O., Portnaya I., Paz Y., Livney Y.D., Microcalorimetric Study of the Effects of a Chaotropic Salt, KSCN, on the Lower Critical Solution Temperature (LCST) of Aqueous Poly(*N*-isopropylacrylamide) (PNIPA) Solutions. *Macromolecules*. **43**, 480-487 (2010)

43. Najafi M., Hebels E., Hennink W.E., Vermonden T., Poly(*N*-isopropylacrylamide): Physicochemical Properties and Biomedical Applications. In: *Temperature-Responsive Polymers: Chemistry, Properties, and Applications;* Khutoryanskiy, V.V., Georgiou, K., Eds.; John Wiley & Sons; 1-34 (2018)

44. Schild H.G., Poly(*N*-isopropylacrylamide): experiment, theory and application. *Prog Polym Sci*. **17**, 163-249 (1992)

45. Li M., Ishihara S., Ji Q., Akada M., Hill J.P., Ariga K., Paradigm shift from self-assembly to commanded assembly of functional materials: Recent examples in porphyrin/fullerene supramolecular systems. *Sci Technol Adv Mater*. **13**, 1-14 (2012)

46. Stone A., Fleischer E.B., The molecular and crystal structure of porphyrin diacids. *J Am Chem Soc.* **90**, 2735-2748 (1968)

47. Hill J.P., Subbaiyan N.K., D'Souza F., *et al*. Antioxidant-substituted tetrapyrazinoporphyrazine as a fluorescent sensor for basic anions. *Chem Commun*. **48**, 3951-3953 (2012)

48. Ishihara S., Hill J.P., Shundo A., *et al*. Reversible Photoredox Switching of Porphyrin-Bridged Bis-2,6-di- tert -butylphenols. *J Am Chem Soc*. **133**, 16119-16126 (2011)

49. Starnes S.D., Arungundram S., Saunders C.H., Anion sensors based on β,β′-disubstituted porphyrin derivatives. *Tetrahedron Lett*. **43**, 7785-7788 (2002)

50. Dolphin D., *The Porphyrins. Physical Chemistry, Part C*, Academic Press, **5**, 303 (2012)

51. Siddiqui S., Spano F.C., H- and J-aggregates of conjugated polymers and oligomers. *Chem Phys Lett*. **308**, 99-105 (1999)

52. Senge M., Ryan A., Letchford K., MacGowan S., Mielke T., Chlorophylls, Symmetry, Chirality, and Photosynthesis. *Symmetry*. **6**, 781-843 (2014)

53. Hestand N.J., Spano F.C., Expanded Theory of H- and J-Molecular Aggregates: The Effects of Vibronic Coupling and Intermolecular Charge Transfer. *Chem Rev*. **118**, 7069-7163 (2018)

54. Maiti N.C., Mazumdar S., Periasamy N., J- and H-aggregates of porphyrin - Surfactant complexes: Time-resolved fluorescence and other spectroscopic studies. *J Phys Chem B*. **102**, 1528-1538 (1998)

55. Zakavi S, Omidyan R, Talebzadeh S. The influence of protonation on the structure and spectral properties of porphine: UV-vis, ^{1}H NMR and *ab* initio studies. *RSC Adv*. **6**, 82219-82226 (2016)

56. Labuta J., Futera Z., Ishihara S., *et al*. Chiral Guest Binding as a Probe of Macrocycle Dynamics and Tautomerism in a Conjugated Tetrapyrrole. *J Am Chem Soc*. **136**, 2112-2118 (2014)

57. Labuta J., Ishihara S., Šikorský T., *et al*. NMR spectroscopic detection of chirality and enantiopurity in referenced systems without formation of diastereomers. *Nat Commun*. **4**, 2188 (2013)

58. Hill J.P., Schumacher A.L., D'Souza F., *et al*. Chromogenic indicator for anion reporting based on an *N*-substituted oxoporphyrinogen. *Inorg Chem*. **45**, 8288-8296 (2006)

59. Ishihara S., Labuta J., Šikorský T., *et al*. Colorimetric detection of trace water in tetrahydrofuran using *N*,*N*′-substituted oxoporphyrinogens. *Chem Commun*. **48**, 3933-3935 (2012)

60. Hunter C.A., Sanders J.K.M., The Nature of π-π Interactions. *J Am Chem Soc*. **112**, 5525-5534 (1990)

61. Ishihara S., Labuta J., Van Rossom W., *et al*. Porphyrin-based sensor nanoarchitectonics in diverse physical detection modes. *Phys Chem Chem Phys*. **16**, 9713-9746 (2014)

62. Cheng H., Fan G-L., Fan J-H., *et al*. Ratiometric theranostic nanoprobe for pH imaging-guided photodynamic therapy. *Nanoscale*. **11**, 9008-9014 (2019)

63. Huang B., Tian J., Jiang D., Gao Y., Zhang W., NIR-Activated "OFF/ON" Photodynamic Therapy by a Hybrid Nanoplatform with Upper Critical Solution Temperature Block Copolymers and Gold Nanorods. *Biomacromolecules*. **20**, 3873-3883 (2019)

64. Zhao Y., Zhang Z., Lu Z., Wang H., Tang Y., Enhanced Energy Transfer in a Donor–Acceptor Photosensitizer Triggers Efficient Photodynamic Therapy. *ACS Appl Mater Interfaces*. **11**, 38467-38474 (2019)

65. Thordarson P., Determining association constants from titration experiments in supramolecular chemistry. *Chem Soc Rev*. **40**, 1305-1323 (2011)

66. Shundo A., Ishihara S., Labuta J., *et al*. Colorimetric visualization of acid–base equilibria in non-polar solvent. *Chem Commun*. **49**, 6870-6872 (2013)

67. Shu X., Wang Y., Zhang S., Huang L., Wang S., Hua D., Determination of trace uranyl ion by thermoresponsive porphyrin–terminated polymeric sensor. *Talanta*. **131**, 198-204 (2015)

68. Yan Q., Jinying Y., Kang Y., Cai Z., Zhou L. and Yin Y., Dual-sensing porphyrin-containing copolymer nanosensor as full-spectrum colorimeter and ultra-sensitive thermometer. *Chem. Commun*., **46**, 2781–2783 (2010)

69. Encyclopedia Britannica, https://www.britannica.com/topic/Nobel-Prize/Physics (web page accessed on June 20, 2020)

70. Günther H., *NMR Spectroscopy: Basic Principles, Concepts and Applications in Chemistry*. 3rd Edition, Wiley-VCH, 734 (2013)

71. Levitt M. H., *Spin Dynamics: Basics of Nuclear Magnetic Resonance*, 2nd Edition, 740, Wiley, (2008)

72. Jacobsen N.E., *NMR Spectroscopy Explained: Basic Principles, Concepts and Applications in Chemistry*. John Wiley & Sons, Inc., Hoboken, New Jersey (2007)

73. Rao B. D. N., Kemple M. D., *NMR as a Structural Tool for Macromolecules. Current Status and Future Directions.* Plenum Press, 382 (1996)

74. Velychkivska N., Starovoytova L., Březina V., Hanyková L., Hill J.P., Labuta J., Improving the Colloidal Stability of Temperature-Sensitive Poly(*N*-isopropylacrylamide) Solutions Using Low Molecular Weight Hydrophobic Additives. *ACS Omega*. **3**, 11865-11873 (2018)

75. Velychkivska N., Bogomolova A., Filippov S.K., Starovoytova L., Labuta J., Thermodynamic and kinetic analysis of phase separation of temperature-sensitive poly(vinyl methyl ether) in the presence of hydrophobic *tert*-butyl alcohol. *Colloid Polym Sci*. 295, 1419-1428 (2017)

76. Odian G., *Radical Chain Polymerization*. In: Principles of Polymerization, 4th edition, John Wiley & Sons, Inc., Hoboken, New Jersey, 198-349 (2004)

77. Spěváček J., Hanyková L., Starovoytova L., ^{1}H NMR Relaxation Study of Thermotropic Phase Transition in Poly(vinyl methyl ether)/D_2O Solutions. *Macromolecules*. **37**, 7710-7718 (2004)

78. Poole C. P. Jr., and Farach H. A. *Relaxation in Magnetic Resonance. Dielectric and Mossbauer Applications.* Academic Press. Elsevier Inc. 408 (1971)

79. Günther H., Hemminger W. F., Flammersheim H.-J., *Differential Scanning Calorimetry*. 2nd Edition, Springer, 310 (2003)

80. Bhattacharjee S., DLS and zeta potential - What they are and what they are not*? J Control Release*. **235**, 337-351 (2016)

81. Schnablegger H., Singh Y., *A Practical Guide to SAXS: Getting acquainted with the principles*. Anton Paar GmbH & P Analytical, 1–99 (2011)

82. Kohlbrecher J., *User Guide for the SASfit Software Package SASfit: A Program for Fitting Simple Structural Models to Small Angle Scattering Data*. 1–517 (2017)

83. Murphy D. B., *Fundamentals of Light Microscopy and Digital Imaging.* Wiley-Liss, Inc. 385 (2001)

84. Owen T., *Fundamentals of UV-visible spectroscopy*. Hewlett-Packard, 142 (1996)

85. Jameson D. M., *Introduction to fluorescence*. 1st Edition Taylor & Francis, 313, (2014)

86. Yusa S-I., Endo T., Ito M., Synthesis of thermo-responsive 4-arm star-shaped porphyrin-centered poly(*N*,*N*-diethylacrylamide) via reversible addition-fragmentation chain transfer radical polymerization. *J Polym Sci Part A Polym Chem*. **47**, 6827-6838 (2009)

87. Starovoytova L., St'astna J., Sturcova A., Konefal R., Dybal J., Velychkivska N., Radecki M., Hanykova L.,. Additive Effects on Phase Transition and Interactions in Poly(vinyl methyl ether) Solutions. *Polymers*. **7**, 2572-2583 (2015)

88. Hofmann C., Schönhoff M., Do additives shift the LCST of poly (*N*-isopropylacrylamide) by solvent quality changes or by direct interactions? *Colloid Polym Sci*. **287**, 1369-1376 (2009)

89. Juranić I., Simple method for the estimation of pK_a of amines. *Croat. Chem. Acta*. **87**, 343–347 (2014)

90. Reeve W., Erikson C. M., Aluotto P. F., A new method for the determination of the relative acidities of alcohols in alcoholic solutions. The nucleophilicities and competitive reactivities of alkoxides and phenoxides. *Can. J. Chem.* **57**, 2747–2754 (1979)

91. Arnett E. M., Wu C. Y., Base strengths of some aliphatic ethers in aqueous sulfuric acid. *J. Am. Chem. Soc.* **84**, 1680–1684 (1962)

92. Zook H. D., Kelly W. L., Posey I. Y., Chemistry of enolates. VI. Acidity scale for ketones. Effect of enolate basicity in elimination reactions of halides. *J. Org. Chem.* **33**, 3477–3480 (1968)

93. Starovoytova L., Spěváček J., Effect of time on the hydration and temperature-induced phase separation in aqueous polymer solutions. ^{1}H NMR study. *Polymer*. **47**, 7329-7334 (2006)

94. Hanykova, L., Spevacek, J., Ilavsky, M., ^{1}H NMR study of thermotropic phase transition of linear and crosslinked poly(vinyl methyl ether) in D_2O. *Polymer*, **42**, 8607-12 (2001)

95. Starovoytova, L., Spevacek, J., Hanykova, L., Ilavsky, M., ^{1}H NMR study of phase separation of uncharged and negatively charged poly(*N*-isopropylacrylamide) in D_2O solutions. *Macromolecular Symposia*, **203**, 239-246 (2003)

96. Hansen Solubility Parameters in Practice (HSPiP) software. http://www.pirika.com/NewHP/PirikaE/logP.html (web page accessed on August 27, 2018)

97. Saleh M.A., Akhtar S., Khan A.R., Viscosity of Aqueous Solutions of *n* -butylamine, *sec* -butylamine and *tert* -butylamine. *Phys Chem Liq*. **39**, 85-97 (2001)

98. Tiktopulo E.I., Bychkova V.E., Rička J., Ptitsyn O.B., Cooperativity of the Coil–Globule Transition in a Homopolymer: Microcalorimetric Study of Poly(*N*-isopropylacrylamide). *Macromolecules*. **27**, 2879-2882 (1994)

99. Flory P. J., Thermodynamics of High Polymer Solutions. *J. Chem. Phys*. **10**, 51 (1942)

100. Huggins M., Some Properties of Solutions of Long-chain Compounds. *J. Phys. Chem*. **46**, 151-158 (1942)

101. Huggins M., Theory of Solutions of High Polymers[1]. *J. Am. Chem. Soc*. **64**, 1712-1719 (1942)

102. Flory, P. J. *Principles of Polymer Chemistry*. Cornell University Press, Ithaka, NY, 672 (1953)

103. Schäfer-Soenen H., Moerkerke R., Berghmans H., Koningsveld R., Dušek K., and Šolc K., Zero and off-zero critical concentrations in systems containing polydisperse polymers with very high molar masses. II. The system water-poly(vinyl methyl ether). *Macromolecules*. **30**, 410–416 (1997)

104. Qian C., Mumby S. J., and Eichinger B. E., Phase diagrams in binary polymer solutions and blends. *Macromolecules*. **24**, 1655–1661 (1991)

105. Moerkerke R., Meeussen F., Koningsveld R., and Berghmans H., Mondelaers W., Schacht E., Dušek K., and Šolc K., Phase transitions in swollen networks. 3. Swelling

behavior of radiation cross-linked poly(vinyl methyl ether) in water. *Macromolecules.* **31**, 2223-2229 (1998)

106. Afroze F., Nies E., Berghmans H., Phase transition in the system poly(*N*-isopropylacrylamide)/water and swelling behaviour of the corresponding networks. *Journal of Molecular Structure*. **554**, 55–68 (2000)

107. Šolc K., Dušek K., Koningsveld R., and Berghmans H., "Zero" and "off-zero" critical concentrations in solutions of polydisperse polymers with very high molar masses. *Collect. Czech. Chem. Commun*. **60**, 1661-1688 (1995)

108. Aida T., Takemura A., Fuse M., Synthesis of a Novel Amphiphilic Porphyrin carrying Water-soluble Polyether Side Chains of Controlled Chain Length. Formation of a Cofacial Molecular Assembly in Aqueous Media. *J Chem. Soc., Chem. Commun*. **26**, 391-393 (1988)

109. Kim T., Ham S., Lee S.H., Hong Y., Kim D., Enhancement of exciton transport in porphyrin aggregate nanostructures by controlling the hierarchical self-assembly. *Nanoscale*. **10**, 16438-16446 (2018)

110. Kuckling D., Adler H.J.P., Arndt K.F., Ling L., Habicher W.D., Temperature and pH sensitive polymers in water-from solution to thin films. *Macromol Symp*. **145**, 65-74 (1999)

111. Wu C., Wang X., Globule-to-coil transition of a single homopolymer chain in solution. *Phys Rev Lett*. **80**, 4092-4094 (1998)

112. Ding Y., Ye X., Zhang G., Microcalorimetric investigation on aggregation and dissolution of poly(*N*-isopropylacrylamide) chains in water. *Macromolecules*. **38**, 904-908 (2005)

113. Wang X., Qiu X., Wu C., Comparison of the coil-to-globule and the globule-to-coil transitions of a single poly(*N*-isopropylacrylamide) homopolymer chain in water. *Macromolecules*. **31**, 2972-2976 (1998)

114. Yamauchi H., Maeda Y., LCST and UCST Behavior of Poly(*N*-isopropylacrylamide) in DMSO/Water Mixed Solvents Studied by IR and Micro-Raman Spectroscopy. *J Phys Chem B*. **111**, 12964-12968 (2007)

115. Tanaka F., Koga T., Kojima H., Xue N., Winnik F.M., Preferential adsorption and Co-nonsolvency of thermoresponsive polymers in mixed solvents of water/methanol. *Macromolecules*. **44**, 2978-2989 (2011)

116. Tanaka F., Koga T., Kojima H., Winnik F.M., Hydration and phase separation of temperature-sensitive water-soluble polymers. *Chinese J Polym Sci*. **29**, 13-21 (2011)

List of publications, conferences contributions, internships and scholarships

List of the author's publications included in the thesis

Publication 1

Starovoytova L., St'astna J., Sturcova A., Konefal R., Dybal J., Velychkivska N., Radecki M., Hanykova L. "Additive effects on phase transition and interactions in poly(vinyl methyl ether) solutions". Polymers, 2015, 7, 12, 2572-2583.

Publication 2

Velychkivska N., Bogomolova A., Filippov S. K., Starovoytova L., Labuta J. "Thermodynamic and kinetic analysis of phase separation of temperature-sensitive poly(vinyl methyl ether) in the presence of hydrophobic *tert*-butyl alcohol". Colloid Polym Sci, 2017, 295, 8, 1419-1428.

Publication 3

Velychkivska N., Starovoytova L., Březina V., Hanyková L., Hill J. P., Labuta J. "Improving the colloidal stability of temperature sensitive poly(*N*-isopropylacrylamide) solutions using low molecular weight hydrophobic dopants". ACS Omega, 2018, 3, 9, 11865-11873.

List of the author's publications not included in the thesis

1. U. Kostiv, Z. Farka, M. J. Mickert, H. H. Gorris, N. Velychkivska, O. Pop-Georgievski, M. Pastucha, E. Odstrčilíková, P. Skládal, D. Horák. "Versatile bioconjugation strategies of PEG-modified upconversion nanoparticles for bioanalytical applications", Biomacromolecules, 2020
2. Janisova L., Gruzinov A., Zaborova O. V., Velychkivska N., Vaněk O., Chytil P., Etrych T., Janoušková O., Zhang X., Blanchet C., Papadakis C. M., Svergun D. I., Filippov S. K. "Molecular mechanisms of the interactions of *N*-(2-hydroxypropyl)methacrylamide copolymers designed for cancer therapy with blood plasma proteins", Pharmaceutics, 12, 106, pp. 1-9, 2020.
3. Chahal M. K., Velychkivska N., Webre W. A., Labuta J., Ishihara S., Ariga K., D'Souza F., Hill J. P. "Increasing the complexity of oxoporphyrinogen colorimetric sensing

chromophores: N-alkylation and beta-substitution", Journal of Porphyrins and Phthalocyanines, 23, 11/12, pp. 1184-1194, 2019.

4. Filippov S. K., Bogomolova A., Kaberov L., Velychkivska N., Starovoytova L., Cernochova Z., Rogers S. E., Lau W. M., Khutoryanskiy V. V., Cook M. T. "Internal nanoparticle structure of temperature responsive self-assembled PNIPAM-b-PEG-b-PNIPAM triblock copolymers in aqueous solutions: NMR, SANS and Light Scattering studies". Langmuir, 2016, 32, 5314-5323.

5. Dibrivnyi V., Marshalek A., Sobechko I., Horak Y., Obushak M., Velychkivska N., Goshko L. "Thermodynamic properties of some isomeric 5-(nitrophenyl)-furyl-2 derivatives", BMC Chemistry, 13,105, pp. 1-11, 2019.

6. Sobechko I., Dibrivnyi V., Horak Y., Velychkivska N., Kochubei V., Obushak M. "Thermodynamic properties of solubility of 2-methyl-5-arylfuran-3-carboxylic acids in organic solvents". Chemistry and Chemical Technology, 2017, 11, 4, 397-404.

7. Sobechko I., Chetverzhuk Y., Horak Y., Serheyev V., Kochubei V., Velychkivska N. "Thermodynamic properties of 2-cyano-3-[5-(phenyl)-2-furyl]-2-propenamide and 2-cyano-3-[5-(4-methylphenyl)-2-furyl]-2-propenamide solutions in organic solvents". Chemistry and Chemical Technology, 2017, 11, 2, 131-137.

8. Dibrivnyi V., Sobechko I., Puniak M., Horak Y., Obushak M., Van-Chin-Syan Y., Marshalek A., Velychkivska N. "Thermodynamic properties of 5(nitrophenyl) furan-2-carbaldehyde isomers". Chemistry and Chemical Technology, 2015, 9, 67, 1-7.

9. Sobechko I.B., Van-Chin-Syan Y.Y., Kochubei V.V., Prokop R.T., Velychkivska N.I., Gorak Y.I., Dibrivnyi V.N., Obushak M.D. "Thermodynamic Properties of Furan-2-carboxylic and 3-(2-Furyl)-2-propenoic Acids", 2014, 88, 12, 2046-2053.

Selected conferences contributions

Oral presentations

Velychkivska N., Starovoytova L., Hill J. P., Labuta J. Investigation of water soluble porphyrin derivatives by means of NMR spectroscopy. Best lecture award in the Workshop "Career in Polymers VIII", Prague, Czech Republic, 2016.

Poster presentations

1. Velychkivska, N., Janisova, L., Bogomolova, A., Kaberov, L., Filippov, S. "Thermoresponsive polymeric systems studied by NMR spectroscopy". 13th International Symposium on Frontiers in Biomedical Polymers, Puerto de la Cruz, Spain, 2019.

2. Velychkivska N., Labuta J. "Water soluble porphyrin derivatives: physicochemical study". 7th World Congress on Biopolymers and Polymer Chemistry, Osaka, Japan, 2018.

3. Velychkivska N., Bogomolova A., Filippov S., Starovoytova L. "Molecular mobility in polymer systems studied by NMR spectroscopy". 9th International Symposium Molecular Mobility and Order in Polymer Systems. St. Petersburg, Russian Federation, 2017.

4. Velychkivska N., Bogomolova A., Filippov S., Starovoytova L. "Interactions of human serum albumin with polymer micelles: NMR study". Discussion workshop on (bio)Macromolecular Ionic Systems. Hrubá Skála, CR, 2017.

5. Velychkivska N., Bogomolova A., Filippov S., Starovoytova L. "Thermodynamic and kinetic analysis of nanoparticle formation of poly(vinyl methyl ether) in the presence of tert-butyl alcohol studied by NMR and ITC methods". Discussion workshop on (bio)Macromolecular Ionic Systems. Hrubá Skála, CR, 2017.

6. Velychkivska N., Starovoytova L. "NMR study of the additive-influenced poly(vinyl methyl ether) and poly(N-isopropylacrylamide) nanoparticle formation". European Polymer Federation Congress 2015. Dresden, Germany, 2015.

Internships

02.2018-07.2018 internship under supervision of Dr. Jan Labuta at the National Institute for Materials Science, Tsukuba, Japan.

11.2016-01.2017 internship under supervision of Dr. Jonathan P. Hill and Dr. Jan Labuta at the National Institute for Materials Science, Tsukuba, Japan.

Scholarship

Visegrad Scholarship № 51910789. "Investigation of stimuli-responsive supramolecular systems studied by NMR spectroscopy" during the period from 10.2019 to 07.2020.

Author's contribution in publications 1-3: 40-65%

Appendix